Anatomical and Functional Organization of the Visual Cortex, and the Effect of Visual Deprivation in Animal Models

Adrian K Andelin

A dissertation

submitted in partial fulfillment of the

requirements for the degree of

Doctor of Philosophy

University of Washington

2018

Reading Committee:

Jaime F. Olavarria, Chair

Steve Buck

Jaime Diaz

Program Authorized to Offer Degree:

Department of Psychology

University of Washington

Abstract

Anatomical and Functional Organization of the Visual Cortex, and the Effect of Visual Deprivation in Animal Models

Adrian K Andelin

Chair of the Supervisory Committee:

Jaime F. Olavarria

Department of Psychology

Despite the fact that the visual system has been the most well-studied of all sensory systems, many questions remain in regard to its structure and function in both human and animal models. While a basic blueprint of the visual system exists across all animal species that sets in place the basic structure prior to the onset of visual experience, it has been well established that this system becomes fine-tuned through experience early in life. Using a variety of techniques and animal models, this dissertation addresses some questions regarding the functional organization and the effect of visual deprivation on the visual cortex of several animal models.

Rodents offer several advantages for studying various aspects of the development, organization and plasticity of the visual system. An important model for studies of visual cortex plasticity is the system of ocular dominance columns (ODC, aggregates of cells with the same

eye preference), which have been extensively studied in many carnivores and primates, but have been thought not to exist in rodents. Our lab recently reported the existence of ODCs in pigmented, Long Evans rats (Laing et al. 2015), but previous reports in albino rats (Diao et al., 1983) point to differences in the binocularity of certain regions of primary visual cortex (V1) and in the role that callosal connections may have in these differences. To explain these strain differences, we hypothesized that albino rats, unlike Long Evans rats, do not have ODCs, and that callosal connections in V1 of albino rats are not patchy, as they are in Long Evans rats. In the first chapter of this dissertation, we present anatomical and electrophysiological experiments supporting our prediction that input from both eyes intermix in the binocular region of V1 in albino rats, without segregating into ODCs, and that callosal connections in albino rats are homogeneously distributed in V1.

In the second chapter, we explore the effect of loss of vision during early development on the surface area of V1. Using histological methods as well as MRI techniques, we examined how the reduction in mature brain surface area varies with age when blindness occurs in rats, ferrets and humans. To compare data across species, we translated the post-conception ages of each species to a common neurodevelopmental event-time scale. We predicted that the critical period for the effect of blindness on the area of V1 ends at a common developmental event-time across species. Our results support our prediction, and also show that the critical period for the effect of blindness on V1 surface area ends well before the visual cortex reaches its normal, mature size.

Much of the research on the organization and function of visual cortex is presently carried out in mice. While a present advantage of mice is the possibility of using genetic tools, a disadvantage is the small size of their brain and visual cortex. In the third chapter, we use multiple anatomical tracers to explore the number, arrangement and internal topographic

organization of extrastriate visual areas in the rabbit, whose brain is about 60 times larger than the mouse brain. Our results show that the visual cortical plan in rabbits closely resembles the plan in mice and rats, suggesting that the rodent plan may be more general, encompassing Lagomorphs and possibly other orders. Our study also underscores the usefulness of the rabbit as an alternative model to rats and mice for projects benefiting from a larger brain.

TABLE OF CONTENTS

LIST OF FIGURES

LIST OF TABLES

INTRODUCTION

The adult structure of the brain results from a combination of the influences of genetics and the environment. Understanding how each of these influences plays into the resulting adult structure can have important implications regarding both species and strain chosen for experimental manipulations, as well as appropriate applications for therapeutic interventions. This dissertation addresses questions regarding the influence of sensory information during development and on the plasticity of the visual cortex, in addition to the effects of species specific genetic abnormalities. Plasticity describes the ability of the brain to adapt to changes in the environment, and is a trait described across species particularly during development. Sensory experiences early in life determine how the brain will function in adulthood. The visual system is among the most well studied systems in this regard.

Previous studies in albino rats reported that a narrow region in lateral striate cortex (V1) is highly binocular, and that input from the ipsilateral eye to this region comes through the corpus callosum. In contrast, a recent study in pigmented Long Evans rats showed that this region is nearly exclusively dominated by responses from the contralateral eye even though it is richly innervated by the callosum. In the first chapter of this dissertation we replicated the previous results in albino rats and tested the hypothesis that the inability of callosal connections to relay input from the ipsilateral eye to lateral striate cortex in Long Evans rats is a consequence of both the existence of ocular dominance columns (ODCs) in V1, and the segregation of callosal connections into patches overlapping ipsilateral eye ODCs in the binocular region of V1 (Laing et al., 2015). We predicted that in albino rats, input from both eyes intermix in the binocular region, without segregating into ODCs, and that callosal connections are not patchy as in Long

Evans rats. Retinal input to V1 was revealed using the transneuronally transported tracer WGA-HRP, and callosal connections were revealed using cortical injections of anatomical tracers.

Confirming our predictions, we found that inputs from both eyes are intermixed in the binocular zone, without segregating into ODCs. Similarly, we found that callosal connections in albino rats are not patchy, but instead are distributed throughout the binocular segment and lateral segment (LS). We propose that, as a consequence of these changes, the binocular region in albino rats includes lateral striate cortex, being therefore larger in size than the binocular region in Long Evans rats. Our findings provide insight about the role of callosal connections in generating binocular cells, and suggest that albino rats may be a useful model for studying factors that regulate the segregation of eye specific input in mammalian visual cortex, as well as the spatial correlation between eye specific domains and callosal connections in striate cortex.

In the second chapter of my dissertation, we examine the influence of sensory input on the developing visual cortex. Blindness during development is known to lead to a reduction in the overall surface area of the primary visual cortex in adulthood. However, there is no established timeline for this effect of deprivation on visual cortex development and it has not been referenced to other neurodevelopmental events in any species. We examined the neuroanatomical consequences of early blindness across three different mammalian species at adulthood. These experiments examine how the reduction in surface area in the mature brain varies with the age of blindness onset in rats, ferrets and humans. We hypothesize that cortical area size correlates with a specific developmental stage across species, suggesting that the eyes regulate cortical development through similar mechanisms in each of the species. Additionally, we examined whether the size of V1 becomes immune to visual deprivation before V1 reaches

its normal adult size by comparing the end of the critical period for visual deprivation with the age at which the visual cortex reaches its adult size in normal rats.

In the third chapter, we examine the anatomy of the rabbit visual system. Previous studies in rabbits have described several extrastriate cortical areas with anatomical connections to V1, however their internal topography is unknown. We addressed this issue using multiple anatomical tracers injected into different regions of V1 of the same animal, and subsequently analyzed the topography in the labeled extrastriate fields. These data support the hypothesis that rabbit extrastriate areas resemble those of rats and mice in both their general location, as well as their internal topography. These findings underscore the usefulness of rabbits as an animal model in studies requiring the use of larger brains than those of rodents.

CHAPTER 1: LACK OF OCULAR DOMINANCE COLUMNS INCREASES THE SIZE OF THE BINOCULAR REGION IN STRIATE CORTEX OF ALBINO RATS

In pigmented, hooded Long Evans rats, inputs from both eyes are anatomically and functionally segregated into ocular dominance columns (ODCs) in the central segment (CS) of striate cortex (V1) (Laing et al., 2015). Interposed between the CS and the lateral border of V1, these authors identified a narrow strip of cortex, named the lateral segment (LS), that is strongly, if not exclusively, dominated by the contralateral eye. Moreover, callosal connections in V1 form both distinct patches that co-localize with ipsilateral eye ODCs in the CS and a dense, continuous band that overlaps the region of contralateral eye input in the lateral segment (LS). This organization mirrors the relationship between eye-specific callosal connections and ODCs described previously in the cat (Olavarria, 2001, 2002), namely, callosal connections correlate with ipsilateral domains in regions corresponding to the CS, and with contralateral domains in regions corresponding to the LS.

In contrast to the findings by Laing et al. (2015) in Long Evans rats, previous studies in albino rats have reported that a region corresponding to the LS in lateral striate cortex is highly binocular, and that input from the ipsilateral eye to this region comes through the callosum (Diao et al., 1983). The observation that the LS in Long Evans rats is strongly dominated by the contralateral eye in spite of being richly innervated by the corpus callosum implies that callosal projections are unable to relay indirect input from the ipsilateral eye to the LS in the Long Evans strain of rats. In this study, we test the hypothesis that this is a consequence of both the functional segregation of eye-specific domains, and the association of callosal patches with ipsilateral eye-specific domains in the CS of Long Evans rats. This hypothesis posits that the co-localization of callosal connections with ipsilateral eye ODCs prevents the ipsilateral eye input

from indirectly reaching the LS via the callosum. It further posits that indirect, interhemispheric passage of eye input to the ipsilateral LS would be facilitated if the inputs from both eyes intermix, and callosal connections do not segregate into patches, in the CS. We therefore predicted that the inputs from both eyes are intermixed, rather than segregated, and that the distribution of callosal connections is homogeneous, rather than patchy, in V1 of albino rats.

In agreement with Diao et al. (1983), our analysis of microelectrode recordings showed that evoked responses are predominantly binocular in lateral striate cortex of albino rats, and that transection of the callosum virtually eliminates input from the ipsilateral eye to this region. To test our anatomical predictions, we analyzed the patterns of retinal input to V1 in tangential cortical sections following monocular injections of the transneuronally transported tracer WGA-HRP. We also analyzed the patterns of callosal connections revealed following multiple intracortical injections of different anatomical tracers. Confirming our predictions, we found that, unlike Long Evans rats, inputs from both eyes do not segregate into ODCs, but instead overlap throughout the CS of albino rats. Moreover, also unlike Long Evans rats, we found that callosal connections do not form distinct patches, but are instead distributed throughout the CS of albino rats, overlapping the diffuse distribution of direct ipsilateral eye input in the CS. We propose that, as a consequence of these changes, the binocular region in albino rats includes the LS, being therefore larger in size than the binocular region in Long Evans rats. These findings suggest that the capacity of callosal connections to contribute to the generation of binocular cells in striate cortex depends to a large extent on factors and constraints determining the modular architecture of eye specific domains in striate cortex, and the spatial correlation between these domains and callosal connections.

MATERIALS AND METHODS

This study used adult Long Evans pigmented (hooded) and Sprague-Dawley albino rats (*Rattus norvegicus)*. Animal procedures were performed according to protocols approved by the Institutional Animal Care and Use Committee at the University of Washington and are in accordance with the animal care guidelines of the National Institutes of Health, USA.

Intraocular and Intracortical Injections of Anatomical Tracers and Histochemical Processing. Intraocular and intracortical tracer injections were performed under anesthesia induced and maintained with isoflurane (5 and 2.5% respectively) in air. In 7 albino rats, a total volume of 6μL of 3% horseradish peroxidase conjugated to wheat-germ agglutinin (WGA-HRP) in saline was pressure injected over 15 minutes through glass micropipettes (50-100 μL tip diameter). The injection site was ~2.00 mm posterior to the corneal limbus, at a depth of ~2.0 mm. Data on ipsilateral eye projections to V1 in Long Evans rats obtained similarly by Laing et al. (2015) were analyzed for comparison.

Callosal connections were labeled following multiple intracortical injections of horseradish peroxidase (HRP, Sigma Co, 25% in saline; total volume = 4.0 μL) into occipital cortex of 8 albino rats. Injections were evenly spaced (0.2 μL each), at a depth of ~800-1000 μm. The tracer was pressure injected through glass micropipettes (50-100 μm tip diameter) over an area extending from ~2 to 7 mm lateral to the midline suture, and 0.0-6.0 mm anterior to lambda suture. The dura was kept intact and moist with saline. Following the injections, the bone chip was repositioned, and the skin was sutured by planes. Data on callosal connections in Long Evans rats obtained similarly by Laing et al. (2015) were analyzed for comparison.

Four days following intraocular injections of WGA-HRP and 2-3 days following intracortical injections of HRP, animals were deeply anesthetized with pentobarbital sodium (100

mg/kg i.p.) and perfused through the heart with 0.9% saline followed by 4% paraformaldehyde (PFA) in 0.1 M phosphate buffer (PB, pH 7.4). Cortices were separated from the brains and flattened for sectioning in the tangential plane, while the remaining brain was left intact for coronal sectioning. The flattened cortices were left between glass slides for 24 hours in 0.1 M PB, after which time the tissue was transferred to a 4% PFA in 0.1 M PB, 20% sucrose solution for 1 additional hour. Tissue blocks to be sectioned in the coronal plane were kept in 4% PFA in 0.1 M PB and 20% sucrose for one or more days. All tissue was cut using a freezing microtome at 60 μm thickness and the sections were collected in 0.1 M PB. Sections were reacted for HRP with 3,3,5,5-tetramethylbenzidine as the chromogen (Mesulam, 1978).

Electrophysiology. Electrophysiological recordings in Long Evans (n = 10) and albino rats (n = 9) were performed under urethane anesthesia (1200 mg/kg i.p.). Atropine sulfate (0.1 mg/kg i.p.) was used to reduce tracheal secretions. Body temperature was kept at 37°C with a heating pad. Pupils were dilated with atropine sulfate ophthalmic solution (1%, Bausch and Lomb), artificial tears (polyethylene glycol eye drops) and silicone oil was used to protect the corneas and the cerebral cortex, respectively. In a separate group of albino rats (n = 13), the splenium of the corpus callosum was transected at the beginning of the recording session by making a parasagittal cut with a #11 scalpel blade in the hemisphere opposite to the recordings, 1mm lateral to the midline, 3 mm deep, and extending posteriorly from 3 to 6 mm measured from the bregma suture. Prior to recording, a window extending from 2 to 7 mm in the mediolateral direction, and from the lambda suture to 5 mm in the anteroposterior direction was drilled into the skull exposing the occipital cortex. The dura matter was left intact. Multiunit activity was recorded with glass-insulated tungsten electrodes (1-2 MΩ; FHC) positioned perpendicularly to the cortical surface, at depths of 500-600 μm, and displayed on an

oscilloscope and an audio monitor. Signals were filtered and amplified using a digital electrophysiology amplifier board (RHD 2132, Intan technologies, LLC) and USB interface board (RHD 2000 series, Intan Technologies, LLC), and stored on a computer for later analysis.

Full field visual stimuli were presented through custom made eye covers housing a white LED for each eye. The eye covers ensured that each eye was stimulated independently from the other eye. A custom made remote control simultaneously sent a signal to one LED as well as the electrophysiology interface board, allowing visually evoked responses to be time-locked to stimulation. Each eye was stimulated separately while the non-stimulated eye was occluded. Visual responses elicited from an eye ceased when the eye was covered, indicating that covering of the eyes was effective in preventing visual stimulation. Electrode penetrations, spaced at least 200 µm apart, were arranged in a grid over the lateral half of V1. In an initial set of experiments in Long Evans and albino rats, the ocular preference of the multiunit activity at each recording site was assessed by comparing the audio responses elicited from each eye, and rated according to the Hubel and Wiesel's 1-7 scale (Hubel & Wiesel, 1962), i.e., responses in group 1 were driven only by the contralateral eye while responses in group 7 were driven only by the ipsilateral eye. Binocular responses were rated in between, with 4 indicating about equal responsiveness to both eyes. In a second set of experiments, designed to test the effect of transecting the callosum on binocularity in V1 of albino rats, the ocular preference of evoked response at each recording site was assessed quantitatively. Action potentials (APs) were collected after filtering and thresholding recording traces of neural activity using a custom Matlab script (ver 2015a; Mathworks, Inc.). The spontaneous activity recorded during 300 milliseconds prior to stimulation was subtracted from responses recorded from each eye during the 300 milliseconds following stimulation onset. These time windows were chosen based on

analysis of peak response times to visual stimulation. For each recording site, counts of the APs for each trial were summed and averaged for each eye. Using these values, a contralateral bias index (CBI) was calculated to evaluate the ocular preference of responses within each of the cortical regions analyzed, according to the formula:

$$CBI = (R\text{contra} - R\text{ipsi}) / (R\text{contra} + R\text{ipsi})$$

R denotes responses, measured as numbers of APs, for stimulations of either the contralateral or ipsilateral eye. This index ranges from -1 (purely ipsilateral response) to +1 (purely contralateral response). Values ~ 0 indicate balanced binocular responses.

Rats with and without callosal transection were perfused immediately at the end of recording sessions, and the recorded hemispheres were flattened for tangential sectioning. The callosotomy was inspected in coronal sections and only cases with a complete transection of the splenium were analyzed.

Data Acquisition and Analysis. Prior to histochemical processing, the tangential sections from flattened hemispheres were digitally scanned at 2400 dpi for identification of the V1 border as revealed by the abrupt transition in the density of myelination pattern upon passing from striate cortex to extrastriate cortex (Richter and Warner 1974; Laing et al. 2012, 2015). The V1 border was delineated with the aid of the filter "trace contour" in Adobe Photoshop CS5 (Adobe Systems, CA). The myelin pattern was optimally displayed in tangential sections passing through Layer 4 (~500–650 μm deep) and was confirmed in 2 or more sections from the same animal. Further information for identifying the border of V1 was provided by the relationship that is known to exist between this border and distinct features of the callosal pattern in V1 (Olavarria

and Van Sluyters 1985; Laing et al. 2012). Following the histological processing for anatomical tracers, digital images of the labeling patterns were obtained by scanning the sections (Epson 4990). The digitized images of myelin and anatomical labeling patterns were aligned with each other in Adobe Photoshop, using the border of V1, the edges of sections, and radial blood vessels as fiducial markers. To reduce sharp increases in density produced by blood vessels and other artifacts, noise filters in ImageJ (ver 1.50e) were used in all images (remove outliers function, radius = 5, threshold = 10) and Gaussian filters ($\sigma = 6$). High-magnification images were obtained using a DMR Leicamicroscope coupled to a Leica DC 300F digital camera.

Analysis of patchiness in the patterns of ipsilateral retino-geniculo-cortical projections and callosal connections.

Area Method. The degree of patchiness of ipsilateral eye and callosal labeling patterns in V1 was quantitatively evaluated using a patchiness index (PI) of area calculated using the formula:

$$PI = 1 - SM/SI$$

SI is the surface area of the 3-D density profile of the labeling distribution over the target region, while SM is the surface area of the projection of SI onto a 2-D plane. Values of the patchiness index (PI) approaching zero indicate low patchiness, i.e., the labeling density landscape fluctuates little (the area of SI approaches that of SM), while values of PI approaching 1 indicate large fluctuations in the labeling density landscape (i.e., area of SI significantly larger than that of SM). SI and SM were calculated using a custom Matlab script. To account for differences in gray scale values across cases, the gray scale values in each image were normalized by dividing them by the mean grey scale value in the image.

SD Method. The degree of patchiness in labeling distributions was also evaluated by calculating the standard deviations of the grey value distributions: images with large variations in labeling density (i.e., high patchiness) contain a wide range of grey values and have large S.D., whereas images with uniform distributions (i.e., low patchiness) are more restricted in their range of grey values and have smaller S.D. To examine whether increases in the tracer reaction times affect the grayscale values, we compared the mean grayscale values across the entire tissue sample across groups, and found that the variance both within and between groups was not statistically significant ($p > 0.05$).

Contour plot analysis. Contour plots of labeled regions of interest were created using the Matlab "contour" function, equally splitting levels of labeling density into successive slices identified by different colors. This method allowed us to calculate the areas of labeled regions at each successive density level as a proportion of the total area of the region examined. To compare with our results in albino rats, we performed similar analyses of Long Evans data from Laing et al. (2015), and some figures adapted from this previous work are illustrated in the present report.

Electrophysiology. In the electrophysiology experiments, the locations of recording sites along with local blood vessels were used as reference were marked on digital images of the intact cortical surface taken immediately before recordings begun. The images were correlated with images of the first, most superficial, tangential sections taken, and the recording sites were matched to the patterns made by electrode penetrations in these sections. The first tangential sections were aligned with deeper sections using the pattern of penetrating blood vessels, section borders, and other landmarks. Following histological processing, the recording sites were assigned to specific regions in V1 that were identified by the pattern of myelination and the

pattern of ipsilateral eye projections labeled by the transport of WGA-HRP. Only penetrations judged to be oriented perpendicularly to the cortical surface were analyzed.

RESULTS

Tripartite Subdivision of V1. To investigate the distribution of retino-geniculo-cortical input to striate cortex in albino rats, we injected the anatomical tracer WGA-HRP into one eye and analyzed the pattern of WGA labeling in tangential cortical sections. As in Long Evans rats, the pattern of labeling was most distinct at the level of layer 4 (Laing et al., 2015). In the hemisphere ipsilateral to the injected eye (Fig. 1B), the transneuronally transported tracer accumulated in a restricted portion of V1, about 1 mm wide, which was separated from the lateral border of V1 by a narrow strip of cortex, about 0.20 mm wide, where the tracer density was markedly reduced or absent. The labeling density was also absent or markedly reduced in the remaining, medial portion of V1, which extended to the medial border of V1 (Fig. 1B). Thus, in albino rats, as in Long Evans rats (Fig. 1A), V1 can be divided into three main subdivisions or segments: 1) The Central Segment (CS), defined as the area containing the ipsilateral retino-thalamo-cortical projection (outlined by segmented lines in Fig. 1); 2) The medial segment (MS), located medial to the CS, presumably representing the peripheral monocular visual field; and 3) The lateral segment (LS), located between the CS and the lateral border of V1. On average, the area of the LS is approximately 25% of the area of the CS. Figure 1C shows the myelin pattern (within black arrows) used for determining the border of V1 in Fig. 1B, indicated by the black line (see Materials and Methods).

In Long Evans rats (Fig. 1A; 2B; 4A), the ipsilateral eye projection forms distinct patches, which, as a group, occupy only about one-third of the total surface area of the CS (Laing et al., 2015), while in albino rats, distinct labeled patches are not observed in the CS. Instead, the

WGA-labeling is distributed rather uniformly, occupying the entire CS (Figs. 1B; 2C-D; 4B-D). Figure 1D shows the WGA-labeling pattern in the hemisphere contralateral to the injected eye in the albino rat shown in Fig. 1B. The WGA-labeling is distributed uniformly throughout V1, including the LS. Moreover, regions of reduced labeling (corresponding to territory innervated by the non-injected eye) are not observed in the CS, as reported in Long Evans rats (Laing et al., 2015). Comparing the labeling patterns in the hemispheres ipsilateral and contralateral to the eye injected with WGA-HRP indicates that the LS does not receive direct (i.e., retino-geniculo-cortical) input from the ipsilateral eye, consistent with the report by Diao et al. (1983) that in albino rats, ipsilateral input to lateral V1 comes exclusively via the corpus callosum. Moreover, this comparison indicates that direct contralateral and ipsilateral projections overlap in the CS, suggesting that these inputs intermix in this region, rather than segregate into separate domains as in Long Evans rats (Laing et al., 2015).

Consistent with previous studies showing that ipsilateral retinal projections are weaker in albino than in pigmented rats (Lund, 1965; Lund et al, 1974), the ipsilateral retinal projection fields are smaller in the dorsal lateral geniculate nucleus (LGN) of albino rats compared with those in Long Evans rats (cf. Fig. 1E, F). Contralaterally, the labeling was uniformly dense throughout the dLGN, except for small dorsomedial regions where the labeling was reduced, presumably corresponding to the ipsilateral eye recipient zone. In the superior colliculus (SC), the contralateral projections in both rat strains was dense and uniform throughout the nucleus, while the ipsilateral projection was weaker in the albino strain (cf. Fig. 1E, F). These labeling patterns also provide evidence that the tracer was taken up and transported evenly by the entire retina following intraocular injections of WGA-HRP.

Figures 2 and 4 further illustrate the differences between Long Evans and albino rats in the patterns of ipsilateral retino-geniculo-cortical projections. In Long Evans rats, the ipsilateral eye projections segregate into densely labeled patches of different sizes and shapes, arranged anteroposteriorly into either single or double strings (Figs. 2A, B; 4A). In contrast, we found that the labeling of ipsilateral eye projections in albino rats was typically less dense and distributed more diffusely and homogenously across the CS (Figs. 1B; 2C-D, and 4B-D). These differences are appreciated more vividly in the 3-D surface plots (Fig. 2A-D, bottom panels) of the labeling density distributions within the rectangular areas demarcated by white segmented lines in each corresponding case in Fig. 2A-D (top panels). In these plots, the z-axis represents the pixel value at each location.

To quantify the differences in the ipsilateral labeling segregation in the CS of Long Evans and albino rats, we took advantage of the fact that the surface area of the 3-D labeling landscapes increases as the patchiness of the labeling distribution increases. We defined a Patchiness Index (PI) of area such that PI = 1-SM/SI, where SI is the surface area of the 3-D density landscape in the analyzed CS region, while SM is the surface area of the projection of SI onto a 2-D plane (see Materials and Methods). Values of PI approaching zero indicate low patchiness, while higher values of PI indicate larger or more numerous fluctuations in the labeling density landscape (see Materials and Methods). We analyzed 8 Long Evans and 7 albino rats, and the average PI for Long Evans rats was 0.162 (SEM = 0.01), while the PI of albino rats was 0.102 (SEM = 0.011) (Fig. 3A), and this difference between both groups was statistically significant ($t_{13} = 3.839$, $p = 0.002$).

The degree of patchiness in WGA-labeling in Long Evans and albino rats was also evaluated by comparing the standard deviations (PISD) of the grey value distributions within a

rectangular region in the CS (see Materials and Methods): high oscillations in labeling density contain a wide range of grey values and have large PISD, whereas low amplitude or no oscillations in labeling density are more restricted in their range of grey values and have smaller PISD. We found a significant difference between the average PISD for Long Evans rats (6.934, SEM = 0.585) and albino rats (3.543, SEM = 0.446), (t_{13} = 4.035, p = 0.001) (Fig. 3B). Together, the results of both analyses suggest that the CS of albino rats does not tend to have large fluctuations in labeling density, and if present, fluctuations tend to be of low amplitude compared to Long Evans rats.

When tangential sections of V1 and their respective contour plots of labeling in albino rats are compared to that of Long Evans, the segregation of ipsilateral eye input was less distinct and of lower amplitude across all albino cases (Figure 4). Albino rats appeared to lack any of the defined ocular dominance domains (ODDs) found in Long Evans rats. Overall, the albino group's periodic fluctuation between local maxima and minima in labeling density tended to be shallower, suggesting significantly less segregation of ipsilateral eye territory relative to Long Evans.

We also analyzed the WGA-HRP labeling density profiles in contour plots generated at ten equally spaced density levels to visualize the proportion of labeled area at each level. Each level was identified by a different color, and the area analyzed was the CS (demarcated by white segmented lines in Fig. 4). Starting at the highest density level, the labeled areas at successive levels are added and the results are expressed as a percent of the area at the bottom level, i.e., the total area of the analyzed region (Fig. 5A). This analysis illustrates how quickly the labeled areas expand to encompass the entire CS. Fig. 5A shows that, compared to Long Evans rats, albinos have less labeling at the densest levels (levels 1-6), and that the labeled area in this group

expands faster at lower density levels. Rather than adding the labeled areas at each successive density level, Fig. 5B plots the proportion of the CS area that is labeled at each level. This figure shows that a significant proportion of the CS area is labeled at high density levels in Long Evans rats, while in albino rats most of the CS area is labeled at relatively low-density levels. Consistent with our analyses of patchiness indices, Fig. 5A, B indicate that, compared to Long Evans rats, albinos tend to have diffuse, low density labeling patterns. K-S tests revealed that differences between groups were significantly different for both additive ($p=0.004$) as well as proportion methods ($p = 0.005$).

Callosal Connections. Patchiness of callosal connections in V1 was analyzed in 8 Long Evans and 8 albino rats using the patch indices used above for ipsilateral eye projections. Figure 6 shows the pattern of HRP-labeled callosal connections in two Long Evans rats (Fig 6A,B) and in two representative albino rats (Fig. 6 C,D). In the lower panels, Fig. 6 shows the 3-D surface plot corresponding to each case for labeling in the CS and LS. In agreement with previous studies in rats (Cusick and Lund, 1981; Olavarria and Van Sluyters, 1985), we observed that the distribution of callosal connections peaks at the border region between areas 17 and 18a, forming a band ~ 0.22 mm wide abutting the border of V1. The labeling in this band is homogeneous throughout its anteroposterior extent, with occasional less dense regions at one or two discrete sites in some cases. By its location and width, this lateral callosal band corresponds closely with the LS described above in albino rats and in Long Evans rats (Laing et al., 2015). From this band, callosal connections decrease in labeling density as they extend over the CS in both strains of rats, but while in Long Evans rats callosal connections form patches in the CS (Fig. 6A, B) (Laing et al., 2015), the distribution is typically homogenous throughout the CS in albino rats (In Fig.6, cf. C, D). Additional examples of callosal patterns in Long Evans and albino rats are

shown in Fig. 8A, and Fig. 8B-D, respectively. Figure 7A shows that the average PIA was 0.536 (SEM = 0.023) for Long Evans rats, and 0.412 (SEM = 0.028) for albino rats, and this difference was statistically significant ($t_{14} = 3.389$, $p = 0.004$). There was also a significant difference in the standard deviations of the grey value distributions (PISD) within the CS between Long Evans rats (43.259, SEM = 3.428) and albino rats (27.942, SEM = 3.26), ($t_{14} = 3.331$, $p = 0.005$) (Fig. 7B).

Finally, the analysis of contour plots (Fig. 9) in 8 Long Evans and 8 albino rats yielded results similar to those obtained for the distribution of ipsilateral eye input to the CS of both rat strains. Fig. 9A shows that, compared to Long Evans rats, albinos have less callosal labeling at the densest levels (levels 1-4), and the labeled area at each level expands faster at lower density levels. Fig. 9B shows that a significant proportion of the CS area is labeled at high density levels in Long Evans rats, while in albino rats most of the CS area is labeled at relatively low density levels. Consistent with our analyses of patchiness indices, Fig. 9A indicates that, compared to Long Evans rats, callosal labeling in albino rats tends to be distributed diffusely over the CS. These inter-strain differences were statistically significant ($p = 0.032$).

When quantified in terms of proportion of total area occupied by each sequential level in the contour plots, the pigmented Long Evans rats once again displayed a larger percentage of the CS occupied by labeling only at the highest levels (1-4). In contrast, few albino rats were observed to have labeling at these densest levels, and the majority of rats in this groups were found to have the largest amount of area in the CS occupied by labeling at much lower levels (5-7), as shown in figure 9B. K-S tests once again revealed that across all levels Long Evans rats were significantly different from albinos ($p = 0.017$).

Electrophysiology. Diao et al. (1983) reported that lateral striate cortex is highly binocular in albino rats, while Laing et al. (2015) reported that evoked responses in the LS of albino rats were strongly dominated by the contralateral eye. To directly examine whether these reported differences were due to the use of different rat strains, we compared the binocularity across the CS and LS in 10 Long Evans rats, 9 intact albino rats, and 13 callosally transected albino rats. The ocular preference of the multiunit activity at each recording site was assessed by comparing the audio responses elicited from each eye, and rated according to Hubel and Wiesel's 1-7 scale, ranging from pure contralateral (1) to pure ipsilateral responses (7) (Hubel and Wiesel, 1962) (see Materials and Methods). Figure 10 shows a diagram of the recordings sites in Long Evans (Fig. 10A) and albino (Fig. 10B) rats. Recording sites are color-coded (see inset) to indicate ocular dominance according to the 1-7 scale of Hubel and Wiesel. The results show that, in the central segment, ipsilateral dominance (scores 5 and 6) is observed in Long Evans, but not in albino rats, consistent with the existence of ODCs in Long Evans (Laing et al., 2015), but not in albino rats. In contrast, in the LS responses are almost exclusively dominated by the contralateral eye in Long Evans rats (score 1 and 2), while they are mostly binocular in albino rats (scores 3 and 4). Our results in albino rats are in close agreement with those reported by Diao et al. (1983) in this rat strain. Likewise, our results from Long Evans confirm the electrophysiological and in situ hybridization findings of Laing et al. (2015). Our physiological results are consistent with our hypothesis that the physiological differences between Long Evans and albino rats reflect strain differences in the organization of retinal input and callosal connections in V1.

Diao et al. (1983) proposed that ipsilateral input to the LS comes via the callosum. To examine the contribution of the visual callosal pathway to the binocularity in V1 of albino rats,

we recorded visual evoked responses in the CS and LS in groups of intact and callosotomized albino rats. We also compared the results to recordings in the CS and LS of intact Long Evans rats. Recording sites across the different segments of V1 in an albino rat are illustrated in Fig. 11A, B. Figure 11 C illustrates the effectiveness of the callosotomy.

To assess the ocular preference of evoked response at each recording site, a contralateral bias index (CBI) was calculated from the counts of action potentials recorded for each trial. This index, defined as CBI = (Rcontra − Ripsi) / (Rcontra + Ripsi), ranges from -1 (purely ipsilateral response) to +1 (purely contralateral response). Values ~ 0 indicate balanced binocular responses (see Materials and Methods).

Confirming our results in Figure 10, we found that, in the lateral segment (Fig. 12A), evoked responses were highly binocular in intact albino rats (CBI=0.16, SEM = 0.049), whereas responses were strongly dominated by the contralateral eye in Long Evans rats (CBI= 0.74, SEM = 0.058) ($t_{13} = 7.496$, $p < 0.001$). However, after callosotomy in albino rats, the contralateral eye became strongly dominant (CBI = 0.82, SEM = 0.057) ($t_{19} = 8.439$, $p < 0.001$), reaching a score similar to that of Long Evans rats (CBI= 0.74, SEM = 0.058) ($t_{14} = 0.866$, $p = 0.401$). The fact that the influence of the contralateral eye in the LS is as high in Long Evans rats as in callosotomized albino rats provides compelling evidence that the bulk, if not all, of the input from the ipsilateral eye to the LS comes via the callosum in albino rats.

In the central segment (Fig. 12B), callosotomy in albino rats shifts the ocular dominance preference from being highly binocular (CBI = 0.11, SEM = 0.068) to being dominated by the contralateral eye (CBI = 0.52, SEM = 0.088), a difference that was significant ($t_{45} = 3.371$, $p = 0.002$). However, this shift is smaller than that observed after callosotomy in the LS (cf Fig.12 A). This increase in contralateral eye dominance in the CS of albino rats after callosotomy

suggests that at least some ipsilateral eye input reaches the CS via the callosum in albino rats. Consistent with this, the CS in intact albino appears to be more binocular (CBI=0.11) than the CS in intact Long Evans rats (CBI=0.33, SEM = 0.053) (t_{50} = 2.446, p = 0.018). These observations suggest that ipsilateral eye input relayed by the callosum may influence not only in the LS, but also some distance into the CS (Lewis and Olavarria, 1995). Alternatively, these observations may simply reflect errors in the location assignment for penetrations near the CS/LS border. Finally, in Long Evans rats, the contralateral eye exerts some dominance in the CS (CBI = 0.33, SEM = 0.053), but not as strongly as in the LS (cf Fig. 1A), which is consistent with the report by Laing et al. (2015) that the LS in Long Evans rats is strongly, if not exclusively, dominated by the contralateral eye.

Traditionally, the region encompassing both the CS and the LS has been designated as the "binocular region" in rats and other species. When assessed by experimental recordings over this "binocular region" in intact Long Evans rats (Fig. 12C), the influence of the contralateral eye is likely to be overestimated over the CS region (CBI = 0.47, SEM = 0.053 in the CS+LS vs. CBI = 0.33, SEM = 0.053 in the CS, cf Fig. 12 B, C) (t_{58} = 2.135, p = 0.037), and underestimated over the LS (CBI = 0.47, SEM = 0.053 in the CS+LS vs. 0.74, SEM = 0.058 in the LS, cf Fig 12A, C) (t_{30} = -2.01, p = 0.054). In contrast, in intact albino rats, binocularity is relatively constant across both the CS and LS (Fig. 12A, B). In summary, in agreement with Diao et al. (1983), our analysis of microelectrode recordings showed that evoked responses are predominantly binocular in lateral striate cortex of albino rats, and that transection of the callosum virtually eliminates input from the ipsilateral eye to this region.

DISCUSSION

Albino rats are characterized by an increased crossed retinal projection, and a reduced ipsilateral retinal projection (Lund, 1965; Lund et al., 1974). In spite of the reduction in the ipsilateral retinal projection, ipsilateral eye responses can be recorded throughout the binocular zone, and are especially robust in lateral striate cortex (Diao et al., 1983), in a region that corresponds to the LS in Long Evans rats (Laing et al., 2015). Our physiological recordings after transection of the corpus callosum confirmed the report by Diao et al. (1983) that ipsilateral input to this region is mediated by the callosal pathway. In contrast, in Long Evans rats this region is nearly exclusively dominated by the contralateral eye in spite of being callosally connected (Laing et al., 2015). To explain why callosal connections are unable to convey ipsilateral eye input to the LS in Long Evans rats, we hypothesized that development of ODCs leads to the formation of callosal patches closely associated with ipsilateral eye ODCs in the CS, which renders callosal connections unable to relay indirect ipsilateral eye input to the LS. As illustrated in Fig. 13A, the LS in the left hemisphere (blue strip) cannot receive transcallosal input from the retinotopically matched nasal retina in the ipsilateral eye (colored yellow) because this retina projects to regions in the contralateral hemisphere that are largely acallosal (colored yellow) due to the close association of callosal connections with ipsilateral ODCs (colored blue) (Laing et al., 2015).

We therefore predicted that, instead of segregating into ODCs, ipsilateral and contralateral eye input intermix throughout the CS of albino rats, allowing the indirect transfer of ipsilateral eye input to lateral striate cortex. Figure 13B represents this prediction and illustrates that if both the yellow and blue eye specific territories intermix in the right CS (blue + yellow =

green), rather than segregate into ODCs, then input from the left hemiretina (yellow) arriving to the right CS (green) would have access to the left LS through the callosum, leading to an increased binocularity in the left LS. Based on the hypothesis that the distributions of eye specific inputs and callosal connections are spatially coupled (Olavarria, 2001, 2002), we also predicted that callosal connections would not be patchy as in Long Evans rats, but would spread over the entire CS (green), reflecting the widespread distribution of ipsilateral eye thalamic input to the CS. Bearing out our predictions, our results from albino rats show that inputs from both eyes are largely intermixed throughout the CS, and callosal connections spread over the CS without forming distinct patches. It should be noted that a widespread distribution of callosal connections may not be necessary for the transcallosal transfer of ipsilateral eye input to the LS in albino rats. Callosal patches could still mediate such transfer because they would innervate areas of intermixed ipsilateral and contralateral eye input to the CS, allowing the ipsilateral eye to gain access to the LS via the callosum.

Lack of ocular dominance columns increases the size of the binocular region in striate cortex of albino rats

Our results extend the results of Diao et al. (1983) by showing that V1 in albino rats is subdivided into three segments, as in Long Evans rats (Laing et al., 2015). These segments consist of the medial, monocular segment (MS), dominated by the contralateral eye, the central segment (CS), receiving direct subcortical input from both eyes, and the lateral segment (LS), receiving primarily direct subcortical input from the contralateral eye (Fig. 1). In each hemisphere, the MS and CS represent the contralateral visual hemifield, with the lateral border of the CS corresponding to the representation of the vertical meridian of the visual field (VM). The LS extends this representation into the ipsilateral visual field (Adams and Forrester, 1968),

which can reach up to 20-30 deg in albino rats (Diao et al., 1987). In this regard, the LS is homologous to the 17/18 transition zone in cats (Payne, 1990; Payne and Siwek, 1991). Moreover, consistent with the report of Diao et al. (1983), our results show that not only the CS, but also the LS, are binocular in albino rats, so a more extensive region of cortex, at least 25% larger, is binocular in albino rats compared to Long Evans rats. As illustrated in Figure 13, the binocular field is hemisected by the VM, and each half is represented only in the opposite CS in Long Evans rats, while in albino rats, each half of the binocular field is also represented in the ipsilateral LS. This increase in the area size of the binocular region implies that binocular neurons are probably more numerous in striate cortex of the albino strain, raising the possibility that albino rats may outperform Long Evans rats in some tasks requiring binocular vision. However, this possibility is not supported by behavioral studies of depth perception in albino and pigmented rats. For instance, Routtenberg and Glickman (1964) reported that albino rats perform worse than Long Evans rats in the cliff test, probably due to factors linked to albinism, such as lower visual acuity. Perhaps comparing the performance in the cliff test of *pigmented* mice, which do not have ODCs (Antonini et al., 1999) and patchy callosal connections (Olavarria and Van Sluyters, 1984), with that of Long Evans rats may reveal an advantage of the "albino" organization in some binocular vision tests.

Why do eye specific inputs segregate in Long Evans rats, but not in albino rats?

In albino rats one would expect that ipsilateral eye projections to V1, although weaker than in Long Evans rats (Lund, 1965, Lund et a., 1974), would segregate, forming perhaps smaller or less densely labeled patches. Instead, we found that input from both eyes largely intermixed throughout the CS, without segregating into distinct eye specific territories. It is possible that segregation of eye specific domains requires the strength of ipsilateral eye input to

rise above a certain threshold, below which segregation does not occur. However, reduction of ipsilateral eye input per se is unlikely to be a major factor because pigmented animals with presumably normal ipsilateral projections can show similar characteristics, namely, a binocular lateral striate cortex, and lack of both ODCs and patchy callosal connections (e.g., mice, Antonini et al., 1999; tree shrews, Bosking et al., 2000). It is possible that mechanisms driving the development of either intermixed or segregated eye specific domains are influenced by factors associated with albinism, and that these factors are also present in some pigmented species. Further comparative studies in albino rats and in other albino and pigmented strains may help in identifying factors associated with the characteristics of eye specific input and callosal connections we observed in albino rats.

Spatial coupling between the distributions of direct eye specific inputs and callosal connections

Laing et al. (2015) showed in Long Evans rats that callosal connections form distinct patches that co-localize with ipsilateral ODCs in the CS. Our present results in albino rats show that ipsilateral eye input and callosal connections do not segregate into distinct patches, but nevertheless remain spatially correlated as they overlap throughout the CS. More generally, previous studies have shown that callosal connections in V1 are patchy in animals with ODCs (e.g., rat, Laing et al., 2015; cat, Olavarria, 2001), whereas in animals without ODCs, callosal connections are not patchy (e.g., mouse, Olavarria and Van Sluyters, 1984; tree shrews, Casagrande and Harting, 1975; Cusick et al., 1985). Thus, species without ODCs may resemble albino rats in that striate cortex is likely to be binocular in regions of lateral striate cortex corresponding to the LS in rats. Consistent with this, the binocular region appears to include lateral striate cortex in both mice (Antonini et al., 1999) and tree shrews (Bosking et al., 2000),

species which lack ODCs. On the other hand, studies in sheep (Pettigrew et al., 1984) show that a region corresponding to the LS in lateral striate cortex is binocular, and that input from the ipsilateral eye to this region comes through the callosum. Thus, it is likely that sheep, like albino rats, lack ODCs. The observation that the distributions of ipsilateral eye input and callosal connections remain spatially coupled whether or not eye specific inputs segregate into ODCs supports the idea that the distribution of callosal connections is specified by bilateral projections from temporal retina. (Olavarria 2001, 2002; Laing et al., 2015). This hypothesis explains why callosal connections correlate with ipsilateral eye domains in the CS of rats and corresponding region in cats, and with contralateral eye domains in the LS of rats and its analogue in the cat, the 17/18 transition zone (Laing et al., 2015; Olavarria, 2001). As discussed above, the intermixing of ipsilateral and contralateral eye input throughout the CS would make it possible for ipsilateral eye input to reach the LS indirectly through the callosum even if callosal connections were patchy in the CS of albino rats. Nevertheless, the observation of widespread callosal connections in the CS of albino rats is interesting because it is consistent with the spatial coupling predicted to exist between the distributions of eye specific inputs and callosal connections in striate cortex in species either with (Olavarria, 2001, Laing et al., 2015) or without (present study) ODCs.

Contribution of callosal connections toward the generation of binocular neurons

The contribution of callosal connections toward the generation of cortical binocular neurons is still a matter of debate. No clear picture has emerged from numerous studies that have used a variety of approaches to determine the extent to which binocularity in visual cortex depends on callosal input (reviewed in Olavarria, 2002). The hypothesis that callosal fibers preferentially link opposite cortical loci that are under the influence of bilateral projections from the same temporal retina (Olavarria, 2001, 2002) sheds light on this debate because it implies

that callosal fibers are not primarily involved in generating binocular cells. As illustrated in Fig. 13, callosal input to a cortical cell largely duplicates the subcortical input from one of the eyes to the same cell. This would allow the direct subcortical input to sustain the binocularity of cortical cells when callosal input is eliminated. This hypothesis leads to the prediction that section of the callosal commissure should not have a significant effect on the binocularity indices recorded in striate cortex of Long Evans rats and cats, in agreement with previous and recent reports (Long Evans rats: Laing et al., 2015; cat: Minciacchi and Antonini, 1984; Conde-Ocaziones et al., 2018). It is interesting to note that cats, as Long Evans rats, have ODCs in V1 (Anderson et al., 1988), but, unlike the LS of Long Evans rats, the cat 17/18 transition zone is binocular. The fact that the ipsilateral eye input to this zone comes via direct subcortical projections (Olavarria, 2001; reviewed in Olavarria, 2002), rather than indirectly via the callosum (Minciacchi and Antonini, 1984; Conde-Ocaziones et al., 2018) supports our hypothesis that the inability of callosal connections to relay indirect input from the ipsilateral eye to lateral striate cortex in Long Evans rats is due to the existence of ODCs in striate cortex.

On the other hand, in some species, binocularity in lateral striate cortex does depend on callosal input, as shown in albino rats (Diao et al., 1983; present study) and sheep (Pettigrew et al., 1984). It is also known that callosal connections contribute to binocularity in some extrastriate areas in Siamese cats, animals in which ipsilateral striate-extrastriate projections are largely monocular (Zeki and Fries, 1980; Marzi et al., 1980). These considerations suggest that generation of binocular cells cannot be regarded as a basic, defining function of visual callosal connections in all species, and in all visual areas. At least in striate cortex, whether callosal input contributes or not to the generation of binocular cells appears to depend on restrictions imposed

by the relationship of callosal connections with the organization of eye specific projections, which in some species segregate into ODCs, and in other species do not**.**

In conclusion, our results show that, in contrast to Long Evans rats, direct eye specific projections do not segregate into ODCs in albino rats. Whether this is related to reductions in the strength of eye specific input, to factors related to albinism, or to other factors present in albino and some pigmented species, remains to be studied. We also found that callosal connections in striate cortex of albino rats do not aggregate into distinct patches as in Long Evans rats. Instead, callosal connections are distributed throughout the CS, overlapping the distribution of ipsilateral eye input in this segment. These results provide further evidence that the organization of callosal connections in V1 is closely coupled to the organization of eye specific inputs, and that changes in the relative distribution of these inputs, i.e., whether they segregate into ODCs or intermix in the CS, can profoundly impact the function of callosal connections in V1. Our findings provide insight about the role of callosal connections in generating binocular cells, and suggest that albino rats may be a useful model for studying factors that regulate the segregation of eye specific input in mammalian visual cortex, as well as the spatial correlation between eye specific domains and callosal connections in striate cortex.

Figure 1: Long Evans and albino rat WGA-HRP ipsilateral eye labeling pattern.

A. Representative case of Long Evans ipsilateral eye labeling (adapted from Laing et al., 2015), note the distinct patches in the central segment of V1. **B.** Representative case of albino ipsilateral eye WGA-HRP labeling. Note the lack of distinct patches in the central segment of V1. **C.** Myelin pattern (arrows) of V1 for albino case shown in (B), used for determining the border of V1. **D.** Labeling in V1 contralateral to the eye injected with WGA-HRP for the albino case shown in Figure (B). **E.** Labeling pattern of LGN (top) and superior colliculus (bottom) of Long Evans rat. **F.** Labeling pattern of LGN and superior colliculus for albino case. Scale bars in A and E = 1.0 mm. In A and B, M = medial segment, C = central segment, L = lateral segment.

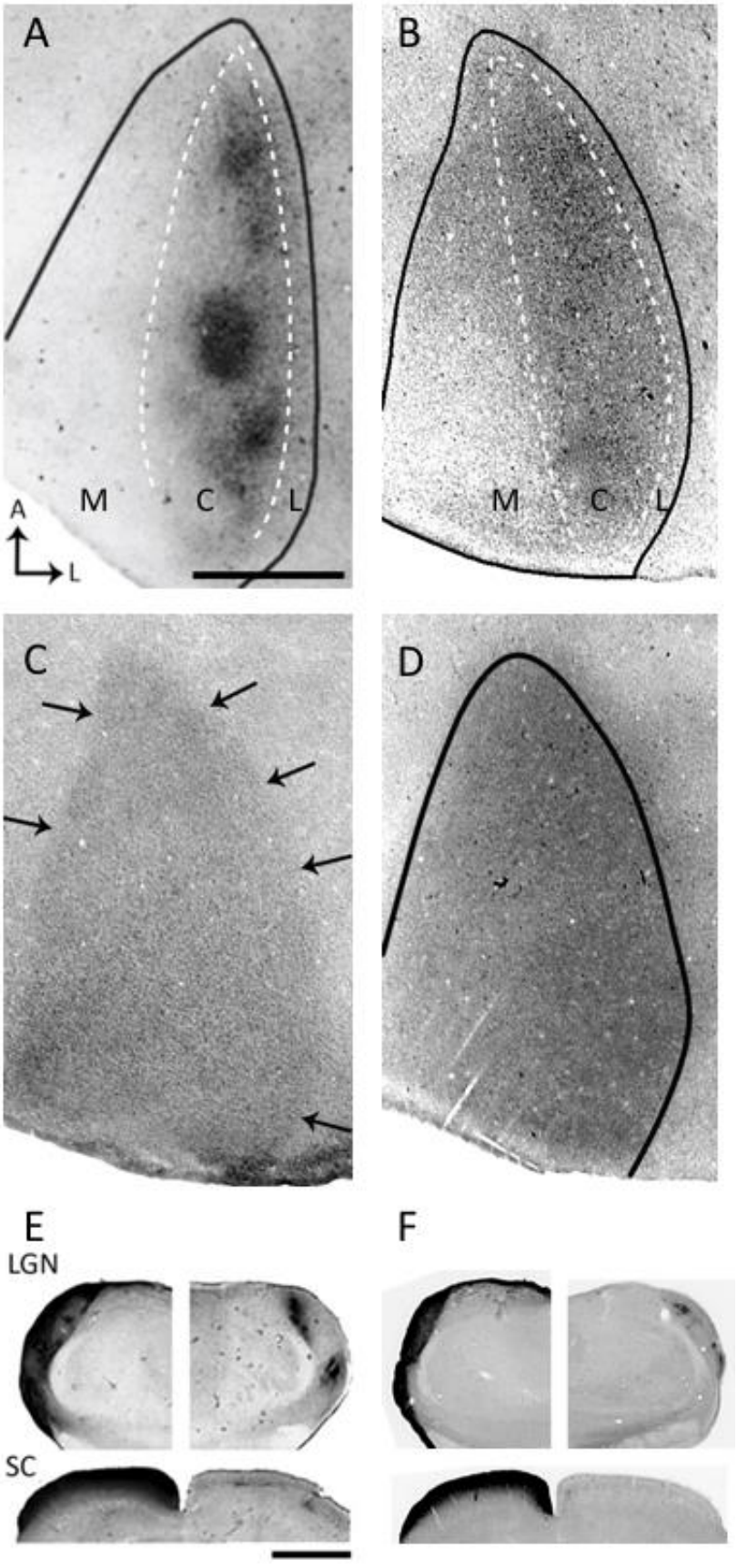
A
M
C
L
A
L
B
M
C
L
C
D
E
LGN
SC
F

Figure 2: WGA-HRP labeling patterns and 3D surface plots for Long Evans and albino rats.

A, B. Two cases of Long Evans rats (top, adapted from Laing et al., 2015) and respective 3D surface plot reconstructions of the labeling pattern (bottom). **C, D.** Two cases of albino rats (top) and respective 3D surface plot reconstructions of labeling patterns. The 3D plots derive from the areas delineated with dashed lines in the top row. Scale bar =1.0 mm.

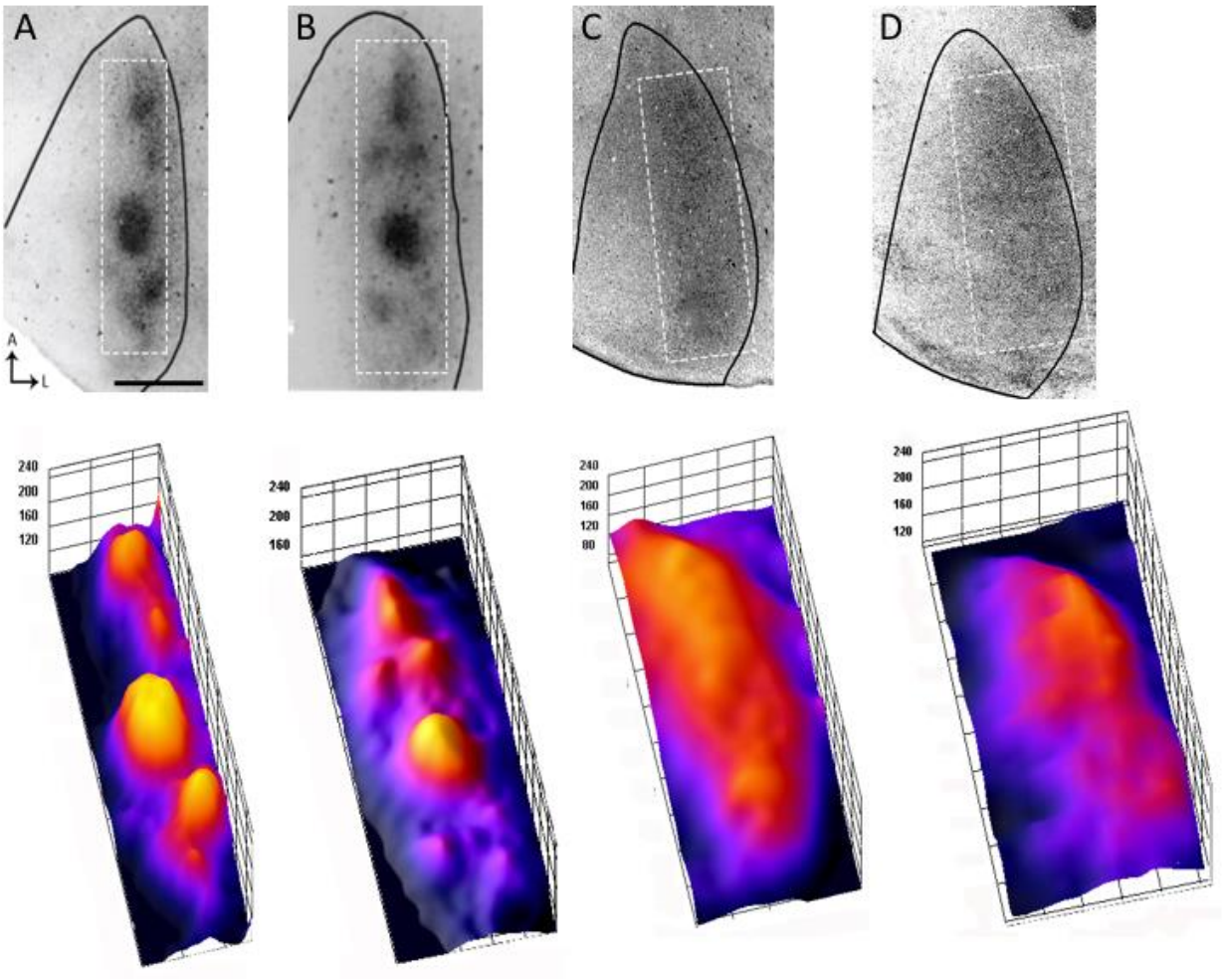
A
B
C
D
A
L
240
200
160
120
240
200
160
240
200
160
120
80
240
200
160
120

Figure 3: Patch Index: Area Method and SD Method for ODCs:

A. Average values of Patch Index Area method for each group on. Long Evans rats (n=8) are significantly different from albino group (n = 7) (p = 0.002). **B.** Average Patch Index Standard Deviation method for Long Evans and the albino group. Long Evans rats (n = 8) are significantly different from the albino group (n = 7) (p = 0.001). Error bars in both graphs denote SEM for each group.

A

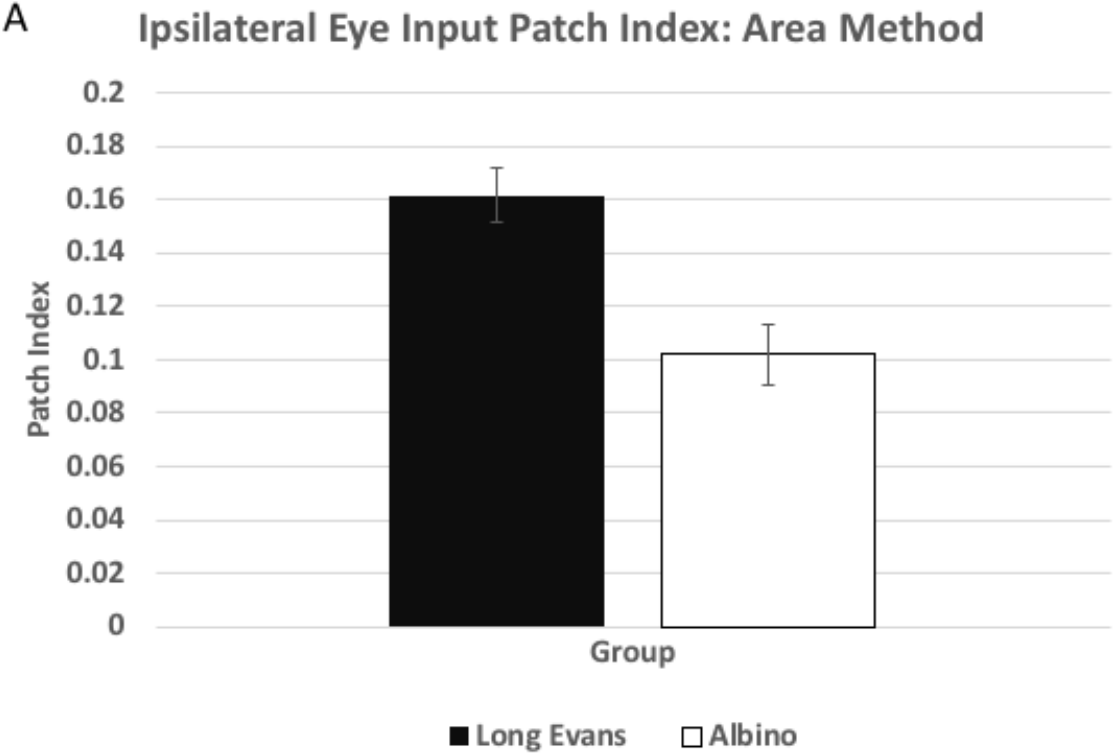
Ipsilateral Eye Input Patch Index: Area Method
0.2
0.18
0.16
0.14
0.12
0.1
0.08
0.06
0.04
0.02
0
Patch Index
Group
Long Evans
Albino

B

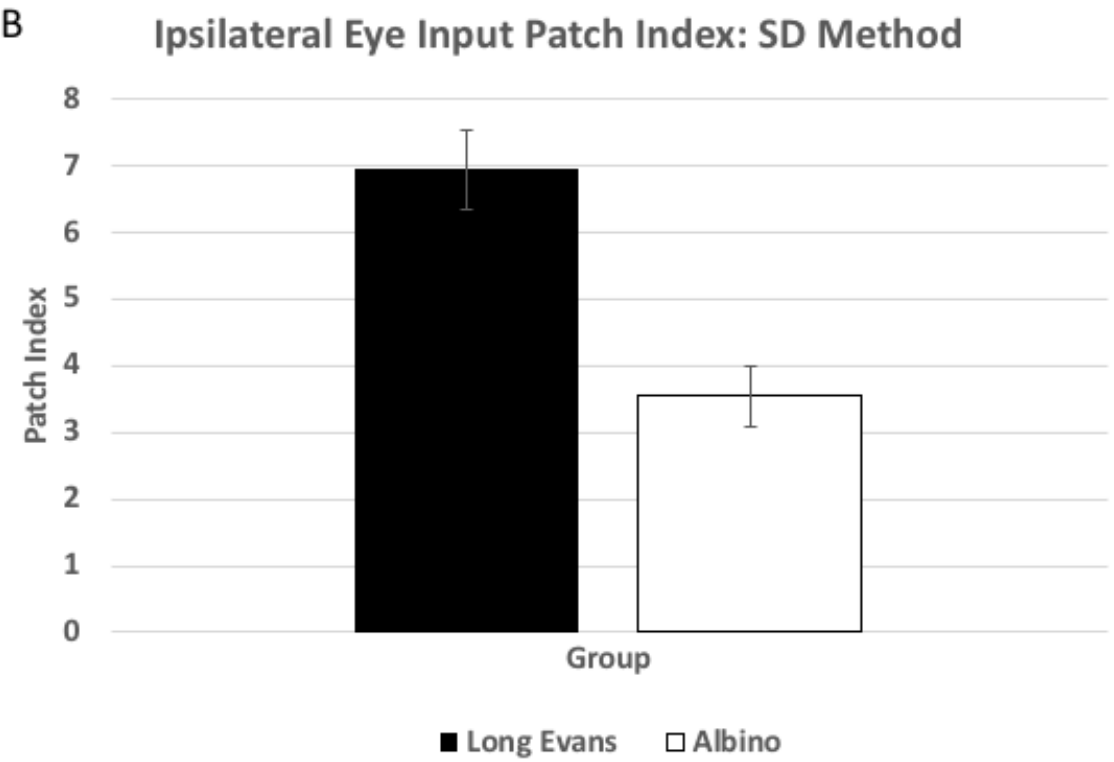
Ipsilateral Eye Input Patch Index: SD Method
8
7
6
5
4
3
2
1
0
Patch Index
Group
Long Evans
Albino

Figure 4: Long Evans and albino rats WGA-HRP labeling and respective contour plots

A. Example of Long Evans rat patchy central segment (outlined by dashed white line) in tissue section (top row), and respective contour plot (bottom row). **B-D.** Three examples of albino rat central segment (dashed white line) in tissue section (top row), and respective contour plots (bottom row). Areas of high density are indicated by bright orange color, while areas of low density are indicated by shades of blue. Scale bar = 1.0 mm.

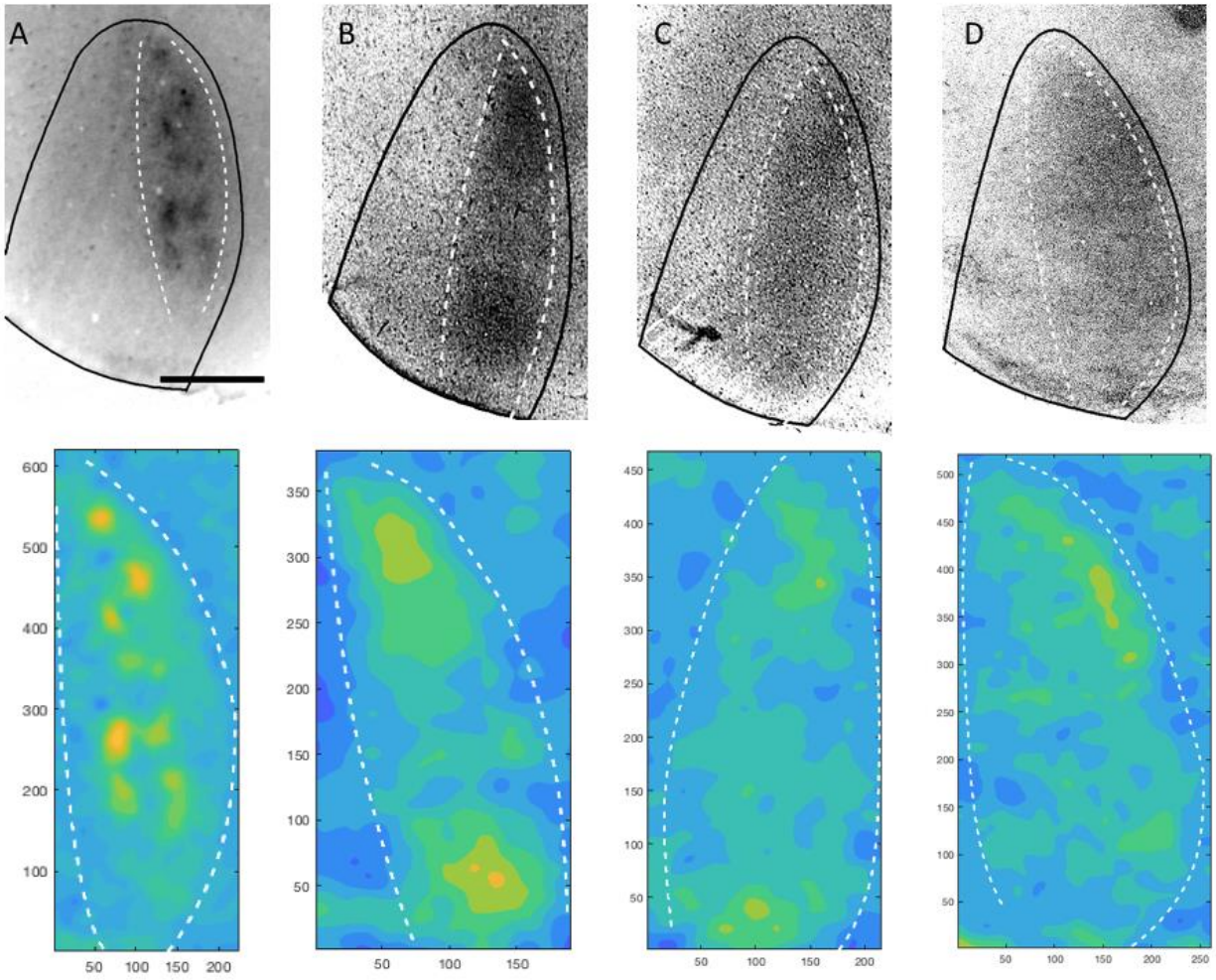
A
B
C
D
600
500
400
300
200
100
50
100
150
200
350
300
250
200
150
100
50
50
100
150
450
400
350
300
250
200
150
100
50
50
100
150
200
500
450
400
350
300
250
200
150
100
50
50
100
150
200
250

Figure 5: Additive and proportion methods for analyzing ODC labeling in Long Evans vs. albino rats.

A. Adding the proportion of the CS occupied by WGA-HRP labeling at each of 10 density levels indicated by different colors reveals that albinos have very little labeling at the densest labeling levels, and that most of the area occupied in contour plots takes place at lower density levels, indicative of more diffuse labeling with no patches. Kolmogorov-Smirnov test reveals that Long Evans rats are significantly different from albino group ($p = 0.004$). **B.** Proportion of labeling occupied at each density level. Compared to Long Evans, albinos have more diffuse labeling patterns that tend to be seen primarily at the least densely labeled levels. K-S test reveal that Long Evans rats are significantly different from the albino group ($p = 0.005$).

A

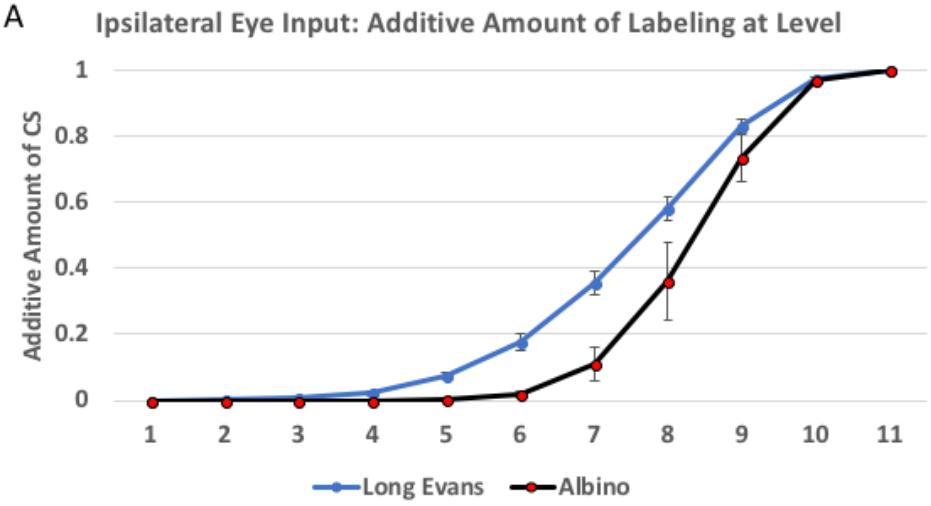
Ipsilateral Eye Input: Additive Amount of Labeling at Level
Additive Amount of CS
1
0.8
0.6
0.4
0.2
0
1 2 3 4 5 6 7 8 9 10 11
Long Evans
Albino

B

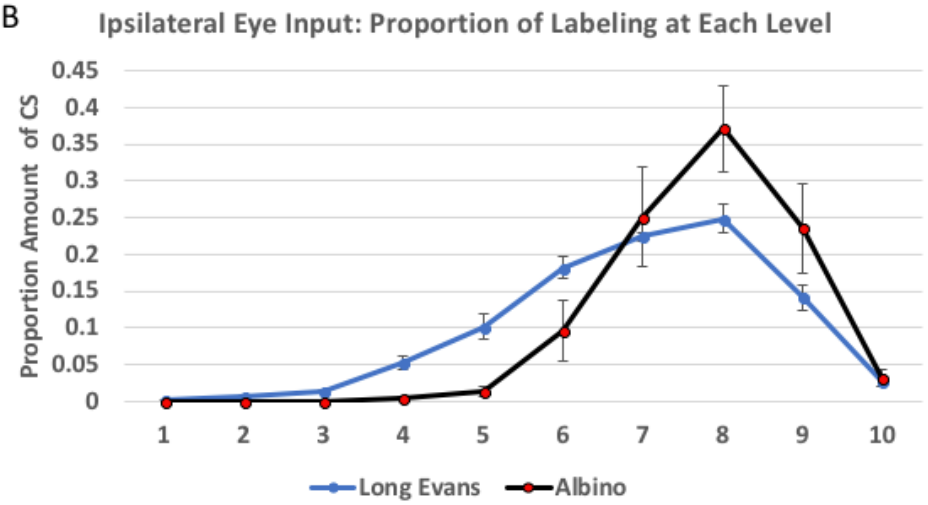
Ipsilateral Eye Input: Proportion of Labeling at Each Level
Proportion Amount of CS
0.45
0.4
0.35
0.3
0.25
0.2
0.15
0.1
0.05
0
1 2 3 4 5 6 7 8 9 10
Long Evans
Albino

Figure 6: Callosal labeling in Long Evans and albino rats.

A, B. Two examples of HRP- labeled callosal patterns in Long Evans rats (top, adapted from Laing et al. 2015) and respective 3D surface plot reconstructions (bottom). **C, D.** Two examples of HRP-labeled callosal patterns albino rats (top) and respective 3D surface plot reconstructions of these cases (bottom). The white lines in the top row indicates the border between striate (V1) and lateral extrastriate cortex. Note that the 3D plots are reconstructed from both the CS and LS. Bright yellow indicates high labeling density; black indicates background. Scale bar = 1.0 mm.

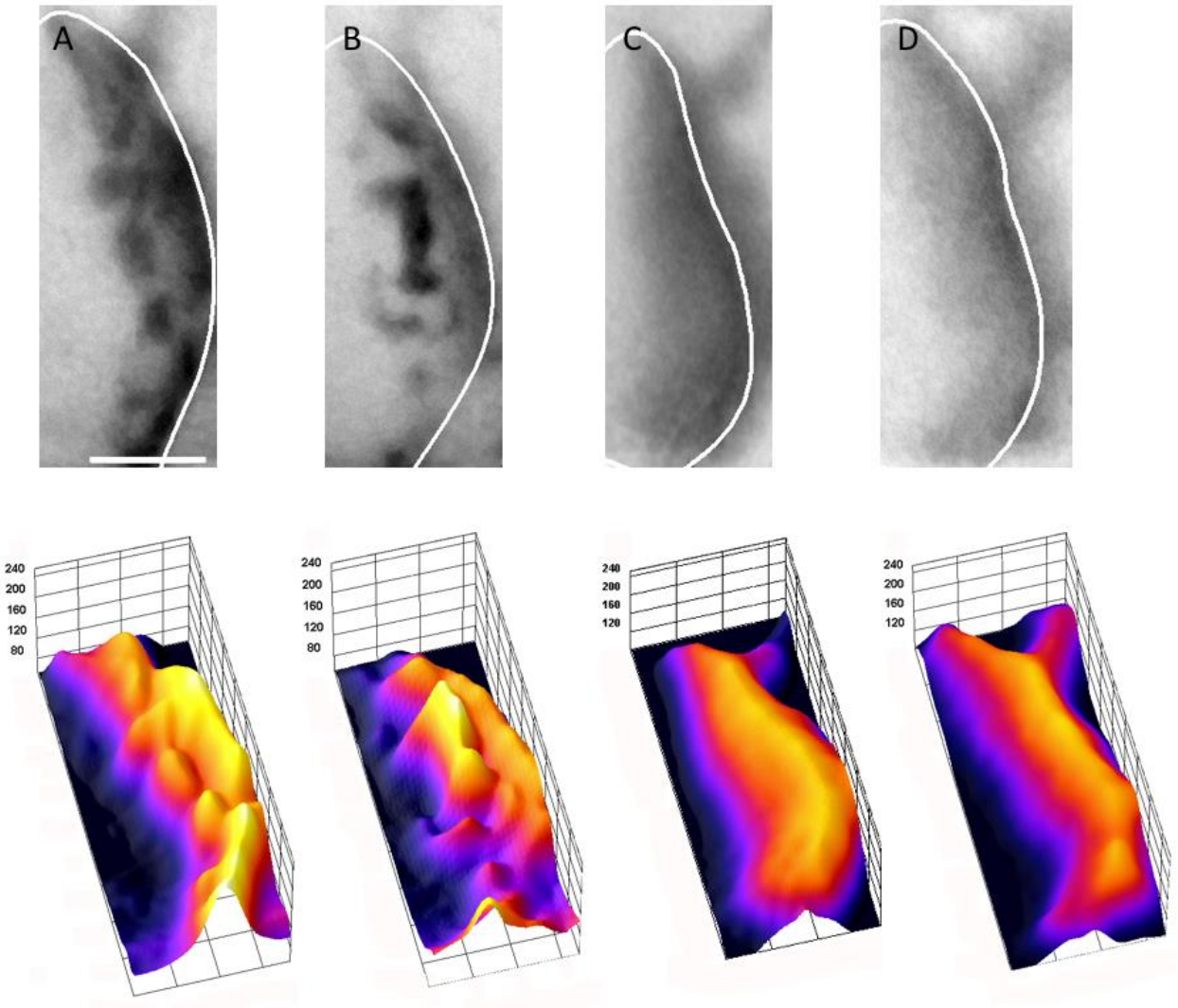
A
B
C
D
240
200
160
120
80
240
200
160
120
80
240
200
160
120
240
200
160
120

Figure 7: Patch Index: Area Method and SD Method for callosal patches.

A. Average values of Patch Index Area method for Long Evans (n = 8) and albino (n = 8) rats. Long Evans rats are significantly different from albino group ($p = 0.032$). **B.** Average values of Patch Index Standard Deviation method for Long Evans (n =8) and albino (n = 8) rats. Long Evans rats are significantly different from the albino group ($p = 0.017$). Error bars in both graphs denote SEM for each group.

A

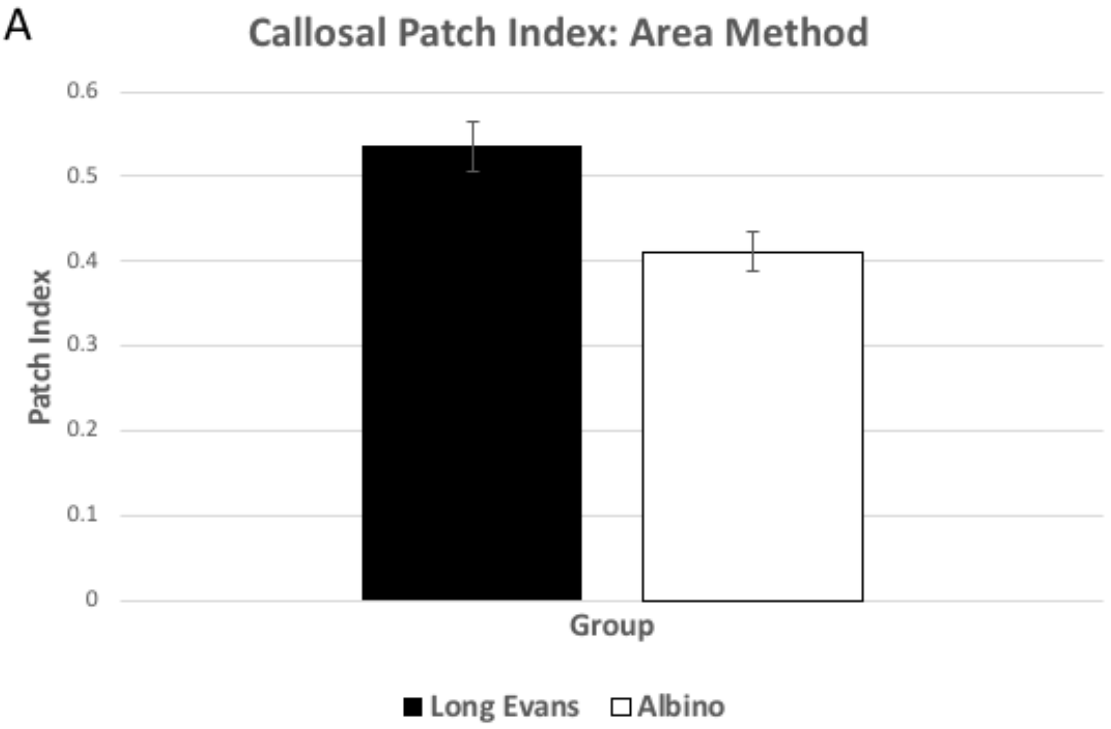
Callosal Patch Index: Area Method
0.6
0.5
0.4
0.3
0.2
0.1
0
Patch Index
Group
Long Evans
Albino

B

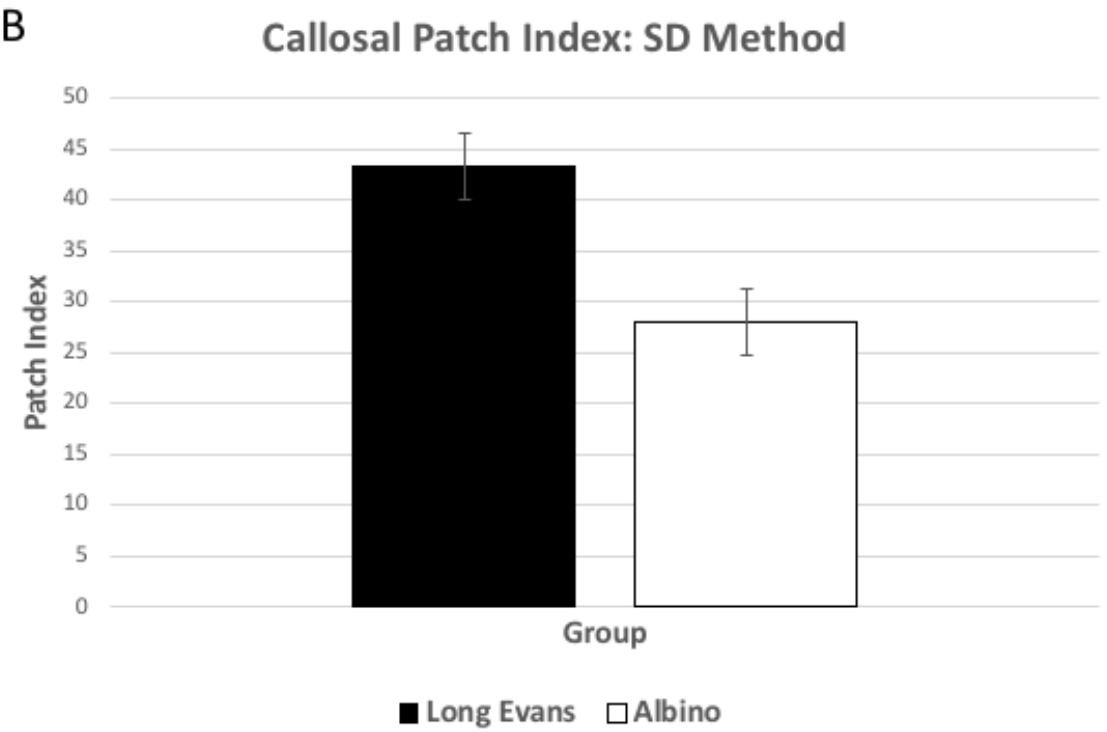
Callosal Patch Index: SD Method
50
45
40
35
30
25
20
15
10
5
0
Patch Index
Group
Long Evans
Albino

Figure 8: Callosal HRP labeling patterns in Long Evans and albino rats, and contour plot reconstructions.

A. Example of patchy callosal connections in a Long Evans rat (adapted from Laing et al., 2015), and respective contour plot (bottom row). **B-D.** Three examples of callosal patterns in albino (top row), and respective contour plots (bottom row). The white lines in the top row indicate the border between striate and lateral extrastriate cortex. The contour plots are derived from the CS (indicated by dashed white lines in the top and bottom rows). Areas of high density are indicated by bright orange color, while areas of low density are indicated by shades of blue. Scale bar = 1.0 mm.

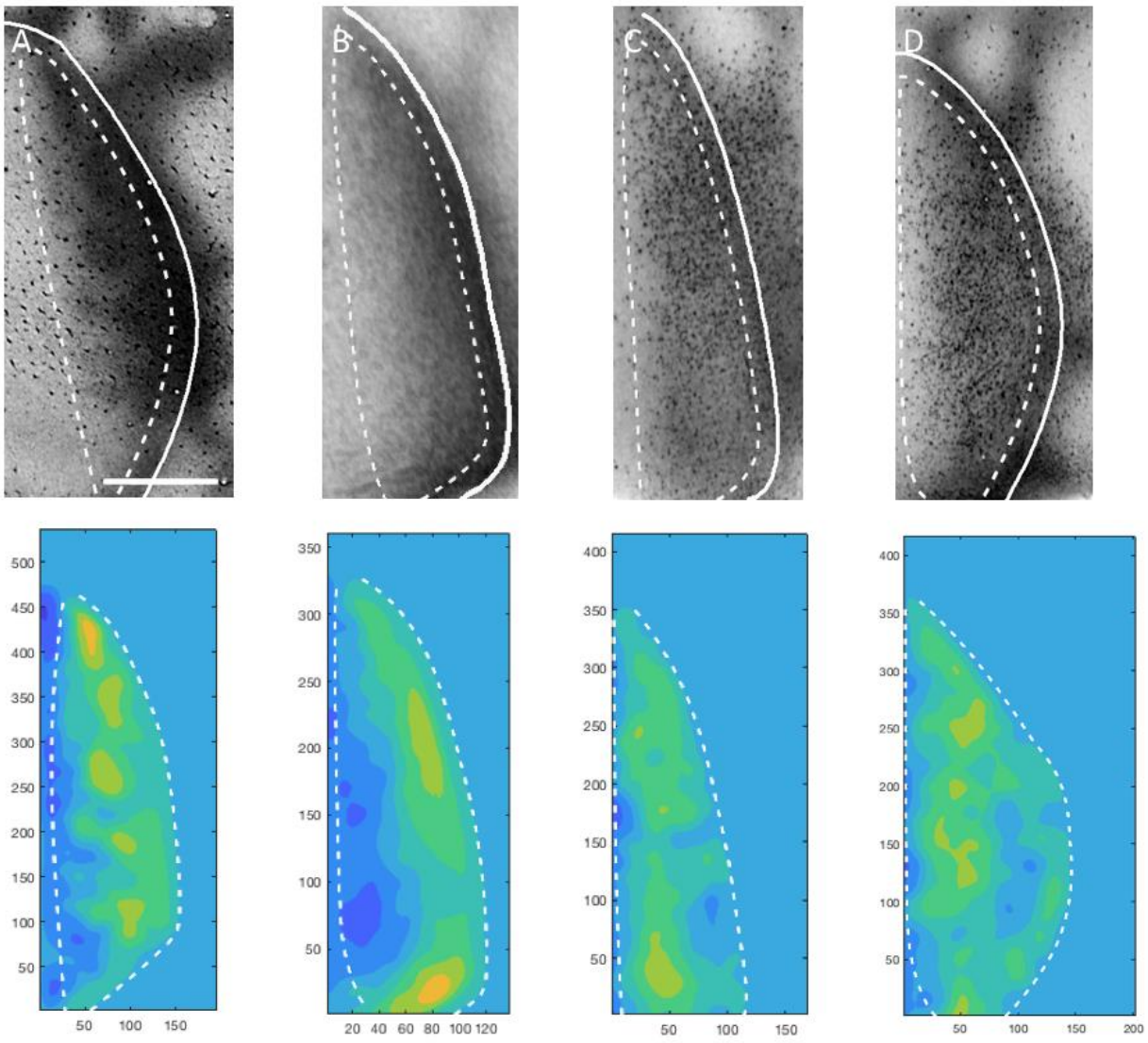
A
B
C
D
500
450
400
350
300
250
200
150
100
50
50 100 150
350
300
250
200
150
100
50
20 40 60 80 100 120
400
350
300
250
200
150
100
50
50 100 150
400
350
300
250
200
150
100
50
50 100 150 200

Figure 9: Additive and proportion methods for analyzing callosal labeling in Long Evans & albino rats

A. Adding the proportion of V1 occupied by HRP labeling at each of 10 density levels indicated by different colors reveals that albinos have very little labeling at the densest labeling levels, and that most of the area occupied in contour plots takes place for lower density labeled areas, indicative of more diffuse labeling with no patches ($p = 0.032$). **B.** Proportion of labeling occupied at each density level. Compared to Long Evans rats, albino rats have more diffuse labeling patterns that tend to be seen primarily at the lowest density levels. K-S test reveals that Long Evans rats are significantly different from the albino group ($p = 0.017$).

A

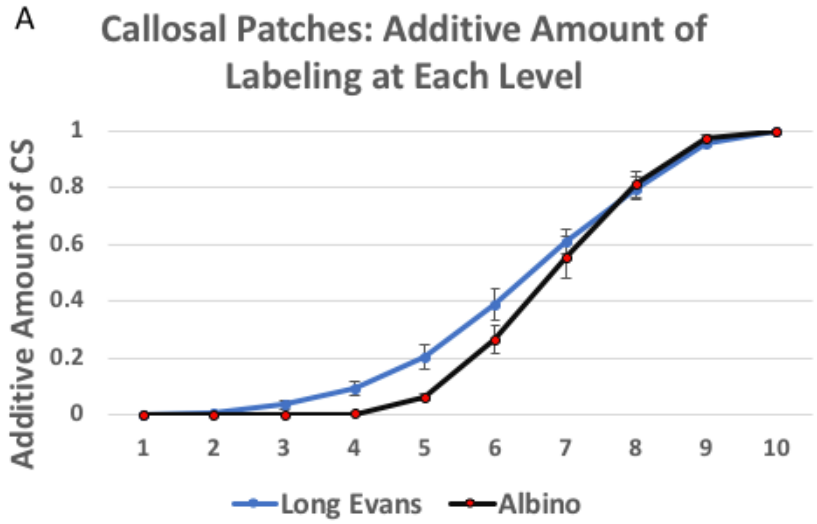
Callosal Patches: Additive Amount of Labeling at Each Level
Additive Amount of CS
1
0.8
0.6
0.4
0.2
0
1 2 3 4 5 6 7 8 9 10
Long Evans
Albino

B

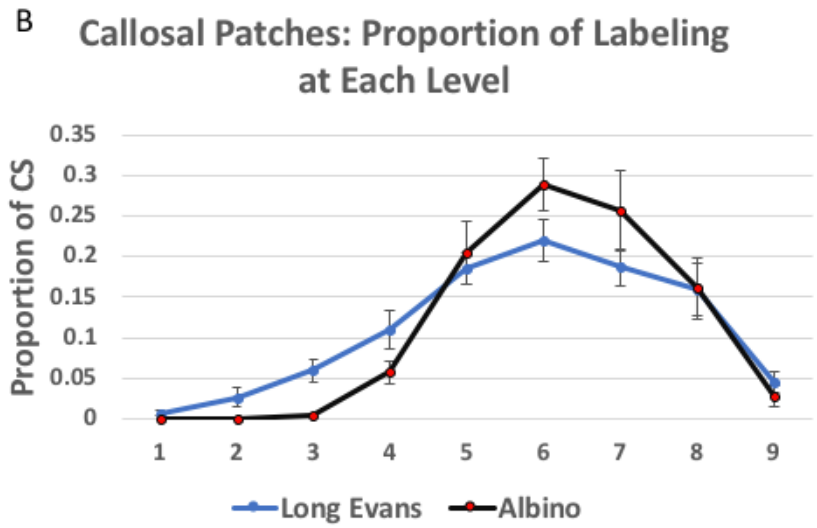
Callosal Patches: Proportion of Labeling at Each Level
Proportion of CS
0.35
0.3
0.25
0.2
0.15
0.1
0.05
0
1 2 3 4 5 6 7 8 9
Long Evans
Albino

Figure 10: Binocularity in the lateral segment is higher in albino than in Long Evans rats. **A, B.** Diagrams of the recordings sites in Long Evans (A) and albino (B) rats. Recording sites are color-coded (inset) to indicate ocular dominance according to the 1-7 scale of Hubel and Wiesel (1962). The CS is indicated by the red lines. **C.** Histogram of responses in the CS as a function of binocularity score for Long Evans (blue) and Albino (orange) rats. Note that ipsilateral dominance (scores 5 and 6) is observed in Long Evans, but not in albino rats, consistent with the existence of ODCs in Long Evans (Laing et al., 2015), but not in albino rats D. Histogram of responses in the LS as a function of binocularity score for Long Evans (blue) and Albino (orange) rats. Responses are almost exclusively dominated by the contralateral eye in Long Evans rats (score 1 and 2), while they are mostly binocular in albino rats (scores 3 and 4). Scale bar in B = 1.0 mm.

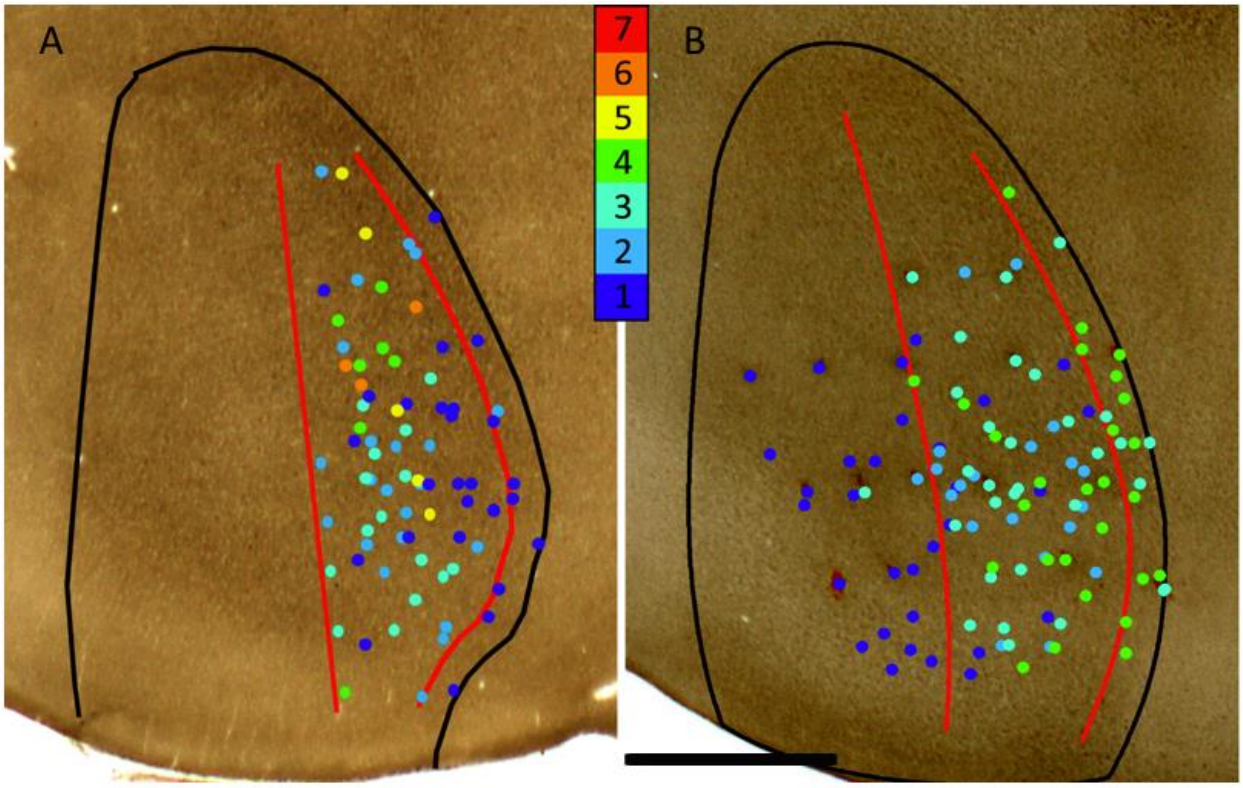
A
B
7
6
5
4
3
2
1

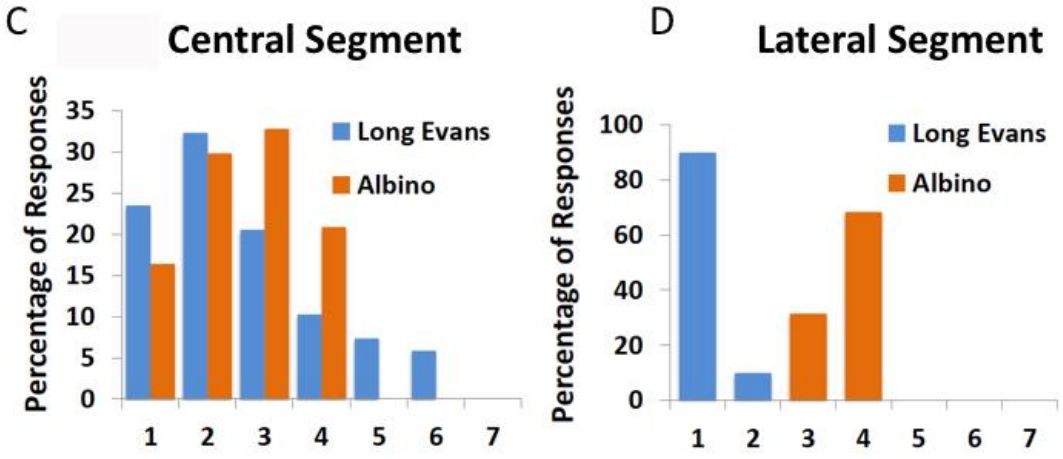
C
Central Segment
Percentage of Responses
35
30
25
20
15
10
5
0
1
2
3
4
5
6
7
Long Evans
Albino
D
Lateral Segment
Percentage of Responses
100
80
60
40
20
0
1
2
3
4
5
6
7
Long Evans
Albino

Figure 11: Recording sites in area V1 of albino rat. Callosotomy in albino rats.

A. Histological section from callosotomized albino showing myelin pattern for V1 (arrows indicate the border of V1). Electrode penetrations (black dots) can be seen across V1. **B.** Same section as in A showing border of V1 (black outline) and several electrode penetrations identified with numbers. The CS is outlined by white dashed line. M=MS, C=CS, L=LS. **C.** Coronal sections show transection of splenium of corpus callosum (arrows) in the top (anterior) two sections. The posterior section, at the level of the superior colliculus, demonstrates that the transection of splenium was complete. The left hemisphere was removed for tangential sectioning (a section is shown in A, B). Scale bars = 1.0 mm. SC = Superior Colliculus; LGN = Lateral Geniculate Nucleus.

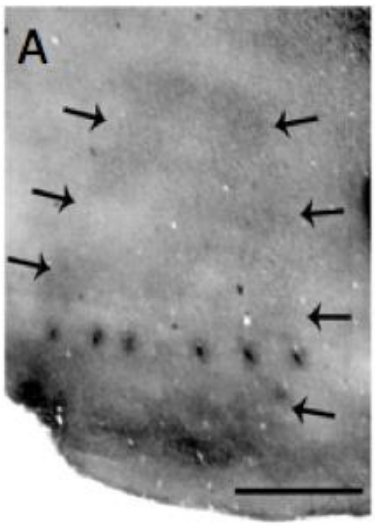
A

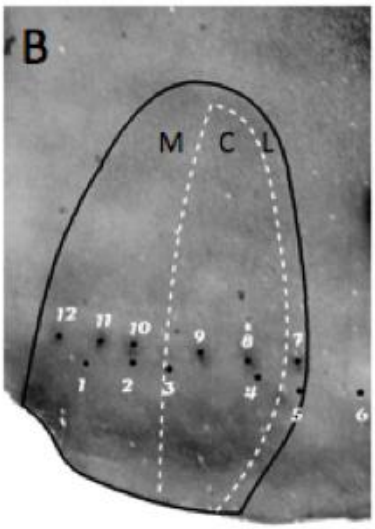
B
M
C
L
12
11
10
9
8
7
1
2
3
4
5
6

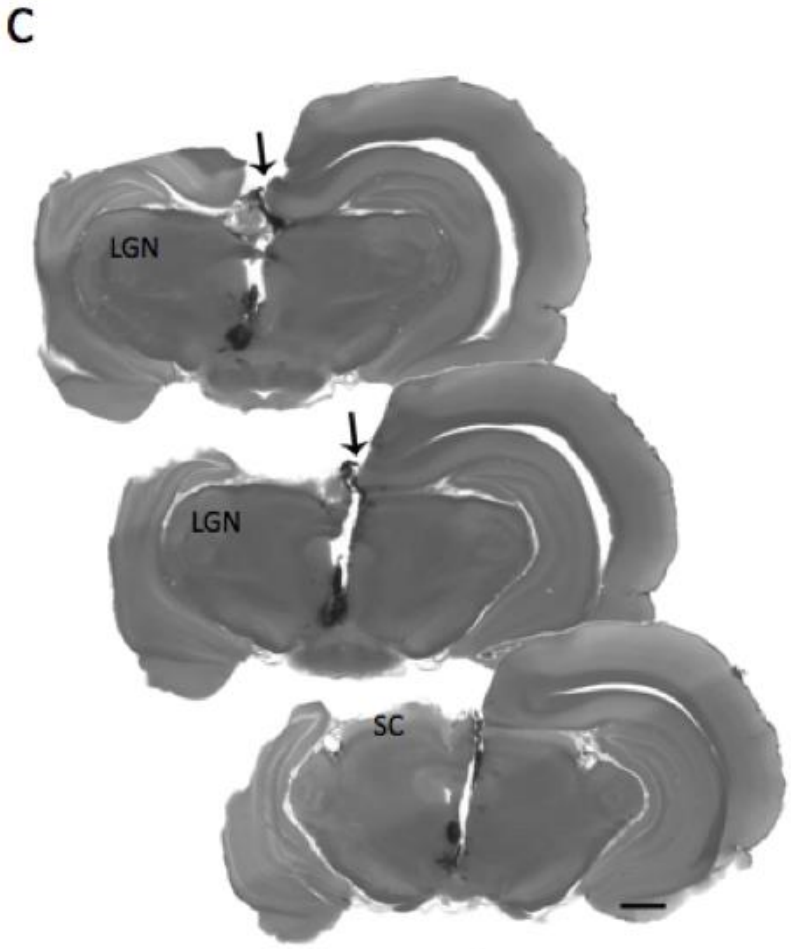
C
LGN
LGN
SC

Figure 12: Quantative analysis of binocularity in pigmented and albino rats: Electrophysiology Contralateral Bias Index (CBI) Scores.

A. Lateral Segment. Evoked responses were highly binocular in intact albino rats (CBI=0.16). After callosotomy, dominance by the contralateral eye increased significantly (CBI = 0.82), reaching a score similar to that of Long Evans rats in the LS (CBI= 0.74). N-sizes for recording sites: Albino: n = 10; Albino Callosotomy: n = 11; Long Evans: n = 5. **B.** Central Segment. In albino rats, callosotomy shifts the ocular dominance preference from highly binocular (CBI = 0.11) to dominated by the contralateral eye (CBI = 0.52). This shift is smaller than that observed in the LS region. In Long Evans rats, the contralateral eye exerts dominance (CBI = 0.33), but not as strongly as in the LS. N-sizes: Albino: n = 19; Albino Callotomy: n = 28; Long Evans: n = 33 **C.** Central Segment + Lateral Segment. In both Long Evans and callosotomized albino rats, there is a small increase in the dominance by the contralateral eye, while no significant change is observed in intact albino rats. N-sizes: Albino: n=30; Albino Callosotomy: n = 39; Long Evans: n = 27.

A

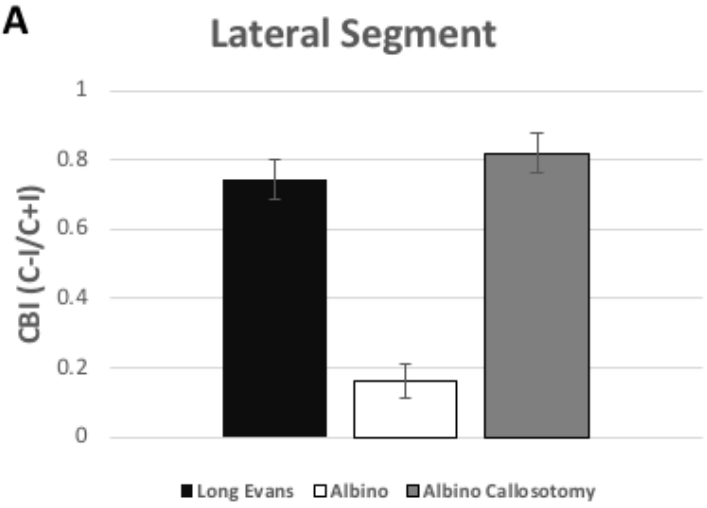
Lateral Segment
CBI (C-I/C+I)
1
0.8
0.6
0.4
0.2
0
Long Evans
Albino
Albino Callosotomy

B

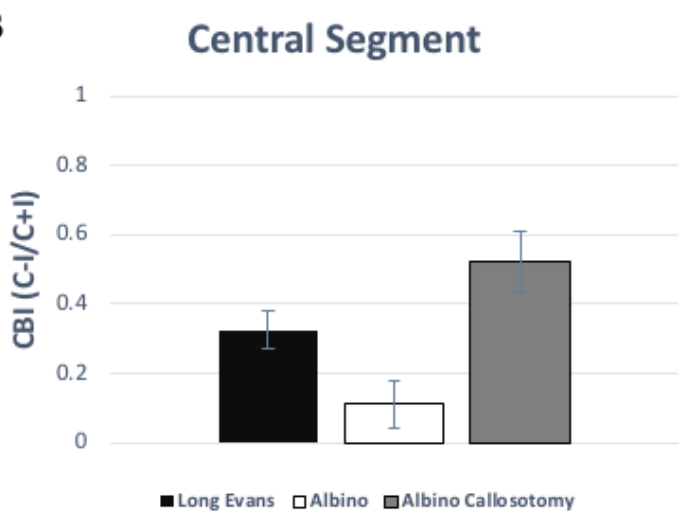
Central Segment
CBI (C-I/C+I)
1
0.8
0.6
0.4
0.2
0
Long Evans
Albino
Albino Callosotomy

C

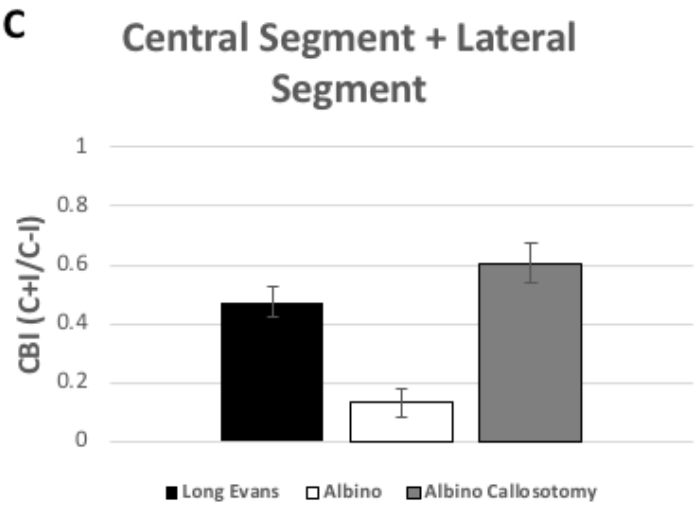
Central Segment + Lateral Segment
CBI (C+I/C-I)
1
0.8
0.6
0.4
0.2
0
Long Evans
Albino
Albino Callosotomy

Figure 13: ODCs and patchy callosal connections reduce binocularity in the lateral segment.

A. In Long Evans rats, the left lateral segment (blue) cannot receive transcallosal input from the ipsilateral eye (yellow) because the contralaterally dominated territories in the right central segment (yellow) are deprived of callosal connections (callosal patches correlate with ipsilateral ODC, colored blue). **B.** In contrast, in albino rats, thalamic inputs from right and left eyes are intermixed in the central segment (blue + yellow = green), allowing the callosal pathway to convey input from the ipsilateral eye to the lateral segment in the left hemisphere, thereby increasing binocularity in this segment (green). The same explanation applies to the right LS, not drawn for simplicity.

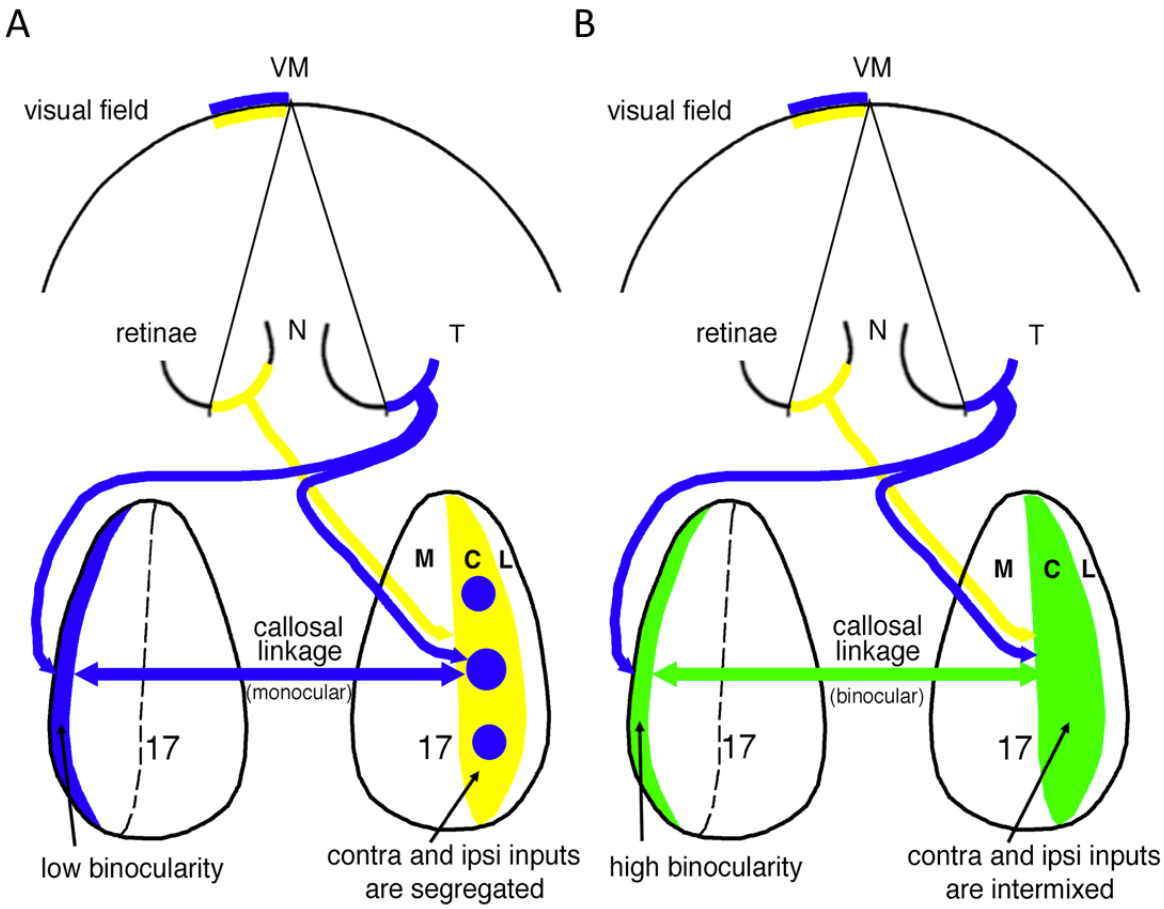
A
VM
visual field
retinae
N
T
M
C
L
callosal
linkage
(monocular)
17
17
low binocularity
contra and ipsi inputs
are segregated
B
VM
visual field
retinae
N
T
M
C
L
callosal
linkage
(binocular)
17
17
high binocularity
contra and ipsi inputs
are intermixed

CHAPTER 2: THE EFFECT OF ONSET AGE OF VISUAL DEPRIVATION ON VISUAL CORTEX SURFACE AREA ACROSS SPECIES

A well-established neuroanatomical consequence of early blindness is a reduction in the surface area of the primary visual cortex (V1) of affected individuals at adulthood. This has been reported in human studies (Park et al., 2009; Jiang et al., 2009), as well as several animal species, including rats (Sugita and Otani, 1984; Laing et al., 2012), mice (Massé et al., 2014), opossum (Karlen and Krubitzer, 2009), ferrets (Reillo et al., 2011; Bock et al., 2012; Olavarria et al., 2012), and rhesus macaques (Rakic, 1988; Dehay et al., 1991; Rakic et al., 1991; Dehay et al., 1996). The extent of the reductions in visual cortex surface area varies with the timing of blindness onset (Rakic, 1988; Rakic et al., 1991; Dehay et al., 1989; Dehay et al., 1996; Karlen and Krubitzer, 2009; Bock et al., 2012; Laing et al., 2012). For example, in rhesus macaques, Rakic et al, 1991, and Dehay et al., 1996 established that enucleation occurring earlier in gestation produced more substantial reductions in striate cortex than when enucleation occurred at ages closer to full gestation. However, the period during which normal development of primary visual cortical surface area requires ocular input is not known.

The typical developmental trajectory of the surface area of V1 involves an initial expansion in surface area (Raznahan et al., 2011; Knutsen et al., 2013), followed by a reduction, or pruning phase (Huttenlocher, 2002; Missler et al., 1993). Building on the radial unit model (Rakic, 1988), the effect of enucleation on the expansion of striate cortex has been linked to modulatory influences that thalamic afferents, by means of diffusible factors, exert over early stages of corticogenesis at the level of the ventricular zone (Dehay et al., 2001), and to interference with the tangential migration of neurons (Reillo et al., 2011). Blindness also results in increased V1 cortical thickness, which has been interpreted as resulting from reduced synaptic

pruning later in development (Anurova et al., 2015; Jiang et al., 2009). Our goal was to identify the critical period for the effect of blindness on cortical surface area across rats, ferrets and humans with respect to this developmental timeline, and to investigate whether early enucleation reduces cortical size by interfering primarily with cortical expansion or with synaptic pruning.

Human studies of blindness have relied on anatomical MRI to measure alterations in visual cortex as a consequence of blindness (Bridge et al., 2009; Ptito et al., 2007; Park et al., 2009; Jiang et al., 2009; Leporé et al., 2010; Anurova et a., 2013). In humans, age of onset of blindness can usually only be estimated from the etiology of blindness (e.g., anophthalmia, retinopathy of prematurity, injury to the eyes, etc.). Furthermore, human studies are almost uniquely conducted at adulthood, and consequently, the reduction in surface cortical area may reflect the effects of blindness on the expansion in surface area that occurs early in development, or to an increase in synaptic pruning, which occurs later in development (Huttenlocher, 1990; Missler et al., 1993). Knowing when the effect of blindness no longer influences the surface area of visual cortex would be useful to further our understanding of the mechanisms controlling cortical growth, and to guide the interpretation of the effects of blindness onset on human cortical surface area development.

To bridge the findings from previous animal studies with the human studies, here we examine how the age of blindness onset affects surface area of V1 at adulthood in rats, ferrets, and humans. To facilitate interspecies comparisons, blindness onset was expressed in terms of a species-independent timeline of neurodevelopmental event times (ET) (Finlay and Darlington, 1995; Darlington et al., 1999; Clancy et al., 2007; Workman et al., 2013). Animal models consisted of rats and ferrets bilaterally enucleated at defined postnatal ages, and sighted control (SC) animals. Human subjects included anophthalmic (in which both eyes fail to develop),

congenitally-blind (in which pattern vision never develops), late-onset blind (following development of relatively normal pattern perception), and normally-sighted controls. We used histological methods in rats and ferrets, a longitudinal structural MRI study in ferrets, and structural MRI data from humans to identify a common developmental endpoint for the effect of blindness on primary visual cortex surface area. We find that the critical period for enucleation ends prior to the completion of cortical expansion, and well before synaptic pruning occurs. Additionally, longitudinal analysis comparing the size of V1 at different postnatal ages in ferrets blinded at post-natal day 7 and their sighted controls, confirmed that enucleation disrupts cortical expansion. Finally, we show that the critical period for the effect of blindness on the surface area of V1 ends before V1 reaches its normal adult size, suggesting that visual cortex expansion remains susceptible to visual deprivation through the perinatal period, followed by a later stage during which expansion is largely independent of ongoing visual input.

MATERIALS AND METHODS

Animal Care

All procedures were approved by the relevant Institutional Animal Care and Use Committee, and were carried out in accordance with the NIH Guide for the Care and Use of Laboratory Animals.

Rats

Animal numbers. A total of 56 rats were included in these experiments. A set of 40 were bilaterally enucleated (BE) at 8 postnatal ages (we denote all ages in post-conception time (PC) to be consistent with translation to event time (ET)). The day of bilateral enucleation (BEP) is indicated with the postnatal day in which enucleation was performed: within 24 hours of birth (BEP0; n=6), BEP10 (n=4), BEP12 (n=5), BEP14 (n=6), BEP16 (n=5), BEP25 (n=5), BEP30 (n=5), BEP45 (n=4). Six sighted rats served as controls (SC). All measurements were made at

maturity (>P60). The additional 10 rats were used to study the development of the surface area of V1 in normally sighted animals, sacrificed at P30
(n=5) and P35 (n=5) (Table 1).

Experimental procedures. Pregnant animals were monitored several times daily and the births of the litters were determined to within 12 hours (the first 24 hours correspond to P0). Rats were injected with ketofen (0.05mg/kg, i.p.) and anesthetized with isofluorane (2-4% in air). After full recovery from surgery, rat pups were either returned to their dams, or to their home cage if the enucleation took place after weaning. Enucleated rats received daily i.p. injections of ketofen for 3 additional days. Upon reaching maturity, experimental as well as control rats were deeply anesthetized with pentobarbital sodium (100mg/kg i.p.) and perfused transcardially with 0.9% saline followed by 4% paraformaldehyde (PFA) in 0.1M phosphate buffer (PB, pH 7.4). A similar procedure was used to anesthetize and perfuse the animals used to study the development of the area size of V1.

A histological approach was used to measure visual cortex surface area. The surface areas of primary visual cortex and remaining isocortex were measured using tangential sections from physically flattened cortical mantles. Brains were removed from the skull and the entire cortical mantle was separated from the brain stem, flattened between glass slides and left in 0.1M PB for 24 hours. The tissue was then transferred to a 4% PFA in 0.1 M PB, 20% sucrose solution for an additional hour and cut tangentially to the cortical surface (60 um sections collected in 0.1 M PB). Unstained tangential sections were scanned (Epson 4990) to identify the border of V1 based on the myelin pattern (Figure 14A, B) (Richter and Warner, 1974; Laing et al., 2015). The myelin pattern was optimally displayed in tangential sections passing through Layer 4 (500–650 µm deep), and the sharp transition from dense to reduced myelination at the border of V1 was

delineated in 2 or more sections from the same animal with the aid of the filter "trace contour" in Adobe Photoshop CS5 (Adobe Systems, CA) (Figure 14A, B). The borders of the cortical mantle and V1 were reconstructed by carefully aligning sections using the edges of the sections, sulci, blood vessels, and other fiducial marks. Data from animals bilaterally enucleated at P0 through P45 were compared to corresponding data from 60-day-old sighted control animals.

Ferrets

Animal numbers. A total of 25 ferrets were examined using live and post mortem MRI. Ferret litters were purchased from Marshall Bioresources (North Rose, NY) and delivered to Oregon Health & Science University (N=23 animals) or Washington University (N=2 animals) on postnatal day five (gestation in ferrets = 41 days), where subsequent procedures were carried out. Thirteen ferrets were included in the comparison of the effect of enucleation at different ages on V1 surface area (Table 2). Of these, nine [BEP7 (n=3), BEP20 (n = 3), SC (n=3)] were part of a previous study (Bock et al., 2012), and an additional four ferrets [BEP7 (n=1), BEP31 (n=2), SC (n=1)] were also included. All were euthanized at adulthood (P120 or older), and their brains were perfused with 4% PFA. Two additional groups of ferrets, BEP7 (n = 3) and SC (n = 3), underwent longitudinal MRI experiments. They were then perfused on day P73 with 4% PFA following previously described procedures (Bock et al., 2012).

Experimental procedures. Ferrets examined by post mortem MRI were euthanized and perfused with 4% PFA. The extracted brains were imaged following previously described procedures for brains analyzed at adulthood (Bock et al., 2012) or at P31 (Bock et al., 2010). In a follow-up longitudinal experiment, BEP7 and SC ferrets were examined using in vivo MRI over the postnatal period from P12 to P29. For both the BEP7 and SC groups, two animals were scanned at P15, P22, and P29, while the third ferret was scanned at P12, P19, and P25, using

experimental procedures (and data from 2 SC animals) described previously (Knutsen et al., 2013). The brains were scanned using an 11.7 T static magnetic field strength magnet interfaced with a small animal imaging gradient system capable of producing highly similar maximum gradient strengths (of 70 G/cm), as well as an identical volume coil transmit/surface coil receive radiofrequency coil configuration.

Following image acquisition and cerebral cortex reconstruction (Bock et al., 2010; Knutsen et al., 2013), gyral/sulcal landmark-based conventions reported previously (see Bock et al., 2012) were used to define boundaries of the isocortex, V1, and extrastriate visual cortex. Briefly, on the ventral lateral surface of the brain, the border of the isocortex corresponds to the fundus of the rhinal fissure, and to the dorsal edge of the corpus callosum on the medial surface of the brain. V1 was defined as the area extending from the fundus of the medial splenial sulcus to the occipital crest (outlined in red in Figures 15, 18). The extrastriate cortical region was defined as the lateral cortical surface extending from the occipital crest to the suprasylvian sulcus ventrally, and a line connecting the dorsal-most point of the suprasylvian sulcus to the midline crest dorsally (outlined in blue in Figure 18).

Humans

Subjects. Data from 51 human subjects were included in the study. The data included 5 participants with anophthalmia (AN), 14 with early-onset blindness (EB, prior to birth), 9 with late-onset blindness (LB, occurring at age 7 or later) and 23 sighted control (SC), collected at three laboratories (Supplementary Table 1). Acquisition procedures were described previously (Bridge et al., 2009; Bock et al., 2015; Jiang et al., 2016; Stevens et al., 2007). Six AN and 9 SC participants were scanned on a 7T Siemens/Magnex system at Oxford University (Bridge et al., 2009). Eleven EB, 5 LB, and 10 SC subjects were scanned in a Siemens 3T Trio with a 12

channel head coil, at Oregon Health & Science University (Stevens et al., 2007). Five EB participants and 4 SC participants were scanned in a Siemens 3T Trio with a 12-channel head coil, at Oxford University (Bridge et al., 2009). A group of 4 LB participants were scanned in a Philips Achieva 3T with a 32 channel head coil. The severe atrophy of optic nerves in these AN individuals was previously confirmed with T1-weighted MR scans (Bridge et al., 2009). (Descriptions of individuals in the AN, EB, and LB are provided in Supplementary Table 1). All participants provided written informed consent in accordance with the Institutional Review Board of each respective site.

***Experimental procedures*.** In humans, consistently detecting the stria of Gennari with MRI is challenging, and its presence is debated in Anopthalamic individuals (Trampel et al., 2011). However, retinotopic mapping of visual cortex with fMRI has demonstrated that cortical topology in and around the calcarine sulcus is closely coupled to the orientation and extent of visual fields (Hinds et al., 2008; Benson et al., 2012), and striate cortex can be estimated with high precision from the cortical folding patterns along the calcarine sulcus in blind individuals (Park et al., 2009; Jiang et al., 2009). All MRI 3D datasets were processed for landmark-based segmentation and surface reconstruction using the Freesurfer software toolkit (http://freesurfer.net/) using the "recon-all" function with default settings. A full description of the processing steps is provided online (https://surfer.nmr.mgh.harvard.edu/fswiki). Briefly, each brain dataset is intensity normalized, skull-stripped, and undergoes a nonlinear transform to align it within Freesurfer's Gaussian Classifier Atlas (GCA). The boundary between white matter and gray matter is determined throughout the brain using intensity, neighborhood and smoothness constraints. The space between the pial surface and white matter boundary is then tesselated, and smoothed to create a cortical ribbon. The cortical ribbon is then parcellated and neuroanatomical

labels of brain areas assigned to each voxel based on probabilistic anatomic information and gyral and sulcal landmarks (Dale et al., 1999; Fischl et al., 2002; Fischl et al., 2004). The reconstructed cerebral cortex surface and boundaries for primary visual cortex for each subject were reviewed by three study staff, blind to the group assignment of the brain. The brain of one congenitally blind (CB) subject was removed due to artifacts resulting from movement during scanning.

Calculation of primary Visual to non-visual Surface Area Ratio (VSAR)

To control for interindividual variability within species in the size of brain structures, we calculated the ratio between the surface area size of V1 and the surface size of another brain structure thought to be unaffected by early blindness. For rats, this surface area ratio (VSAR) was calculated by dividing the area size of V1 by the surface area of the remaining isocortex, including extrastriate visual cortex, because previous studies have shown that the surface area of rat extrastriate cortex is not significantly affected by early enucleation (Laing et al., 2012). In ferrets, early enucleation reduces the area size of both striate and extrastriate cortex (Bock et al., 2012), and therefore, VSAR was defined as the surface area of V1 divided by the surface area of all non-visual isocortex (i.e., excluding both V1 and extrastriate visual cortex). For humans, VSAR was defined as the surface area of V1 divided by the surface area of the primary motor cortex, identified relative to gyral and sulcal landmarks in FreeSurfer (Dale et al., 1999). This normalization procedure not only provides an internal scaling factor for each subject, but also reduces potential biases introduced by differences in the scanners and scan parameters used to acquire the data from human subjects.

Across-species comparison

The VSAR measure from each experimental group can also be compared to the VSAR of sighted adults of the same species, to provide an unbiased measure of the percentage of reduction in surface area as a consequence of age at blindness onset. Specifically, to directly compare the effect of age at blindness onset on surface area reduction of V1 across species, the VSAR of each experimental group was expressed as the percentage of the corresponding SC group (% VSAR = $100*VSAR_{blind}/VSAR_{SC}$).

All data are expressed in a common developmental timeframe, using the "translating time" regression model developed by Finlay and colleagues (Workman et al., 2013; see also, http://www.translatingtime.org). This model provides a regression equation that translates early neurodevelopmental events into species-independent event time (ET) that spans early brain development, allowing for the prediction of 271 developmental events across 18 mammalian species. The parameters of ET and post-conception (PC) age (in days) are related through the expression

$$ET = (\ln(PC)\text{-}Constant)/Slope$$

Species-specific *Constant* and *Slope* parameters are given in Table 2 of Workman et al. (Workman et al., 2013). PC at birth for rats = 21 days, ferrets = 41 days, and humans = 270 days.

Statistical analyses

The effects of visual deprivation on V1 surface area measured at adulthood can be characterized by a linear function, reflecting the relationship between age at blindness onset and the resulting reduction of V1 surface area. The linear model provides an estimate of the time (ET_C) at which visual deprivation no longer affects V1 surface area expansion. Subsequent to this event time, V1 surface area should remain at asymptote, at a value equal to the V1 surface

area of sighted control conspecifics. We estimated the ET at which binocular enucleation no longer reduced the visual surface area relative to adult SC animals of the same species, using a non-linear piecewise regression model. The model uses a two-segment fitting algorithm: a linear estimate of the best fitting line to the data with values less than 100% of adult VSAR and a flat line reflecting the values that do not differ from the mean of the adult VSAR value. (i.e., the ET at which VSAR reaches asymptote relative to 100% of adult VSAR. The piecewise model has four variables:

$$\textit{Percent of Adult VSAR } (y) = [(m*x + b \mid x<ET_c),\ (m*t.x + b \mid x> ET_c)\ ]$$

Where (b) is the y-intercept, (m) is the linear regression slope, (x) is age of blindness onset (expressed in ET), and (ET_c) is the ET at which percent of adult VSAR reaches asymptote. ET_c denotes the event time at which blindness onset no longer reduces V1 surface area (i.e., the measurement of VSAR is 100% of the adult control VSAR). All analyses were carried out with R (*https://www.r-project.org/*) using the *nls* function, and an iterative minimization of least squares approach to find the value of ET_c.

RESULTS

The effect of age of visual deprivation onset on adult primary visual cortex surface area

Rats. Figure 14 shows the flattened primary visual cortex of a SC rat at P60 (Figure 14A), and of a BEP12 rat (Figure 14B), also sacrificed at P60, illustrating the reduction in surface area as a consequence of enucleation. Figure 14C shows VSAR as a function of the event time at which enucleation was performed. The area size of V1 in rats bilaterally enucleated on P0 (BEP0, ET = 0.43) through P45 (BEP45, ET>1) are plotted as a percent of the area size of V1

in adult SC rats (all animals were sacrificed at P60). In adult SC animals, approximately 8% of cortical surface areas is occupied by V1. In contrast, in animals enucleated at P0, the surface area of V1 measured at maturity is reduced to roughly 6% of the cortical surface area, in agreement with previous studies (Laing et al., 2012).

Early enucleation (e.g., BEP0, ET = 0.43) produced much larger reductions in VSAR than later enucleations, with a strong linear relationship between age of enucleation and percent adult VSAR, over the measured age range (Figure 14C). The asymptote for the effect of enucleation on VSAR occurred at $ET_c = 0.82$. The regression model produced a strong fit to the data (adjusted $R^2 = 0.73$). Asymptote occurred at 97% of the adult SC surface area (Fig 14C); the estimated ET at 100% based on the slope of the linear regression line was ET = 0.86, corresponding to postnatal age = 22.6 days. This analysis indicates that enucleation at this age or later no longer affects the surface area expansion V1 in the rat.

Ferrets. In this species, most of primary visual cortex resides on the caudal and medial part of the brain, and its borders can be readily identified by sulcal landmarks (Figure 15A). Fig. 15B shows insets of V1 in five animals enucleated at BEP7 and in 5 SC animals. Figure 15B also illustrates that early enucleation reduces cortical folding within primary visual cortex: the posterior sulcus observed in adult control animals (yellow arrows in Figure 15B) is not observed in adult ferrets enucleated at P7 (PC = 48, ET = 0.54). The effect of enucleation on the area size of V1 was analyzed at adulthood in ferrets enucleated at P7 (ET=0.54), P20 (ET=0.65), and P31 (ET=0.72) (Table 2). Relative to the size of area V1 in sighted controls, we observed that the surface area of V1 is reduced in enucleated ferrets, with a graded effect of age of deprivation similar to that observed in rats (Figure 15C). The regression model used suggests that enucleation ceases to affect the surface area of V1 at $ET_c = 0.77$, corresponding to postnatal age

= 39 days, about a week after eye opening (P31, ET = 0.72). Table 3 lists the regression model parameters and significance of the piecewise regression models for enucleated and sighted controls rats and ferrets.

Humans. Human data came from of 3 groups of subjects blinded at different ages. In one group, blindness was due to anophthalmia (AN), in which the midbrain, diencephalon and cortex never receive retinal input because retinal projections fail to develop. We confirmed the severe atrophy of optic nerves in these AN individuals with T1-weighted MR scans (Bridge et al., 2009). The early blind group (EB) consisted primarily of individuals with retinopathy of prematurity (ROP). Unlike AN subjects, the midbrain, diencephalon and cortex of EB subjects receive retinal input before the onset of blindness, which occurs neonatally. The late blind (LB) group consisted of individuals who, after relatively normal visual development, lost their vision due to disease or accidents affecting the eyes at 7 years of age or later (Table 4).

Primary visual and primary motor cortex for a representative SC are shown in Figure 16A. As in rats and ferrets, the reduction of the VSAR in humans depends on the age of blindness onset (Figure 16B). To characterize the differences between the groups of blind individuals we used a non-parametric test to determine if the rank of age of blindness onset produced a monotonic increase in VSAR. Based on our rat and ferret data, we predicted that both AN and EB groups would have smaller VSAR than LB and SC groups, which would have similar VSAR values. This was born out by a non-parametric estimates of group differences with conditional Wilcoxon-Mann-Whitney tests (Munzel and Hothorn, 2001). Significance level was maintained at $P < 0.05$ across group comparisons. In both AN and EB groups, the VSAR was significantly smaller than in the SC group, but the LB group did not differ significantly from the SC group (Figure 16B).

A subset of EB participants had some residual light sensitivity or had a history of minimal light perception prior to onset of complete blindness. To determine if minimal diffuse

light sensitivity influenced surface area, we compared VSAR measurements between EB individuals with residual light perception (n = 5, mean = 1.92±0.18), to those without residual light perception (n = 9, mean = 1.98±0.15). For both subgroups of EB subjects, the VSAR is approximately equal to the mean VSAR for EB subjects overall (Table 4). We found no evidence for differences between those EB with light perception and those without light perception (Wilcoxon rank sum test: $Z = 0.38$, $p = 0.72$). In fact, it is worth noting that subjects in the EB group with light perception had a smaller mean VSAR than subjects without light perception, the opposite of what would be expected if light exposure alone was adequate to sustain surface area expansion.

Rat-ferret-human comparisons

To investigate the developmental correspondence of the effects of blindness onset on the area size of V1 across rats, ferrets and humans, we plotted the data from these species on a common timeline of neurodevelopmental event times. Figure 17 combines our data on the effects of age of blindness onset on the area size of V1 from rats (circles), ferrets (diamonds) and humans (inverted triangles) using a weighted regression taking into account the number of cases for each data group. For each species, VSAR is expressed as a percentage of the mean of their respective SC group's VSAR. The age of blindness onset is converted to the developmental event time scale defined by Workman et al. (Workman et al., 2013).

Unlike the experimental animal data, in which the age at enucleation is known precisely, blindness onset is rarely known precisely for AN and EB individuals (Verma & Fitzpatrick, 2007). For AN humans, we used PC78 (ET = 0.32) as the approximate time of blindness onset, which corresponds to the event time in which optic axons reach the dorsal lateral geniculate nucleus in normal visual development. Severe ROP, as was the case in our EB subject group, is

detectable four weeks prior to the normal 40 week (PC = 270 days) gestation period for humans, corresponding to a blindness onset age of PC242 (ET = 0.62). In the LB group blindness occurred over a broad age range well above the range of the ET scale; therefore, these data were excluded from the graph. (All but 2 LB subjects were post-adolescent. In the remaining 2 subjects, blindness occurred at ages 7 and 12, so it can be presumed that cortical expansion was virtually complete). As shown in Figure 17, the model fit was very good (adjusted $R^2 = 0.74$), and the cross-species ETc = 0.87, in good agreement with the ETc estimated for rats and ferrets separately.

Early blindness attenuates visual cortex expansion

The finding that the critical period for the effect of blindness ends relatively early in the developmental timeline suggests that the effect of visual deprivation on surface area might result from attenuated expansion of visual cortex, rather than by increasing the synaptic pruning that typically occurs at later stages of development (Anurova et al., 2015). However, as the effect of delayed blindness onset was assessed at adulthood, after both expansion and pruning have taken place, it remains possible that both processes are compromised by visual deprivation. To more directly examine whether early enucleation reduces cortical expansion, we carried out longitudinal MRI measurements of VSAR during the expansion phase of cortical maturation, from P11 (ET = 0.57) through P28 (ET = 0.70), in three ferrets enucleated at P7 (ET=0.54) and three SC ferrets.

Figure 18A illustrates that by age P11, gyral and sulcal folds, although rudimentary, provide sufficient information to delineate striate (red borders), extrastriate (blue borders), and isocortical (yellow borders) boundaries. By P25, these landmarks are highly similar to the pattern observed in adult brains. Figure 18C shows that, over the period from P11 through P28 (ET 0.57

to 0.70), striate cortex in the control animals (open symbols) expands linearly at a rate of 2.5 mm^2/day. Differences between BEP7 (closed symbols) and SC animals are apparent by P14 (ET=0.6), one week following enucleation. VSAR of the immature cortex is significantly reduced in BEP7 animals compared to controls ($Z(4)= 1.964$, $p=0.05$) (Fig. 18B). These findings were replicated in a cross-sectional analysis performed on post mortem tissue for separate groups of 3 BEP7 and 3 SC ferrets at P31 (ET = 0.72) (data not shown). Notably, VSAR in the BEP7 animals measured prior to P31 was 77% of the SC animals in the longitudinal measurements, and 85% for animals assessed at P31 in the post mortem analysis, which corresponds well with the 75% of SC VSAR observed in mature ferrets enucleated at P7 (Figure 15). Thus, the effects of early enucleation are similar in magnitude regardless of whether measurements are made at P14 (ET=0.6), well before pruning begins, or in the adult animal. This strongly suggests that perturbed cortical expansion, rather than enhanced pruning, is the primary mechanism underlying reduced V1 surface area in visually deprived animals.

Blindness ceases to affect the surface area of area V1 well before expansion of V1 is complete

Is expansion of visual cortex susceptible to the effects of blindness until V1 reaches its normal adult size? Answering this question is important for understanding the role of visual input in the maturation of visual cortex. In the rat, Duffy et al. (1989) reported that V1 surface area expansion continues beyond P27, past the age at which our data indicate that enucleation no longer affects the size of area V1 (P22.6, ET = 0.86) (Figure 14C). To determine the end of the growth period, we measured the size of V1 at P30 (n=5), P35 (n=5), and P60 (n= 6) in control rats and plotted these data, and that from Duffy et al., (1989), in Figure 19 (blue symbols). We applied the piecewise regression model to these developmental rat data, and estimated that VSAR asymptotes at $ET_{dev} = 1.06$. This result, together with our data from the BE rats, indicates

that blindness starting by ET = 0.86 no longer has a significant effect on the expansion of V1 even though V1 is still significantly smaller (by about 25%) than its adult size. Table 3 lists the regression model parameters and significance of the piecewise regression models used for the rat developmental data.

Meta-analysis of extant data: generalization to other species

We extended our analysis to data from other investigations on the effect of visual deprivation on the size of V1 including histological studies in rhesus macaques (Rakic et al., 1991; Dehay et al., 1996), rats (Sugita and Otani, 1984; Laing et al., 2012), ferrets (Reillo et al., 2011), short -tailed opossum (Karlen and Krubitzer, 2009), cat (Olavarria and Van Sluyters, 1995), as well as MRI-based studies of blind human subjects (Park et al., 2009; Jiang et al., 2009). In agreement with our present results, this meta-analysis suggests the existence of a graded dependence of the area size of V1 on the age of blindness onset that is consistent across species, yielding an $ET_c = 0.81$ (Figure 20, black symbols).

In a similar manner, extant data on the development of the area size of V1 in sighted individuals can also be directly compared to the present findings. Such data include studies in rats (Duffy et al., 1998), cats (Duffy et al., 1998; Rathjen et al., 2003), macaques (Rakic et al., 1991; Dehay et al., 1991; Purves and LaMantia, 1993; Dehay et al., 1996; Horton and Hocking, 1996), and human (Lyall et al., 2015). This yields an estimated value of $ET_{dev} = 0.93$ (Figure 20 blue symbols). Comparison of this value with the estimated value of $ET_c = 0.81$ obtained for the meta-analysis of the effect of enucleation on the area size of V1 confirms our observation that the effect of visual deprivation ceases its effect on V1 surface area expansion prior to the normal completion of V1 surface area expansion, and extends it to many other mammalian species.

DISCUSSION

A wide variety of studies in both animals and humans have reported that early blindness results in reduced V1 surface area. However, the critical period for this effect, and its relationship to cortical expansion, is not yet understood. Here we show that the period of susceptibility to blindness as a function of age of deprivation is remarkably consistent across species once data have been represented in a common developmental event-time framework (Workman et al., 2013). This critical period spans early to mid-cortical expansion, and ends before cortical expansion is complete, and well before cortical pruning begins. The effects of the enucleations have been linked to disruption of normal, prenatal thalamic influences on cortex development (Rakic, 1972; 1988; Reillo et al., 2011l; Moreno-Juan et al., 2017).

Analysis of the results presented here indicate that enucleations performed at or after postnatal day P22 (ET = 0.86) in the rat and P39 (ET=0.77) in the ferret cease to affect the surface area expansion of V1. In humans, reductions in surface area were observed for both AN (ET = 0.32) and EB (ET = 0.62) groups as compared to SC, and these reductions were similar in magnitude to those found in animal models. However, the VSAR in the LB group did not differ significantly from SC group. Since blindness in the LB group occurred at ages corresponding to ET >1, we could not determine with accuracy the end of the critical period for V1 surface area reductions in humans. A meta-analysis in which we combined our data from rats, ferrets and humans with animal and human data from previous studies, indicates that the end of the critical period for the effect of blindness on the area size of V1 is reached at $ET_C = 0.81$. In humans, this suggests that blindness would be expected to influence the surface area of V1 only if the onset occurs before post conception day 483 (postnatal day 213). Given that, in visually normal individuals visual acuity is correlated with cortical surface area (Duncan and Boynton, 2003),

this result has interesting translational implications in cases of sight recovery. For example, a study examining individuals who suffered from congenital cataracts until the ages of 8-17 years of age found severe acuity losses, even many months after surgery (Kalia et al., 2014). It is possible that losses in V1 surface area are related to these impairments in pattern vision.

The effect of blindness on surface area ends before cortical expansion is complete

The period during which the surface area of V1 is susceptible to blindness is relatively protracted compared to other critical periods in cortical development. For example, the critical period for the effect of visual input on corticocortical connection patterns in rats is confined to an approximately 2-day time interval from P4 to P6 (ET = 0.53-0.58) (Olavarria et al., 1987; Olavarria and Hiroi, 2003; Laing et al., 2012). Similarly, in ferrets, the period in which the pattern of visual callosal connections is susceptible to enucleation ends during the third postnatal week (ET= 0.65) (Bock et al., 2012). In contrast, our estimate of the end of the critical period for surface area is ETc = 0.77, suggesting that visual input continues to regulate the size of visual cortex well after the corticocortical connections of visual cortex have been specified. Cortical expansion occurs relatively late in the neurodevelopmental timeline compared to the establishment of corticocortical connections. For example, while corticocortical connections in rats appear mature by P12 (ET = 0.69) (Olavarria and Van Sluyters, 1985), the area of V1 reaches its adult size more than two weeks later. In rats, we found that V1 reaches its adult size by P40 (ET= 1.06). This result is in good agreement with data for the growth of V1 in the cat (Duffy et al., 1998) showing that by 12 weeks of age (ET = 0.97) the areal extent of V1 is adult-like. Thus, visual input regulates multiple aspects of cortical development through mechanisms that operate during different time windows.

One potential consequence of cortical expansion occurring relatively late in the developmental timeline is that it may allow the specification of V1 intra-cortical connections to match the statistics of visual input. Some aspects of visual development are surprisingly slow to reach a mature state. For example, human foveal development, reflected by cone packing density and foveal diameter does not reach adult measures until some time after 45 months postnatal (Yuodellis and Hendricson, 1986). In visually normal individuals there is a two- to three-fold variation in the size of the optic tract, the volumes of the magnocellular and parvocellular layers of the LGN, and the surface area and volume of V1. Importantly, this variation is coordinated within the visual system of any one individual. That is, a relatively large V1 is associated with a commensurately large LGN and optic tract, whereas a relatively small V1 is associated with a commensurately smaller LGN and optic tract (Andrews et al., 1997). These variations seem to influence visual performance: visual acuity is correlated with cortical surface area (Duncan and Boynton, 2003), both as a function of eccentricity, and across individuals. This relationship across the hierarchy of the human visual pathway suggests that the development of its different parts is interdependent (Andrews et al., 1997), and may explain why cortical expansion occurs relatively late in the neurodevelopmental timeline.

Our data from rats indicate that enucleation ceases to influence the area size of V1 by P22 (ET= 0.86), at a time when the size of V1 is about 66% of its normal adult size, and about two weeks before V1 reaches its normal adult size. Similarly, in ferrets, the critical period for the effect of enucleation on the area size of V1 ends by P39 (ET = 0.77), but normal cortical expansion continues at least until P59 (ET = 0.87, unpublished findings). In humans, cortical expansion is even more prolonged; cerebral cortex reaches approximately 95% of its adult volume by 6 years of age (Giedd et al., 2015). Our present analysis suggests that the critical

period for visual deprivation ends by ETc = 0.81, the 7th postnatal month in humans. Thus, visual cortical expansion seems to consist of an initial stage that is susceptible to visual deprivation, and a later stage during which expansion is largely independent of ongoing visual input. Our meta-analysis including data from previous studies in other species suggests that these results can be generalized to many mammalian species.

The neurodevelopmental context for the effects of visual deprivation on surface area

The use of a common developmental event-time framework permits the cross-species comparison of the critical period for the effect of visual deprivation on cortical surface area. Enucleation in rats and ferrets, or blindness onset in humans at event times 0.25, 0.5, or 0.75 (see Figure 20), are associated with primary visual cortical surface areas at maturity that are approximately 50%, 70%, or 90% of the surface area of primary visual cortex in normally-sighted controls, respectively. At event time 0.25, retinal axons have begun to form the optic tract, but their terminals do not reach the lateral geniculate nucleus until an event time of 0.319 (Workman et al., 2013). Thalamic axons from the LGN influence mitogenic activity within subcortical lamina of the occipital lobe (Dehay et al., 2001; Dehay and Kennedy, 2007; Reillo et al., 2011), and synapse onto subplate neurons of the developing primary visual cortex between ET 0.3-0.53 (post-conception age 28 to P6 in the ferret) (Johnson and Casagrande, 1993; Herrmann et al., 1994). According to Reillo et al. (2011), a special type of progenitor cells leads to the generation of a class of glial cells that promote tangential dispersion of radially migrating neurons, and thereby facilitates growth in surface area of the cortical sheet. Disruption of the thalamic afferents through early enucleation in ferrets at P2 (ET=0.49) reduces the density of these progenitor cells which in turn is associated with a reduction in cortical surface area (Reillo et al., 2011). Thus, the approximately 30% reduction in visual cortex surface area observed in

early enucleated animals (Figures 14 and 15) and anophthalmic subjects (Figure 16), who are deprived at the equivalent of event time 0.32 or earlier, is consistent with the idea that visual deprivation reduces cortical surface area by interfering with the effect of these progenitor cells on surface area expansion. At an event time of 0.5, retinal axons innervate the thalamus; thalamic axons have synapsed with subplate, but not layer IV neurons. Neurogenesis of cortical neurons is essentially complete, but intracortical synaptogenesis has yet to begin, and the eyes have not yet opened (Workman et al., 2013). Early blind individuals were deprived of retinal input beginning approximately in the second half of human gestation (ET=0.62). At this event time myelination of the optic radiations is complete, and myelination of the optic tract is underway. Within cortex, synaptogenesis as well as differentiation of individual cortical layers is underway. It remains to be seen whether the effects seen in EB subjects and animals enucleated later in development simply reflect the asymptotic effects of cortical tangential expansion, or whether the smaller reduction in visual cortex size observed in these individuals also involves perturbation of the initial formation of visual cortical circuits.

Human vs. animal data

One limitation of studies examining the effects of visual deprivation on cortical anatomy in humans is that it is extremely difficult to systematically examine the effects of age of deprivation in the human population. While it is possible to find relatively homogenous subject groups affected with anophthalmia or early blindness, it is essentially impossible to examine the effects of age within prenatal development, and extremely challenging to find a subject group where deprivation systematically spans early childhood development.

Another limitation of human studies is that visual deprivation results from a variety of pathologies that differ widely both in disease mechanism (e.g. photoreceptor disease vs. optic

nerve damage) and in the extent of visual deprivation (no retinal signals vs. light perception). Thus, while blindness in the rats and ferrets in this study was induced by bilateral enucleation, within our human populations, most individuals maintained at least some retinal projections. Indeed, five of the EB subjects and most of the LB subjects had low light perception (but no form perception) (Supplementary Table 1). It should also be noted that, due to the etiology of blindness, the timing of blindness onset could not be determined with precision in many EB and LB cases. Perhaps surprisingly, the presence of residual light perception did not seem to influence cortical surface area in EB individuals. No significant difference in cortical surface area was found across the EB individuals with and without light perception. Moreover, when projected onto a common developmental timeline, EB individuals showed similar magnitudes of reductions in surface area as observed in enucleated animals. This failure to find a difference between enucleation and light deprivation due to photoreceptor loss suggests that the mechanisms underlying later tangential expansion can be disrupted by loss of pattern vision, as well as by the absence of the retino-LGN-V1 projection.

Translating data from several species into a common developmental time scale revealed a striking similarity across species both in the size of the reduction of surface area, and in the relationship between the graded reduction in visual cortical surface area and the age of blindness onset. This allowed us to estimate that visual deprivation starting at ETc = 0.81 no longer affects the surface area of V1. In humans, this event time corresponds to post conception day 483 (postnatal day 213). We also found that the critical period for the effect of visual deprivation ends long before cortical expansion is complete. Efforts to confirm these event times for humans will require finding subject groups whose blindness onset spans early childhood development, including the first year of life.

Summary and future directions

Our findings suggest that visual deprivation disrupts early stages of cortical expansion; the critical period for the effect of visual deprivation on V1 surface area occurs during a developmental time window when progenitor cells are generating glial cells that later promote tangential dispersion of radially migrating neurons, thereby facilitating cortical sheet growth. In humans, this critical period ends near the first year of life, suggesting that the age of deprivation may play a significant role in anatomical specification up to that age. Thus, this critical period may have translational importance when considering the likely success of sight recovery procedures in individuals blinded before the first year of life. Visual deprivation during later stages of cortical expansion, or during cortical pruning had little or no effect on V1 surface area. No significant difference was found between EB individuals with light perception and those without, suggesting that, at postnatal stages, it is the absence of patterned vision that is important. Further work will be needed to understand the mechanisms by which loss of visual input disrupts V1 cortical expansion, and why their influence ceases at the end of the critical period determined in this study.

Table 1: Rat Group Measures

Group	Enucleation Age	Sample Size	Event Time	V1 Surface Area	Cortex Surface Area	Ratio V1:Cortex	% Adult VSAR
BEP0	P0	6	0.43	9.3	166.9	0.06	73.3
BEP10	P10	4	0.66	12.0	181.3	0.07	86.8
BEP12	P12	5	0.70	12.5	181.7	0.07	90.0
BEP14	P14	6	0.73	13.2	185.2	0.07	93.3
BEP16	P16	5	0.76	13.0	179.1	0.07	94.8
BEP25	P25	5	0.89	13.3	182.4	0.07	95.7
BEP30	P30	5	0.95	13.7	186.5	0.07	96.5
BEP45	P45	4	1.10	13.9	185.8	0.07	98.2
SC	> P60	6	1.30	14.3	185.5	0.08	100.0

Table 2: Ferret Group Measures. Full term is at gestation day 41

Group	Enucleation Age	Sample Size	Event Time	V1 Surface Area	Extrastriate Surface Area	IsoCortex Surface Area	Ratio V1:Ctx	% of SC V1 Ratio
BEP7	PC48	4	0.54	55	123	781	0.083	77.7
BEP20	PC61	3	0.65	65	138	852	0.090	84.2
BEP31	PC72	2	0.72	70	112	774	0.105	98.1
SC	>119	4		67	133	759	0.107	100.0

Table 3: Piecewise regression parameter estimates for Enucleated Rats, Sighted Rats (for developmental of V1 area size), and Enucleated Ferrets

	Parameter Estimate	Standard Error	T-value
Rat: Enucleated			
y-intercept (b)	62.36987	3.57268	17.457***
Slope (m)	38.68413	4.80825	8.04***
Asymptote (t.x)	0.95412	0.05165	18.473***
Rat: Sighted, for (development of V1 area size)			
y-intercept	-26.37	13.27	-1.92
Slope	119.64	15.36	7.79***
Asymptote	1.056	0.04	27.08***
Ferret: Enucleated			
y-intercept	13.68	20.89609	0.65
Slope	105.31	33.77021	3.12*
Asymptote	0.772	0.06684	11.56***
* 0.01, ** 0.001, *** < 0.001			

Table 4: Human Group Measures. Surface area means (standard deviations)

Group	N	Event Time	V1 Surface Area	M1 Surface Area	Ratio V1:M1	% SC VSAR
AN	5	0.32	2068 (408)	1177 (176)	1.76	71.2
EB	13	0.65	1908 (427)	1004 (145)	1.90	77.0
LB	9	-	2101 (398)	923 (167)	2.28	92.2
SC	23	-	2449 (293)	992 (122)	2.47	100.0

Supplementary Table 1: Human subject details

Group	Age	Gender	Onset	Description
Anophthalmic (AN)				
ano1	21	F	0	Isolated bilateral anophthalmia, right with orbital cyst
ano3	33	F	0	Isolated bilateral anophthalmia
ano4	20	M	0	Isolated bilateral anophthalmia
ano5	25	M	0	Isolated bilateral anophthalmia
ano6	26	M	0	Isolated bilateral anophthalmia
Early Blind				
eb-ohsu03	53	F	0	etiology unknown; minimal light perception until 6 years old. no light perception
eb-ohsu04 †	50	F	0	Retinopathy of prematurity; no light perception
eb-ohsu05 ‡	40	F	0	Retinopathy of prematurity; diffuse minimal light perception
eb-ohsu06	44	M	0	Retinopathy of prematurity; no light perception
eb-ohsu07	45	F	0	Retinopathy of prematurity; no light perception
eb-ohsu08	56	F	0	Retinopathy of prematurity; no light perception
eb-ohsu09	52	M	0	Retinopathy of prematurity; no light perception
eb-ohsu12	55	F	0	Retinopathy of prematurity; diffuse minimal light perception
eb-ohsu22	36	M	0	Retinopathy of prematurity; no light perception
eb2	51	F	0	Retinopathy of prematurity; low light perception until retina detached at 25 years;
eb6	60	M	0	Retinopathy of prematurity; no light perception
eb7	36	F	0	Retinopathy of prematurity; low light perception until 14 years
eb8	30	M	0	Leber's congenital amaurosis; low light perception
eb10	38	M	0	Glaucoma from birth, light perception until 7 years in right eye, no light perception in left eye; unknown etiology, possible rubella virus in pregnancy
Late Blind				
lb-ohsu01	62	M	20 (60)	Diabetes; Glaucoma

lb-ohsu02	36	F	22 (26)	Glaucoma
lb-ohsu03	61	M	16 (43)	Retinitis Pigmentosa
lb-ohsu05	52	M	7 (40)	Rigors; Glaucoma
lb-ohsu06	58	M	12 (53)	Congenital Cataracts
lb-uw2	42	F	34 (41)	optic neuropathy
lb-uw3	62	F	42 (59)	glaucoma; corneal problems
lb-uw4	52	M	28(48)	retinitis pigmentosa
lb-uw5	63	M	30's(40)	retinitis pigmentosa

Sighted Controls for Anophthalmic Subjects		
con18	31	M
con19	30	F
con21	22	F
con24	22	F
con25	26	M
con27	27	F
con28	25	F

Sighted Controls for Early and Late Blind Subjects		
sc-ohsu01	51	M
sc-ohsu02	59	F
sc-ohsu03	58	M
sc-ohsu04	47	F
sc-ohsu05	50	F
sc-ohsu06	45	M
sc-ohsu07	57	M
sc-ohsu08	53	F
con8	29	M
con9	24	F
con10	30	F
con15	30	F
con16	26	M

†Right hemisphere omitted from analysis.

‡Left hemisphere omitted from analysis.

Figure 14. Primary visual cortex surface area as a function of age of deprivation onset in bilaterally- enucleated rats.

Profiles of V1 and cortical mantle revealed in tangential sections for **A.** a control P60 rat and **B.** a BEP12 P60 rat. In both visual cortices, heavily-stained myelinated regions allow delineation of primary visual cortex (dashed black line). Insets illustrate the reduced surface area of a BEP12 hemisphere compared to control (scale bars = 1 mm). **C.** Primary visual to non-visual cortex surface area ratios (VSAR) expressed as the percent of adult visual surface area ratio, for rats enucleated over an age range extending from P0 (ET = 0.43) to P45 (ET> 1). The broken line indicates the piecewise regression line of best fit. Vertical dotted line indicates end of the effect of enucleation (ETc). In rats, gestation is 21 days.

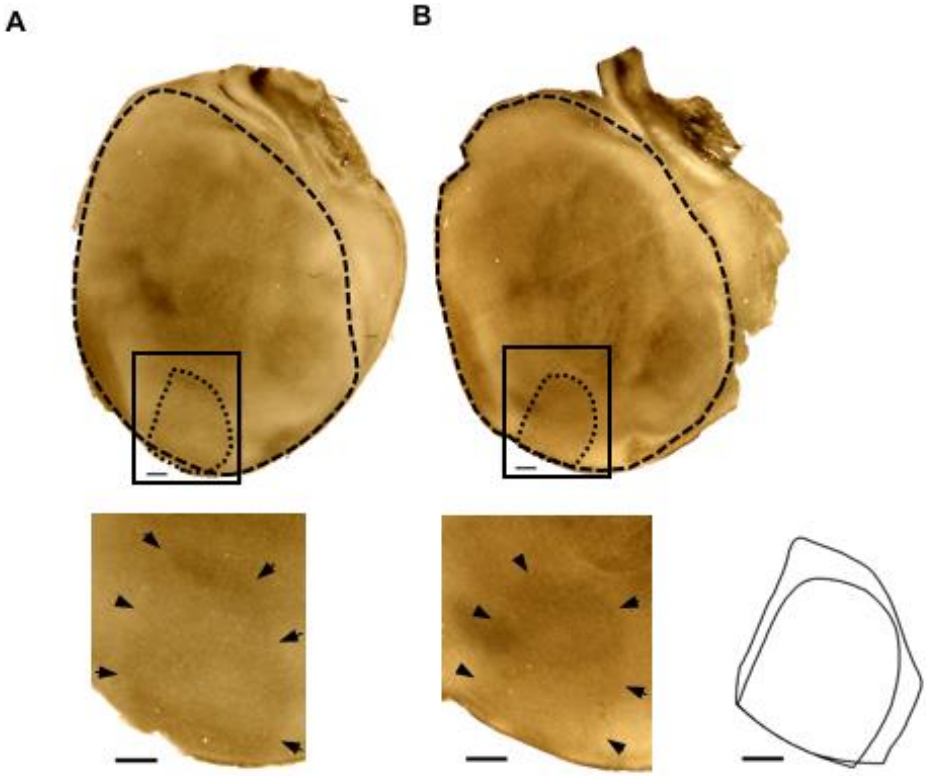
A
B

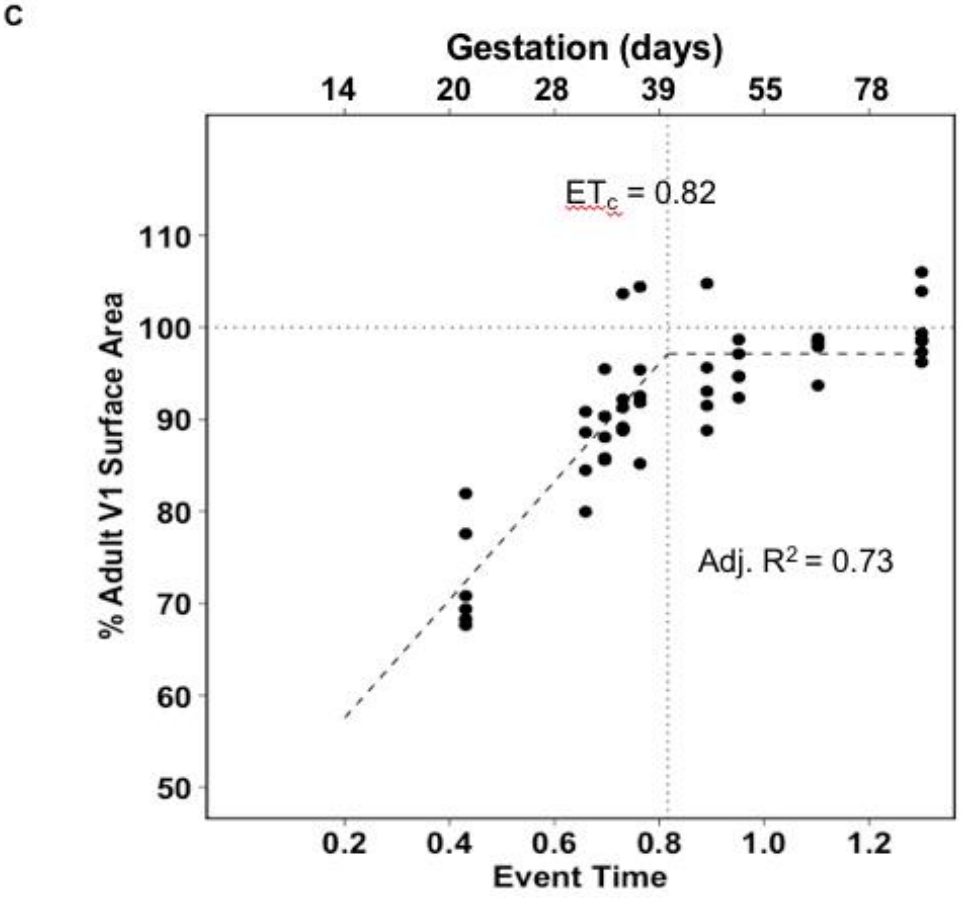
C
Gestation (days)
14
20
28
39
55
78
ET$_c$ = 0.82
Adj. R^2 = 0.73
% Adult V1 Surface Area
110
100
90
80
70
60
50
0.2
0.4
0.6
0.8
1.0
1.2
Event Time

Figure 15. Primary visual cortex surface area reduction as a function of age of deprivation onset in bilaterally-enucleated ferrets.

A. The primary visual cortex resides on the medial occipital surface, indicated by dashed white boundaries in caudal/ventral views of the ferret brain. **B.** The surface area of the primary visual cortex (enclosed by dashed white boundaries) of BEP7 ferrets is reduced compared to controls. The absence of the shallow sulcus that is present in control brains (yellow arrows) in brains from BEP7 animals contributes to the difference in visual cortex surface area. **C.** Quantification of primary visual cortex surface areas by MRI reveals pronounced reductions in the primary visual to non-visual surface area ratio in early enucleates (P7, ET = 0.54), with graded effects of enucleation on the primary visual to non-visual surface area ratio for later enucleations (P20, ET = 0.65 and P31, ET = 0.72). Broken line indicates best fit of the piecewise regression. Vertical dotted line indicates end of the effect of enucleation (ETc). In ferrets, gestation is 41 days.

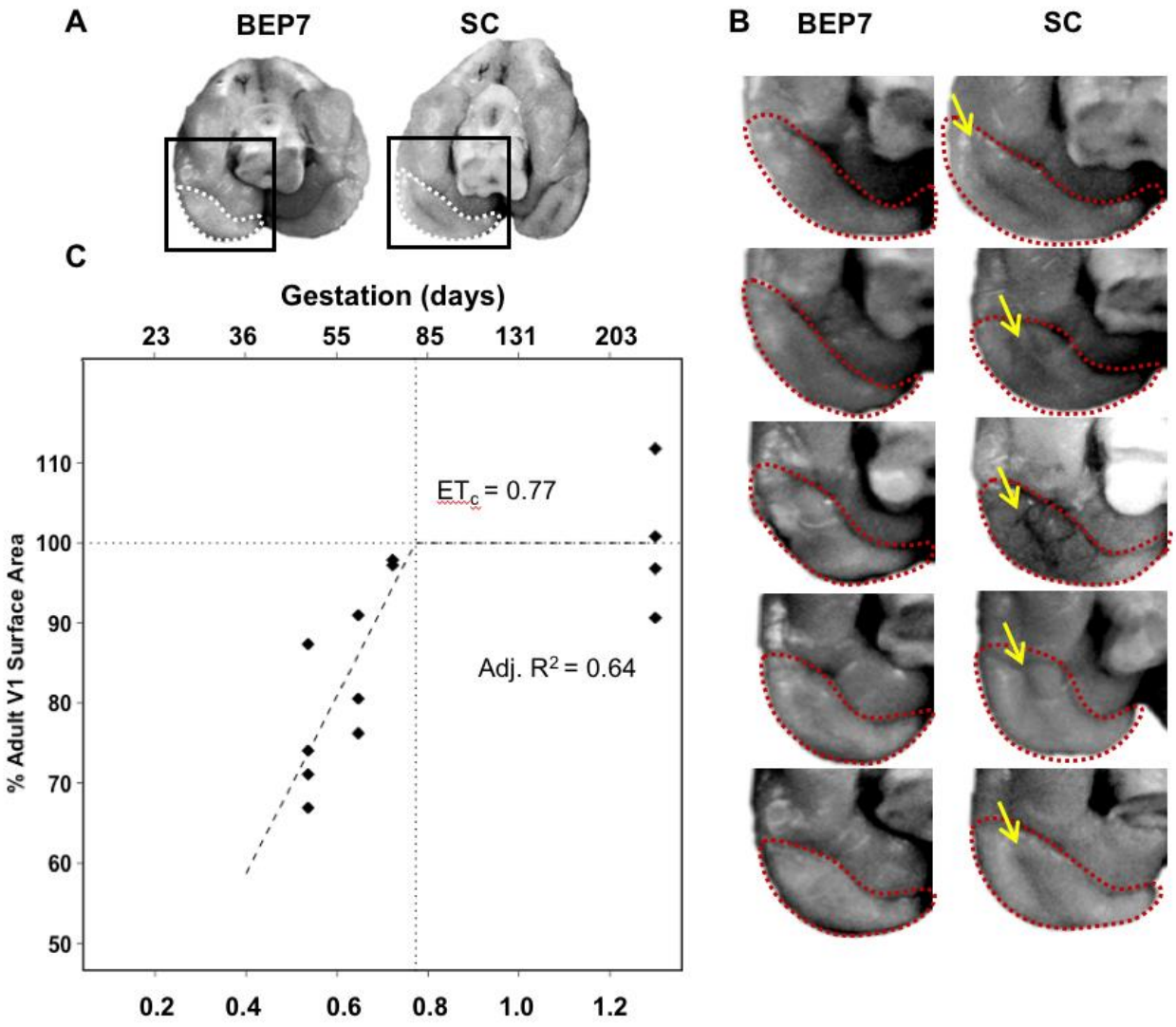
A
BEP7
SC
B
BEP7
SC
C
Gestation (days)
23
36
55
85
131
203
% Adult V1 Surface Area
110
100
90
80
70
60
50
0.2
0.4
0.6
0.8
1.0
1.2
ET_c = 0.77
Adj. R² = 0.64

Figure 16. Primary visual cortex surface area reduction for varying causes of blindness in humans with anophthalmia (AN), early-onset blindness (EB) late-onset blindness (LB) and sighted controls (SC) (see Methods, for group details).

A. For a SC subject, the region of cerebral cortex assigned to V1 (left column) and M1 (right column) is indicated by red areas bounded by yellow. A fiducial surface is shown in the top row and an inflated surface is shown in the bottom row. **B.** V1/M1 ratios expressed as a percentage of SC mean V1:M1 ratio (= 100%) are shown for AN, EB, LB, and SC groups. Significant V1/M1 surface area ratio reductions are observed for AN and EB (asterisks) but not LB relative to SC. (* $P < 0.05$, corrected for multiple comparisons)**.** Open symbols = right hemisphere; black symbols = right hemisphere.

A

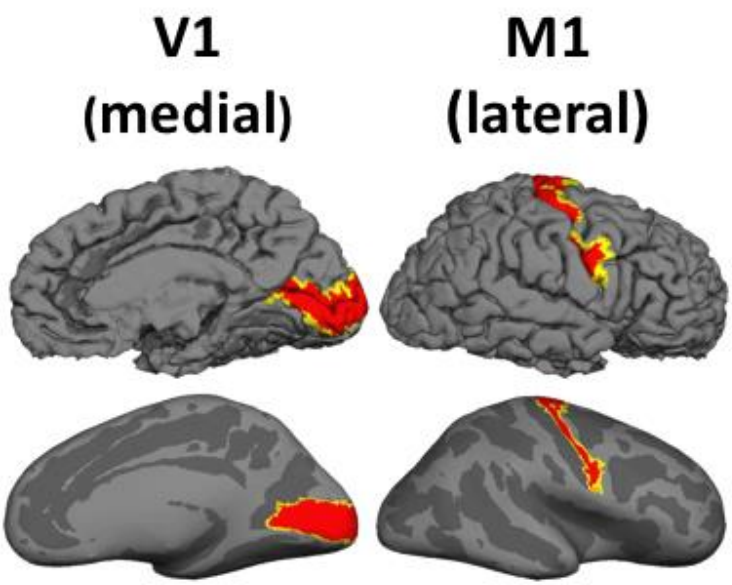
V1
(medial)
M1
(lateral)

B

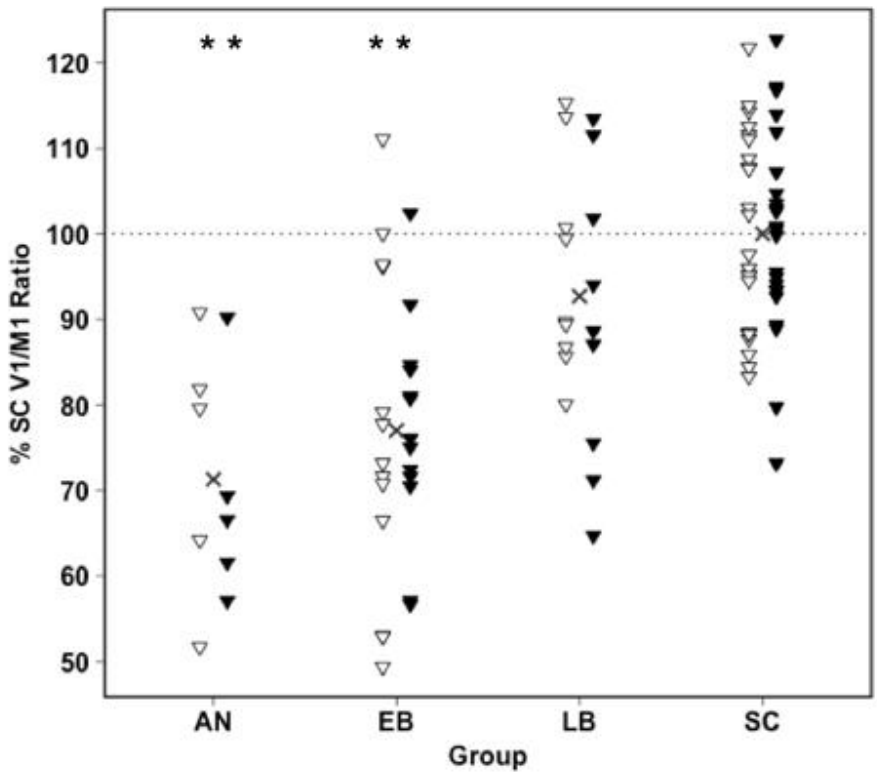
* *
* *
120
110
100
90
80
70
60
50
% SC V1/M1 Ratio
AN
EB
LB
SC
Group

Figure 17. Effect of age of blindness onset on the area size of V1. Data from each of the three groups of blind subjects in the current study fit with a piecewise regression model. The model yields an estimate of $ET_c = 0.87$ as the event time at which blindness no longer affects the size of V1 surface area.

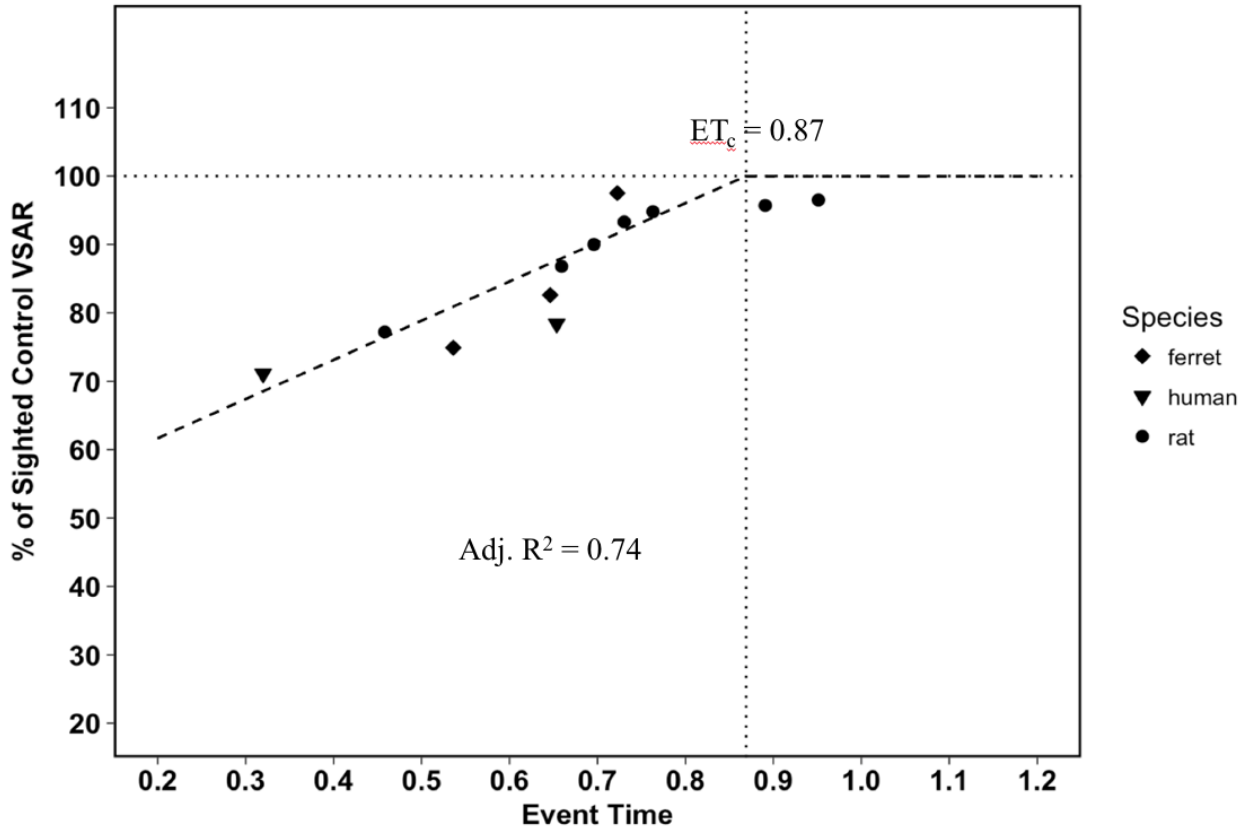
% of Sighted Control VSAR
110
100
90
80
70
60
50
40
30
20
0.2
0.3
0.4
0.5
0.6
0.7
0.8
0.9
1.0
1.1
1.2
Event Time
ETc = 0.87
Adj. R2 = 0.74
Species
ferret
human
rat

Figure 18. Longitudinal MRI anatomical analysis in three SC ferrets and three ferrets enucleated at P7.

The visual cortical surface area is reduced in the immature brain of P7 enucleated ferrets, compared to that in immature brains of control ferrets. **A.** Lateral (left) and medial (right) views of the right hemisphere of a control ferret brain at ages P11, P18, P25, and P31. Gyri and sulci appear as they do in a mature brain, which enables delineation of striate (red) and extrastriate (blue) visual cortex, as well as isocortex (yellow) boundaries following previously established conventions (Bock et al., 2012). **B.** Plots of the average of the left and right primary visual cortex surface area for 3 control (open symbols) and 3 BEP7 (black symbols) ferrets illustrating the surface area expansion over time. **C.** VSAR plotted for the same animals, as in b, illustrating the reduction in surface area in the BEP 7 ferrets induced by the enucleation.

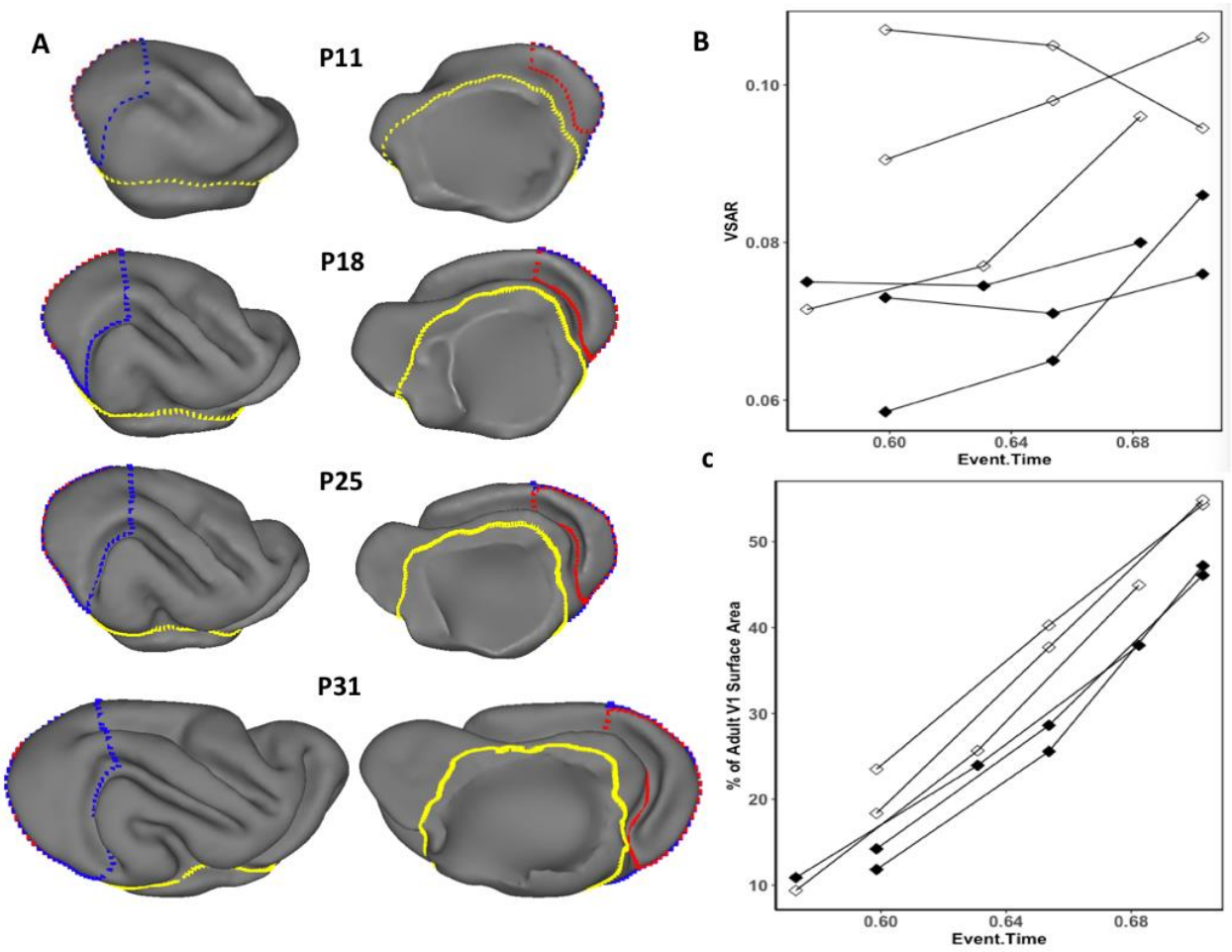
A
P11
P18
P25
P31
B
VSAR
0.10
0.08
0.06
0.60
0.64
0.68
Event.Time
C
% of Adult V1 Surface Area
50
40
30
20
10
0.60
0.64
0.68
Event.Time

Figure 19. Comparison of the effect of age of blindness onset on the area size of V1 with the normal development of V1 in sighted rats.

Data from the enucleated rats in Figure 14C (black circles) are plotted with data from normally developing rats sacrificed at ages P11, P15, P20 and P27 replotted from Duffy et al. (1998), and P30 and P35 collected in the present study (blue circles). Because Duffy et al. (1998) did not report measurements for the non-visual isocortex, the surface area values for V1 were normalized by dividing them by the size of V1 measured in the respective adult sighted control rats and the ratio was expressed as % of adult size of V1. Exact ages of the adult rats from Duffy et al. (1998) were not specified, but were set to ET = 1.3 (> P69).

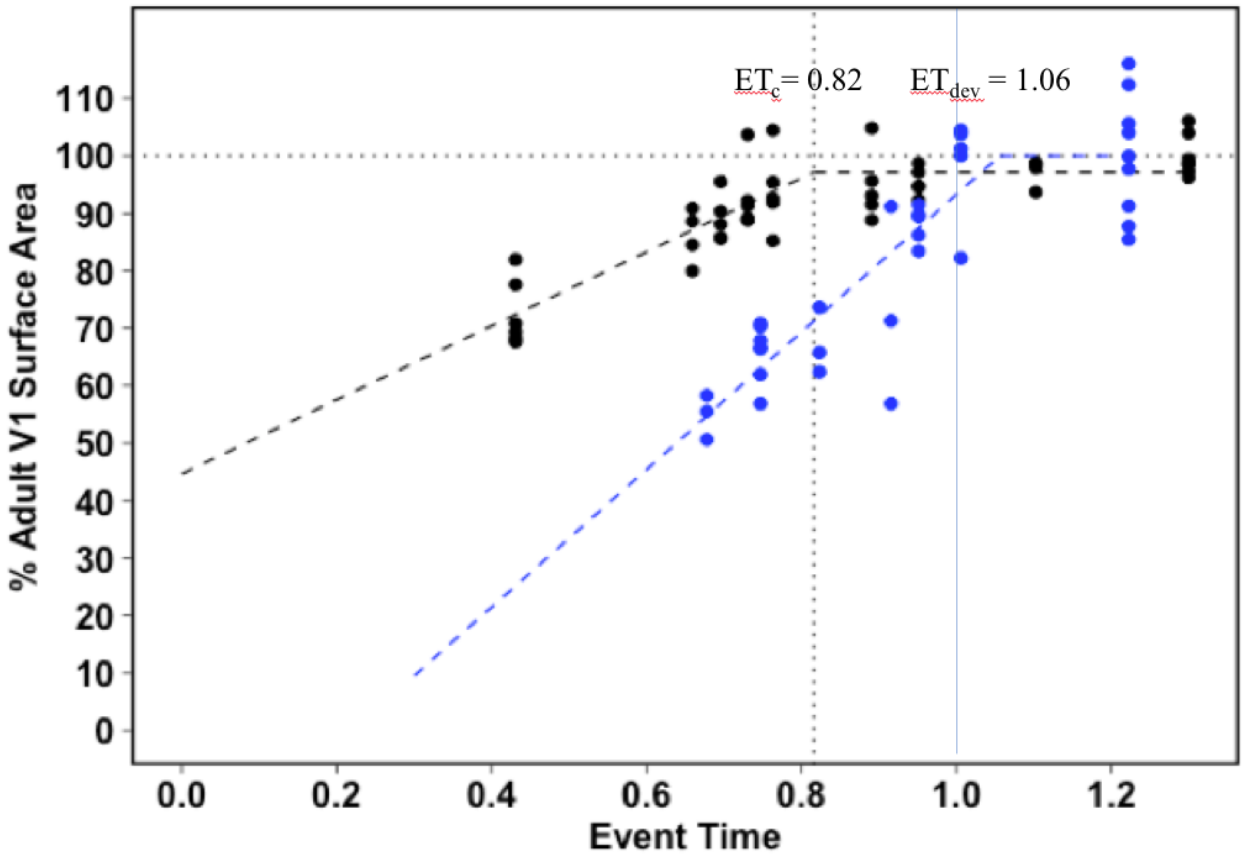
ET$_c$ = 0.82
ET$_{dev}$ = 1.06
% Adult V1 Surface Area
110
100
90
80
70
60
50
40
30
20
10
0
0.0
0.2
0.4
0.6
0.8
1.0
1.2
Event Time

Figure 20. Inter-species comparison of enucleation effect and development of V1.

Our current data on the effect of blindness (open symbols), presented in figure 17, are plotted together with data from published studies on the effect of blindness on the size of V1 in different species (black symbols). Data for the development of the area size of V1 in normal, sighted individuals come from published studies in different species (blue symbols). The black and blue segmented regression lines were weighted by the sample size (either one or several cases) for each data point. Dashed horizontal line corresponds to 100% of sighted control VSAR, while dotted vertical lines indicate the intersection points marking the event times for the estimated asymptote for the blind ($ET_c = 0.81$) and sighted ($ET_{dev} = 0.93$) non-linear fits. These event times indicate the end of the critical period for the effect of enucleation on the area size of V1, and the event time at which area V1 reaches its normal adult size in sighted individuals, respectively. This inter-species comparison confirms our observation that blindness ceases to affect the surface area of area V1 well before expansion of V1 is complete can, and extends it to many mammalian species. Extant data on the effect of visual deprivation on the size of V1 come from histological studies in rhesus macaques (Rakic et al., 1991; Dehay et al., 1996), rats (Sugita and Otani, 1984; Laing et al., 2012), ferrets (Reillo et al., 2011), short-tailed opossum (Karlen and Krubitzer, 2009), cat (Olavarria and Van Sluyters, 1995), as well as MRI-based studies of blind human subjects (Park et al., 2009; Jiang et al., 2009). Extant data on the development of the area size of V1 in sighted individuals include studies in rats (Duffy et al., 1998), cats (Duffy et al., 1998; Rathjen et al., 2003), macaques (Rakic et al., 1991; Dehay et al., 1991; Purves and LaMantia, 1993; Dehay et al., 1996; Horton and Hocking, 1996), human (Lyall et al., 2015).

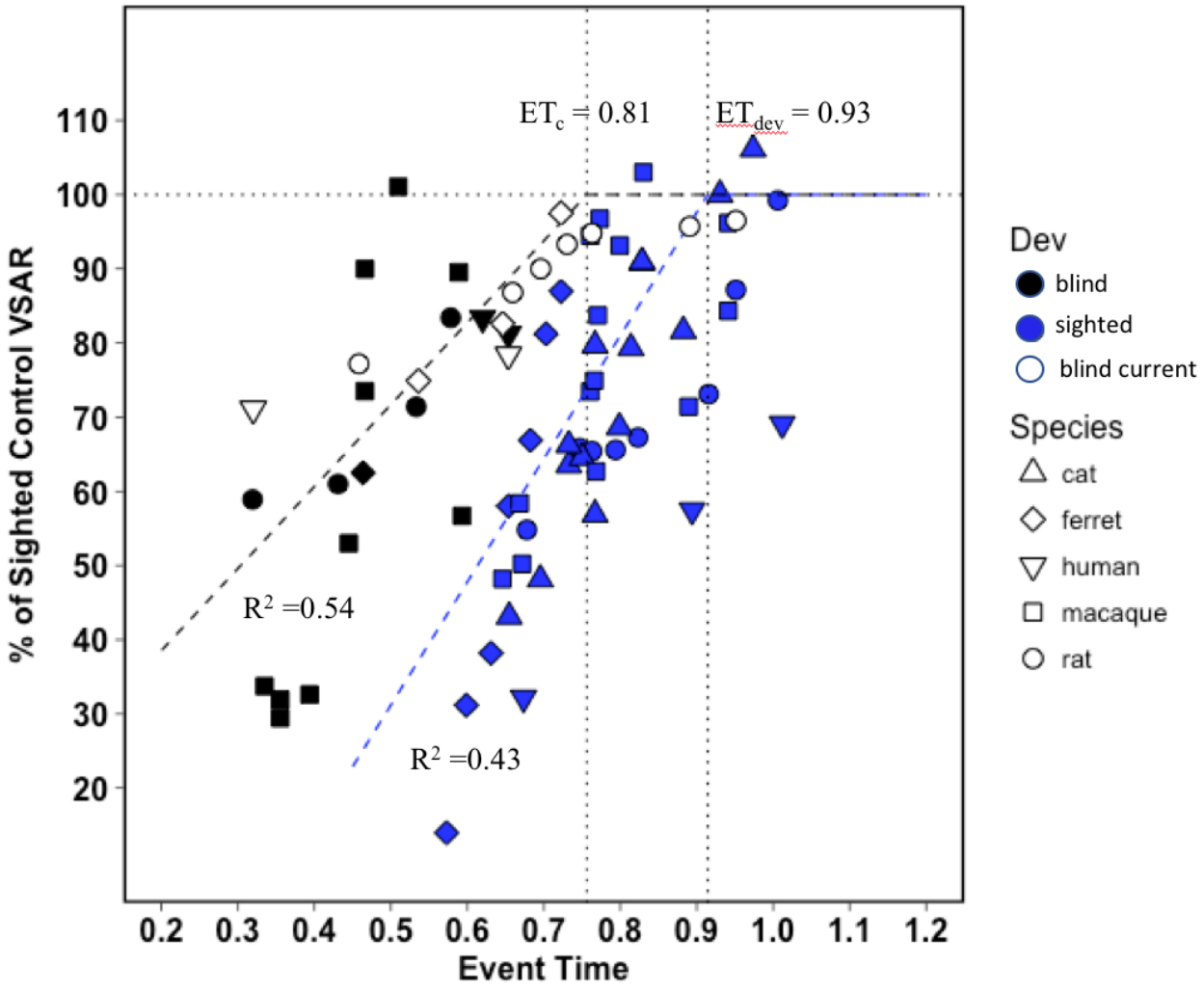
ET$_c$ = 0.81
ET$_{dev}$ = 0.93
R^2 =0.54
R^2 =0.43
% of Sighted Control VSAR
Event Time
110
100
90
80
70
60
50
40
30
20
0.2
0.3
0.4
0.5
0.6
0.7
0.8
0.9
1.0
1.1
1.2
Dev
blind
sighted
blind current
Species
cat
ferret
human
macaque
rat

CHAPTER 3: VISUAL INTERHEMISPHERIC AND STRIATE-EXTRASTRIATE CORTICAL CONNECTIONS IN THE RABBIT: A MULTIPLE TRACER STUDY

An important goal of visual system studies in animals is to understand vision in humans. In past decades, emphasis has been placed on studying carnivores and non-human primates based on the belief that advanced species resemble humans in both behavior and brain organization more closely than less advanced species, such as rodents, whose visual system has been widely assumed to be much simpler by comparison. However, numerous studies in rats and mice have convincingly shown that the occipital cortex surrounding primary visual cortex (V1, striate cortex) is significantly more elaborate than previously thought, consisting of about a dozen of interconnected, topographically organized extrastriate visual areas (Montero et al., 1973; Olavarria & Torrealba, 1978; Olavarria, 1979; Olavarria & Montero, 1981; Olavarria & Montero, 1984; Olavarria & Montero, 1989; Olavarria et al., 1982; Espinoza & Thomas, 1983; Sanderson et al., 1991; Montero, 1993; Coogan & Burkhalter, 1993; Schuett et al., 2002; Wang & Burkhalter, 2007; Garrett et al., 2014). This knowledge, together with the availability of genetic and molecular tools, especially in mice, have triggered a surge of studies using rodents as models for advancing our understanding of cortical visual processing in mammals. Indeed, recent advances include evidence that visual areas in rats (Coogan & Burkhalter, 1993; Vermaerke et al., 2014) and mice (Garrett et al., 2014; Marshel et al., 2011; Roth et al., 2012; Wang et al., 2011; Wang et al., 2012; Glickfield et al., 2014; Laramée & Boire, 2015) are functionally specialized and organized into processing streams that resemble the temporal and parietal parallel processing streams of primates, and that progressive functional transformations along these pathways conform to general hierarchical principles. While these and other studies have also pointed out differences between rodents, carnivores and primates (Vermaercke et al., 2014;

Laramée & Boire, 2015; Kaas & Balaram, 2014), they nevertheless highlight the usefulness of rodents as models in mammalian visual research.

However, the small size of the brains in rats and especially mice presents some challenges, such as greater difficulty in locating and recording from small cortical areas. Experiments benefiting from, or requiring larger brains, such as studies using stimulating/recording microelectrode arrays to explore the potential for chronic recordings in visual cortex (Porada et al., 2000) or for restoring vision (Chai et al., 2008; Sun et al., 2013), have often used rabbits, a Lagomorph whose brain is lissencephalic as in rats and mice, but about 6 and 30 times larger than the brain of rats and mice, respectively. Rabbits have also been used in a variety of other investigations involving the visual cortex, including cross-modal (Newton et al., 2002) and MRI and fMRI studies (Miller et al., 2008) but at present limited information about the organization of visual cortex beyond V1 is available in this species (Thompson et al., 1950; Hughes & Wilson, 1969; Woolsey et al., 1974; Towns et al., 1977; Mathers et al., 1977; Bousefield, 1978; Hughes & Vaney, 1982). Studies of the distribution of extrastriate fields labeled following single anatomical tracer injections into rabbit V1 reported that the arrangement of extrastriate areas connected with V1 closely resembles the arrangement of visual areas in rats and mice (Montero, 1981; Müller-Paschinger & Tömböl, 1989), and suggested that the "rodent" visual cortical plan may be more general, encompassing species within the Lagomorphs, and perhaps other orders (Montero, 1981; Montero, 1993).

Whereas these previous anatomical studies identified extrastriate areas connected with V1, they were unable to reveal their internal topography due to the use of only single V1 tracer injections. To address this issue, in a group of albino rabbits we injected multiple distinguishable tracers into different regions of V1 in the same animal and analyzed the topography of resulting

extrastriate labeled fields with reference to the patterns of callosal connections and myeloarchitecture revealed in tangential sections of the flattened cortex, an approach that has been fruitful for delineating the location and topography of extrastriate visual areas in several species (Olavarria & Montero, 1984; Olavarria & Montero, 1989; Olavarria & Montero, 1990). We also revealed the patterns of callosal connections in a group of Dutch belted rabbits to investigate possible differences in the overall organization of this interhemispheric pathway between albino and pigmented strains of rabbits.

MATERIALS AND METHODS

Surgery was performed in 5 albino and 5 adult Dutch belted rabbits (weighing approximately 2000-2500 g) anesthetized with ketamine hydrochloride (33 mg/kg, im) and xylazine hydrochloride (5 mg/kg, im), supplemented with atropine sulfate (0.05 mg/kg sc). Procedures followed protocols approved by the Institutional Animal Care and Use Committees.

Tracer Injections. To reveal the distribution of callosal connections in the right hemisphere, total volumes of about 9.0 -10.0 μL of a solution of horseradish peroxidase (HRP, Sigma Type VI, St. Louis, MO; 30% in saline) were injected into about 50-60 sites across occipital cortex in the left hemisphere. To reveal striate-extrastriate connections, small volumes (0.02–0.1 μL) of several additional tracers were injected at different loci in striate cortex of the right hemisphere (approx. 4.0–10.0 mm from the midline; 4.5–14.0 mm posterior to bregma). These tracers included the anterograde tracer ^{3}H-proline (25 μCi/μL solution in saline, L-[2,3-^{3}H] proline, specific activity 40.0 Ci/mmol, New England Nuclear, USA) and up to three retrogradely transported fluorescent tracers (rhodamine beads, RB, green beads, GB, LumaFluor, Naples, FL, USA, concentrated stock solution, and fast blue, FB, Sigma Co, St Louis. MO, 10%

in DW). The approximate area of effective tracer uptake for restricted injections was estimated as described previously (Laing et al., 2012). All tracers were pressure-injected through glass micropipettes (50–100 μm tip diameter) using brief pressure pulses.

Histochemical Processing. After 3-5 day survival, animals were deeply anesthetized with pentobarbital sodium (100 mg/kg ip) and perfused through the heart with 0.9% saline followed by 4% paraformaldehyde in 0.1 M phosphate buffer (pH 7.4). The right cortical mantle was resected, flattened between glass slides, and sectioned tangentially (60μm thick sections) as described previously (Laing et al., 2012). The rest of the brain received additional fixation and was cut into 60μm thick coronal sections. The transport of ^{3}H-proline was revealed in sections processed for autoradiography (Cowan et al., 1972), with an exposure time of 6 weeks at 4^{o} C, while HRP labeling was revealed using tetramethylbenzidine as the chromogen (Mesulam, 1978). A series of tangential sections was processed for myelin (Gallyas, 1979).

Data Acquisition and Analysis. Digital images of the myelin- and HRP-labeling patterns were obtained by scanning photographs of the histological sections at 2400 dpi using an Epson 4990 scanner. The distribution of cells labeled with fluorescent tracers were acquired with a custom, computer-assisted microscope system. Tangential sections throughout the depth of the cortex were examined to ensure that injections analyzed were restricted to grey matter.

The left hemispheres were extensively infiltrated with HRP and the ipsilateral visual thalamic nuclei were uniformly and densely labeled with reaction product (Figure 21A), indicating that HRP was effectively transported from the injected cortex. In the right hemispheres, the locations of the injection sites into V1 (Thompson et al., 1950; Hughes & Vaney, 1982) were confirmed by analyzing the distribution of labeled fields within the ipsilateral dorsal lateral geniculate nucleus of the thalamus (dLGN) (Weyand & Shadlow, 1986) (Figure

21B).

Using Adobe Photoshop CS2 (Adobe Systems), digitized images of anatomical tracers and myelin labeling patterns from the same animal were carefully aligned with each other using the border of V1, the edges of the sections, blood vessels, and other fiducial marks. Cells labeled by the injections of RB, GB and FB were represented by red, green and blue dots, respectively, and overall labeling patterns were reconstructed from 3-4 sections. ^{3}H-proline labeling was visualized under dark field microscopy and represented by outlines of densely labeled regions. Callosal connections were illustrated either by photographic images, by outlines of the areas containing dense accumulations of HRP labeling, or by thresholded versions prepared after first applying a median filter to reduce noise, followed by a high-pass filter to remove gradual changes in staining density across the entire image. The results were carefully inspected to confirm that these versions accurately represented the labeling pattern observed in the sections. Figures were prepared using Adobe Photoshop CS2, and all imaging processing used, including contrast enhancement and intensity level adjustments, were applied to the entire images.

RESULTS

Myeloarchitecture. Heavily myelinated areas are observed in occipital, temporal and parietal regions (Figure 22A). Figure 22B relates the myelination pattern to the cytoarchitectonic map of the rabbit cortex (Fleischhauer et al., 1980). Striate cortex (area V1) appears as an oval region of dense myelination with sharp and smooth borders (Figure 22A). The medial border of V1 coincides with the lateral sulcus (Figure 22). Fleishhauer et al. (1980) subdivided V1 into a lateral region (Oc2), which is binocular (Hughes & Wilson, 1969; Hughes & Vaney, 1982), and a medial monocular region (Oc1), but the border between these subdivisions is not as apparent in

the myelin pattern (Figure 22) as it is in other species, for example the squirrel (Paolini & Sereno, 1998). Area Oc3.1, immediately lateral to V1, includes the physiologically defined area V2 (Hughes & Wison, 1969). Area Oc3.1 is less densely myelinated than V1, but more myelinated than neighboring temporal areas Te2.1 and Te2.2. In parietal cortex, heavily myelinated regions include Poc1 (the barrel field), the rest of primary somatosensory cortex (S1), and Poc3 (second somatosensory cortex, S2). In temporal cortex, densely myelinated regions include primary auditory cortex (Te1), and a region within the most posterior and ventral portion of temporal cortex (Te3) (Figure 22B). In medial extrastriate cortex, the border between cytoarchitectonic areas Oc3.2 and Rsgβ (Fleischhauer et al., 1980) was not obvious in myelin stained tangential section. We therefore identified this region as cingulate area 29d (Vogt et al., 1986).

Pattern of callosal connections. The patterns of callosal connections were revealed in albino (Figures 23A and 23B) and Dutch belted rabbits (Figures 23C-E). Dense accumulations of retrogradely HRP-labeled cell bodies and anterogradely labeled terminations formed a band straddling the lateral border of V1. Often, this band had a beaded appearance, consisting of a series of distinct patches of about 0.75 mm in diameter, separated by about 1.5 mm (arrows in Figures 23A-C). In some cases, patches were present throughout most of the lateral border of V1 (Figures 23A and 23B), while in other cases they were apparent only in posterior regions of V1 (Figure 23C). At some places, pairs of patches (opposing arrows in Figure 23B) were separated by a narrow region of low labeling density centered at the lateral border of striate cortex. The callosal band at the lateral border of V1 was consistently narrow posteriorly (0.7-1.0 mm in width), but it often tended to increase in width in more anterior regions of V1, reaching about 2.5 mm at its widest region in some cases (Figure 23C). It is unlikely that the patchiness

and anteroposterior difference in width are due to incomplete infiltration of HRP because HRP labeling in the ipsilateral dLGN was uniformly dense throughout the nucleus (Figure 21A).

In extrastriate cortex callosal connections formed patches and bands, and in some cases callosal bands partially or completely encircled areas devoid of callosal connections in lateral extrastriate cortex (Figure 23). The appearance and location of several of these callosal features were consistent across rabbits and proved useful when comparing patterns of striate-extrastriate connections from different animals. No major differences between albino and pigmented rabbits were observed in the distribution of callosal connections (Figure 23).

Striate-extrastriate connections. Striate-extrastriate connections were studied only in albino rabbits (n = 5). Tracer injections into V1 were placed in regions representing upper and lower visual fields, as well as nasal and temporal fields (Figure 24). Labeled fields of different sizes were observed in lateral extrastriate cortex. The largest fields were typically arranged anteroposteriorly forming a first tier consisting of 4-5 fields located immediately lateral to V1, in area Oc3.1, while 2-3 smaller fields formed a second tier distributed more laterally in Oc3.1 and in neighboring temporal areas Te2.1, Te2.2 and Te3. In medial extrastriate cortex, within area 29d, labeled cells usually formed an elongated field. We identified putative retinotopically-organized areas based on the analysis of local, systematic displacements of labeled fields in response to displacements of injection sites in V1. As in previous studies in the rabbit (Montero, 1981; Müller-Paschinger & Tömböl, 1989), we have tentatively adopted the nomenclature established in the rat, in which visual areas are named according to their location relative to V1 (Montero et al., 1973; Olavarria & Montero, 1984).

The case shown in Figures 25A and 25B illustrates the distribution of extrastriate labeled fields resulting from injection sequences oriented along either the mediolateral or anteroposterior

axes in V1. From these data we tentatively identified several visual areas in lateral extrastriate, which are summarized in Figure 25C. Figure 25A illustrates that a mediolateral sequence injections across the width of V1 (from temporal to nasal representations in the lower visual field) results in a mirror image distribution of labeled fields in area Oc3.1. The FB- and GB-labeled fields are elongated anteroposteriorly, occupying portions of areas that we identify as areas AL (anterolateral) and LM (lateromedial) by their locations relative to V1 and the callosal pattern (Figure 25C). The largest field of tritiated proline is restricted to area LM, while the two more lateral smaller fields of tritiated proline suggest the existence of additional areas lateral to LM. This animal also received an injection of RB more posteriorly in V1 (Figure 25B). Figure 25B shows a sparse field of RB-labeled cells in anterior portions of area AL, and a robust elongated field in posterior portions of putative area LM, whose position was more posterior than the fields produced by the other 3 anterior injections. Further posteriorly, a callosal band extends across areas Te2.2 and Te3 in a lateroposterior direction separating two additional RB-labeled fields and partially overlapping with a FB-labeled field. The location and topography of the areas separated by this callosal band suggest that they correspond to areas PL (posterolateral) and P (posterior) described in the rat and mice (Olavarria & Montero, 1984; Olavarria & Montero, 1989) (Figure 25B and C). The field of FB-labeled cells overlapping the callosal band is assumed to straddle the border between PL and P (Figure 25B and C).

Note that in area AL, the fields of FB- and GB-labeled cells occupy more posterior portions than the field of RB-labeled cells, and the reverse is true in LM, namely, FB- and GB-labeled cells occupy anterior regions of LM while RB-labeled cells occupy posterior regions of this area. As a result, while a region free of RB-labeled cells separates the fields of RB-labeled cells in AL and LM, the fields of FB- and GB-labeled cells appear to form continuous fields

extending from anterior LM to posterior AL. In area PL, the distribution of RB- and FB-labeled cells reverses with respect to the distribution in area LM, i.e., FB-labeled cells are posterior, while RB-labeled cell are anterior. Thus, as the injection site in V1 moves from anterior to posterior, the labeled fields move anteriorly in AL and PL and posteriorly in LM, suggesting that, as in the rat, the anteroposterior axis in V1 (from lower to upper visual field representations) maps along the same direction in LM, but in the reverse direction in areas AL and PL. The anteroposterior map in PL appears to reverse again in area P.

The RB-labeled field in LM extends further laterally at both its anterior and posterior ends forming two tongues. The posterior tongue is long, extending into areas Te2.1 and Te2.2 (field labeled LI, laterointermediate, Figure 25B and C), while the anterior tongue is short with only a few RB-labeled cells seen beyond the lateral border of area Oc3.1 (field labeled LLa, laterolateral anterior, Figure 25B and C). Note that both of these tongues of RB labeling are located between patches of callosal connections and overlap with the two small lateral fields of tritiated proline, providing support to the idea that these two regions may correspond to two separate visual areas. Sparse RB labeling was observed in area Te3. Finally, labeling in medial area 29d suggests a mirror image representation of the mediolateral axis in V1, but RB labeling was not strong enough in this region to map the anteroposterior axis in V1.

Figure 26 provides further evidence that a mediolateral injection sequence (GB-FB-RB) produces a mirror image sequence of labeled fields (RB-FB-GB) in LM. Moreover, this sequence reverses again (GB-FB-RB) as FB-labeled cells and RB-labeled cells are found immediately lateral to the GB-labeled field (indicated by an arrow). This small, labeled field straddles the Oc3.1/Te2.1 border and extends into Te2.1. It appears to correspond to the area occupied by both the posterior isotope-labeled field and the posterior tongue-like RB-labeled

field described in Figure 25B. Together, these data provide further evidence that this region may correspond to area LI in the rat, in which the mediolateral map reverses with respect to that in LM (Thomas & Espinoza, 1987). Thus, in Figure 26, the GB-labeled field indicated by the arrow (temporal visual field representation) would mark both the lateral border of LM and the medial border of LI. More posteriorly, Figure 26 shows separate labeled fields that may correspond to areas PL and P described above. While distribution of RB-and FB-labeled cells in LP suggests a mirror image of the corresponding injection sites in V1, the topography in P is not clear. Immediately lateral and posterior to LP, in area Te3, we tentatively identify area TP (temporal posterior area, see below). Labeling could not be assigned with certainty to area AL. In medial extrastriate cortex, a narrow field of labeling was oriented anteroposteriorly, but its topography was not apparent.

Additional data on the mapping of the anteroposterior axis in V1 are presented in Figures 27 and 28. Following an injection of FB in a region of V1 representing lower visual fields, two dense, slightly separated FB-labeled projection fields were observed lateral to V1, in regions likely corresponding to areas AL and LM (Figure 27A). Comparing these data with data from an injection of RB placed more posteriorly, in regions representing upper fields (Figure 27B), shows that the distribution of RB-labeled cells is more extensive, occupying more anterior regions in AL as well as more posterior regions in LM. These displacements in opposite direction are consistent with data in Figure 25 suggesting that the anteroposterior map in V1 has the same orientation in LM, but is inverted in AL. A small field of FB- and RB-labeled cells is observed lateral to the larger RB- and FB-labeled fields associated with areas AL and LM. This small field appears to be in a region corresponding to area LLa, and the fact that FB-labeled cells are located more anterior than the RB-labeled cells suggest that the anteroposterior axis in V1 is

mapped along the same orientation in area LLa. Further posteriorly, this case shows labeled fields resembling those seen in Figures 25 and 26, in regions that appear to correspond to areas LI, PL, P and TP. Anterior to AL, there was sparse FB and RB labeling in a narrow region delimited laterally by a callosal band. This region may correspond to area RL (rostrolateral, Figure 27B) described in the rat (Coogan & Burkhalter, 1993;Thomas & Espinoza, 1987) and mouse (Wang & Burkhalter, 2007). Labeling similar to that described in Figures 25 and 26 was observed in medial extrastriate cortex.

Figure 28A correlates the pattern of callosal connections (outlined in yellow) and the labeled fields resulting from injections of tritiated proline (black outlines), RB and FB with the underlying myeloarchitecture. The injection of tritiated proline in anterior V1 (lower visual fields) produced a circular labeled field in area Oc3.1, which likely straddles the border between areas AL and LM. A smaller labeled field is located immediately lateral, in an area we tentatively identify as area LLa (Figure 28B). Another isotope-labeled field was observed anteriorly in area Oc3.1, in a region we identify as area RL. This region is less densely myelinated than the rest of area Oc3.1. The injection of RB was placed more posteriorly in V1 and, consistent with the topography of areas AL and LM described above, the RB-labeled fields in AL and LM appear to fuse at the site of the large isotope-labeled fields, presumably at the border between AL and LM, where the representations of lower visual fields in AL and LM meet. However, unlike this isotope-labeled field, RB-labeled fields extended more anteriorly in AL and more posteriorly in LM, occupying regions that represent higher elevations. A tongue-like RB-labeled field extended laterally between callosally labeled regions. This field overlapped with the small, lateral isotope-labeled field, supporting the existence of a small area we call LLa in this region (see Figures 25B and 27B). In putative area RL, the RB labeling was located

further lateral than the isotope labeling, suggesting that RL is topographically organized. In posterior regions, the RB injection produced labeled fields in areas Te2.2 and Te3 (Figure 28B) that resemble the labeling localized in areas PL, P and TP in Figures 25, 26 and 27. The RB- and FB-labeled fields in area TP occupy a portion of a densely myelinated area observed in Te3 (Figure 28A), and the separation between these fields suggests that area TP is topographically organized. Labeling in this region was observed following injections into different V1 sites, suggesting that area TP represents a large portion of the visual field. The injection of FB was placed very close to the posterior and medial border of V1, in a region representing peripheral portions of the upper visual field. In lateral extrastriate cortex, FB-labeled cells accumulated in lateral area Oc3.1, in approximately the same location occupied by the GB-labeled field in Figure 26 (black arrow), and by the two more posterior isotope-labeled fields in Figure 25B. These results support the interpretation drawn from Figures 25B and 26 that peripheral visual fields are represented at the boundary between putative areas LM and LI. A small FB-labeled field was located at the posterior end of lateral extrastriate cortex, likely in area P, and a few FB-labeled were located in area AL. In medial extrastriate cortex, elongated FB- and RB-labeled fields overlapped extensively in the anteroposterior direction, while along the mediolateral axis they were segregated, suggesting a mirror-image representation of the mediolateral axis in V1.

In a final case (87-1) we revealed the projections from an injection of tritiated proline placed at the medial border of posterior V1, in a region roughly similar to the FB injection in Figure 28. We observed a labeling pattern resembling that produced by the FB injection in Figure 28 (data not shown). In both cases the distribution of labeling in lateral extrastriate cortex was rather restricted, suggesting that extreme upper peripheral visual fields are not represented in all extrastriate areas.

DISCUSSION

Callosal connections. We confirmed studies showing that callosal connections form a band that straddles the lateral border of V1 (Shadlow et al., 1978; Clarke et al., 1992). Our results extend these previous observations by showing that in lateral extrastriate cortex of both albino and pigmented rabbits callosal connections form patches and several band-like regions oriented mediolaterally at different anteroposterior levels. In some cases, a band of callosal labeling was observed in anterior portions of medial extrastriate cortex. The location of several of these callosal features was constant across animals of both strains. However, we did not typically observe ring-like callosal configurations encircling separate extrastriate cortical regions, as described in rodents [6] and some marsupials (Bravo et al., 1990; Martinich et al., 2000).

The callosal band at the V1/Oc3.1 border often had a beaded appearance in both albino and Dutch belted rabbits. The presence of callosal patches along this band is in agreement with previous reports in rabbits (Ledoux et al., 1987) and squirrels (Gould, 1984). A recent study in Long Evans rats correlated distinct periodicities in the pattern of callosal connections in V1 with ipsilateral ocular dominance columns (Laing et al., 2014), but a similar correlation may not exist in rabbits and squirrels because no evidence of ocular dominance columns has been found in these species (Holländer & Hälbig, 1980; Weber et al., 1977). It remains possible that callosal projection patches at the V1 border in rabbits and squirrels relate to orientation selectivity or other forms of functional segregation (Bousfield, 1977).

Relative to the width of V1, the callosal zone in V1 is narrower in rabbits than in rats (Hughes & Wilson, 1969; Olavarria & Van Sluyters, 1985). A possible explanation comes from relating the width of the binocular regions in V1 and the projections from temporal retina in both

species. The binocular region in rabbit V1 (Hughes & Wilson, 1969; Jijiwa, 1973) is narrower than in rats and other species, reflecting the fact that the rabbit temporal retina is relatively small due to the more lateral placement of the eyes (Hughes & Vaney, 1982). Moreover, as in the rat (Cowey & Perry, 1979), the entire temporal retina of rabbits projects both ipsilaterally and contralaterally (Provis & Watson, 1981). Consistent with the hypothesis that the width of the callosal zone in V1 reflects the extent of temporal retina from which crossed projections originate (Olavarria & Li, 1995), the width of the callosal zone in V1 matches the width of the binocular region in V1 in both rats (Laing et al., 2014) and rabbits (Hughes & Wilson, 1969; Jijiwa, 1973). Thus, relative to the width of V1, the difference in the width of the V1 callosal zone between rabbits and rats may simply reflect the difference in the width of the binocular zone between these species. It is worth adding that both the width of the binocular region in rabbit V1 (Thompson et al., 1950; Hughes & Wilson, 1969), as well as the strength of the ipsilateral eye input to this region (Choudhury & Gent, 1973) tend to decrease posteriorly, which may explain our observation that the width of the callosal zone in rabbit V1 tends to decrease posteriorly.

Striate-extrastriate connections. Our results extend previous studies and provide further evidence that extrastriate areas identified anatomically in the rabbit (Montero, 1981; Müller-Paschinger & Tömböl, 1989) resemble the pattern of visual areas in the rat not only in their general location with respect to V1, but also in their internal topography. Our data are also consistent with the interpretation that, as in the rat, lateral extrastriate areas connected with V1 are arranged primarily in two tiers. Figures 29A and B show a tentative diagram of the distribution and internal topography of extrastriate visual areas derived from this study. To facilitate comparison with studies in rodents, a diagram of visual areas in the rat is illustrated in

Figure 29C. The anteroposterior and mediolateral oriented arrows (Figure 29B) summarize the displacements of the injections sites in V1 and the resulting displacements of labeled fields in some of the identified extrastriate areas. Most injections into rabbit V1 labeled fields widely distributed in the areas delineated in Figures 29A and B, with the exception of very medial and posterior injections (see Figure 28). The latter injections produced more restricted labeling patterns, suggesting that only some extrastriate areas contain representations of extreme upper and temporal regions of the visual field. Representations that are either incomplete or biased toward particular regions of visual space have also been described in mice (Garrett et al., 2014).

In rats (Figure 29C) and mice, areas AL, LM, PL and P form a tier located adjacent to the lateral border of V1. In these areas, the representation of the mediolateral axis in V1 (from temporal to nasal visual fields) is inverted, such that tracer injections into medial or lateral regions of V1 produce labeled fields away or close to the lateral border of V1 in lateral extrastriate cortex, respectively (Montero et al., 1973; Olavarria & Torrealba, 1978; Olavarria, 1979; Olavarria & Montero, 1981; Olavarria & Montero, 1984; Olavarria & Montero, 1989; Olavarria et al., 1982; Espinoza & Thomas, 1983; Sanderson et al., 1991; Montero, 1993; Coogan & Burkhalter, 1993; Schuett et al., 2002; Wang & Burkhalter, 2007; Garrett et al., 2014, Vermaercke et al., 2014; Marshel et al., 2011; Thomas & Espinoza, 1987). We observed a similar topography in the homonymous areas in the rabbit. The similarity extended to the representation of the anteroposterior axis in V1 (from lower to upper visual fields). As in the rat and mice, we observed that the anteroposterior axis in V1 maps along the same direction in area LM, but in the reverse direction in both AL and PL. Our data (Figure 25) also suggest that the map reverses again in P. Opposite orientations of the elevation maps in LM and AL are illustrated by the fact that labeled fields in LM and AL originating from progressively more

anterior loci in V1 (representing progressively lower visual fields) moved closer and closer together, eventually merging. As such, the most anterior V1 injection results in a single field at the putative border between AL and LM (see isotope labeled field in Figure 28B). We also identified area RL whose location in anterior lateral extrastriate cortex resembles that of area RL in rats (Thomas & Espinoza, 1987; Coogan & Burkhalter, 1993) and mice (Wang & Burkhalter, 2007). In these rodents, area RL is often associated with a small anterior callosal ring, and in some rabbits callosal connections form a ring-like configuration in this region (Figure 23).

In agreement with Montero (1981), we observed that area LM is the largest area in lateral extrastriate cortex, and that is elongated in the anteroposterior direction. On the basis of its location, size and topographic organization, we concur with Montero's suggestion that LM corresponds to an area called V2 in previous electrophysiological studies in the rabbit (Hughes & Wilson, 1969; Woolsey et al., 1974; Hughes & Vaney, 1982), and that it is likely homologous to visual area V2 described in primates, carnivores and other species (Rosa & Krubitzer, 1999).

In addition to the first tier of areas located immediately adjacent to the lateral border of V1, we identified a second tier of smaller areas. In one of these, area LI, the mediolateral topography was a mirror image of that in LM, as in rats (Olavarria & Montero, 1984; Espinoza &Thomas, 1983; Montero, 1993; Vermaercke et al., 2014) and mice (Olavarria & Montero, 1989; Wang & Burkhalter, 2007). A small area called LL has been identified further laterally in rats (Olavarria & Montero, 1984; Espinoza &Thomas, 1983; Montero, 1993; Vermaercke et al., 2014) and mice (Olavarria & Montero, 1989), in which the mediolateral topography reverses again, resembling the map in LM. While next to LI we may have failed to identify an area corresponding to area LL in rats and mice, we tentatively named LLa a small area we identified further anteriorly (Figure 29A). The second tier is somewhat variable in the rat, and in some

studies area LLa has been identified anterior to LL (Olavarria & Montero, 1984; Thomas & Espinoza, 1987). Thus, it is possible that area LLa in the rabbit may correspond to area LLa in the rat and mouse (Garrett et al., 2014).

The densely myelinated area we observed in Te3 may correspond to a heavily myelinated area, called TP (temporal posterior), described in approximately this region in the squirrel (Kaas et al., 1989; Wong & Kaas, 2008) and agouti (Dias et al., 2014). The portion connected with V1 may correspond to a visually responsive area in rabbit temporal cortex described in previous physiological and anatomical studies (Mathers et al., 1977; Bousfield, 1978). In the rat, it may correspond to a region connected with V1 described in perirhinal cortex (Olavarria & Montero, 1984; Montero, 1993; Coogan & Burkhalter, 1993) (see area PR, pararhinal, in Figure 29(c)), and to the caudal temporal area (Vaudano et al., 1991), while in the mouse it may correspond to area 36p (Wang & Burkhalter, 2007).

We did not observe projections anterior to V1 that could correspond to area A (anterior) in rats (Olavarria & Montero, 1984) and mice (Wang & Burkhalter, 2007). Likewise, we did not observe projections to a site in somatosensory cortex called S in rats (Olavarria & Montero, 1984) and mice (Olavarria & Montero, 1989). Medially, in area 29d, we observed connections with an elongated region that we tentatively called area M (medial, Figure 29A). Labeling from different injections usually overlapped extensively, but in some animals the anteroposterior axis in V1 was represented as in V1, while the mediolateral axis in V1 was represented as a mirror image. This region may correspond in part to area AM described in the rabbit [36], and areas PM, AM, and M described in rats (Olavarria & Montero, 1984; Espinoza & Thomas, 1983; Montero, 1993) and mice (Olavarria & Montero, 1989; Wang & Burkhalter, 2007; Garrett et al., 2014; Roth et al., 2012). More detailed experiments will be necessary to correlate labeling in

medial cortex with the architectonic subdivisions recognized by Fleishhauer et al. (1980) in this region.

In addition to areas V1 and V2, a previous physiological study (Woolsey et al., 1974) described three small visual areas in regions corresponding approximately to areas AL and LLa in the present study. Further posteriorly, the same study described an additional small area in regions that may correspond to area PL or TP in this study. These findings support the notion that areas identified anatomically in the rabbit likely correspond to separate representations of the visual field, as it has been demonstrated in the rat and mice. Additional studies combining electrophysiological and anatomical methods will be required to further explore the topography and interconnectivity of the areas identified in this and previous anatomical studies (Montero, 1981; Müller-Paschinger & Tömböl, 1989).

Conclusion

Our study provides further information about the location and topography of extrastriate areas connected with V1 in the rabbit, and relates these areas to the patterns of callosal connections and myeloarchitecture. Our results should facilitate the interpretation of additional mapping and hodological data obtained in the rabbit with electrophysiological and other techniques, and contribute toward comparative studies of the organization of visual cortex in mammals. In view of the similarity that appears to exist between rabbits, rats and mice, the rabbit offers an alternative model for further studies of the "rodent" visual cortical plan, especially for projects benefiting from a larger brain.

Figure 21: Cortical injections of HRP and fluorescent tracers.

A. Areas stained with HRP reaction product following multiple cortical injections of this enzyme. Arrows indicate borders of V1. The dLGN and LP are densely and homogeneously labeled by the transport of HRP (from case albino 86-21, Figure 25). Lateral is to the left, ventral is down. **B**. Topographic retrograde labeling in dLGN and LP (lower panel) following injections of FB (blue) and red beads into V1 (upper panel) (from case albino 86-20, Figure 28). Lateral is to the right, ventral is down. dLGN: dorsal lateral geniculate nucleus, LP: latero posterior nucleus of the thalamus. Sale bars = 2 mm.

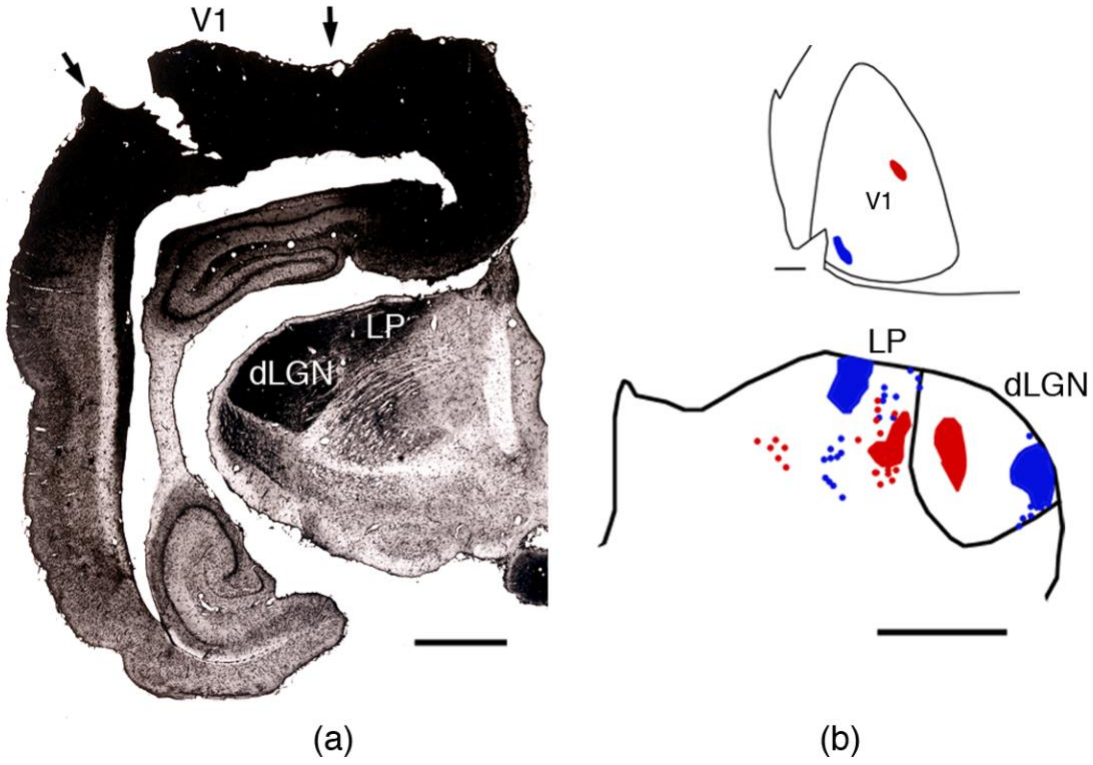

(a) (b)

Figure 22: Myeloarchitectonic and cytoarchitectonic borders. Case albino 86-20.

A. Cortical myeloarchitecture. Arrows and arrowheads indicate areas of dense myelination. **B.** Relation of myelination pattern to cytoarchitectonic map. Segmented line indicates the lateral sulcus. Medial is to the left, posterior is down. Oc: area occipitalis, Te: area temporalis, Prh: area perirhinalis, Poc: area postcentralis, 29d: cingulate area 29d, S1: primary somatosensory cortex, S2: secondary somatosensory cortex, A: auditory cortex. Scale bar = 2 mm.

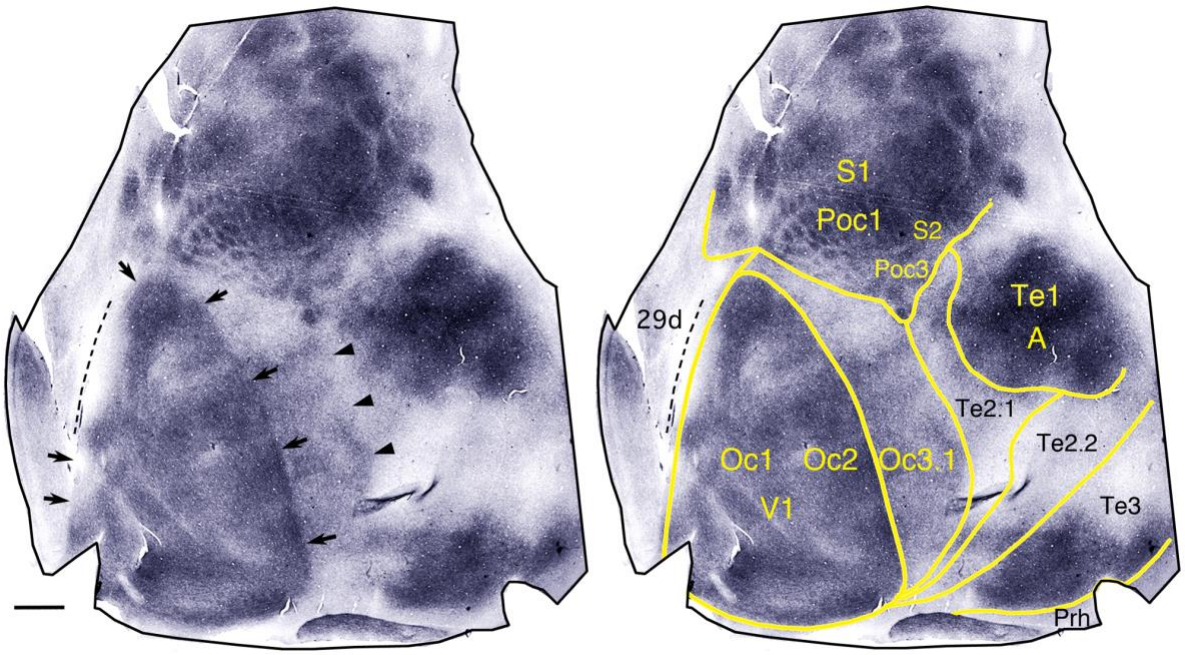

(a) (b)

Figure 23: Patterns of callosal connections in the right hemisphere revealed following multiple injections of HRP into the opposite hemisphere. (**A.** and **B.**) Albino rabbits (cases 86-12 and 87-1, respectively). (**C.-E.**) Dutch belted rabbits (cases R53, R5 and R6, respectively). Arrows indicate bead-like patches. Opposing arrows in (**B**) illustrate a double patch. Numbers indicate corresponding areas in the five cases shown. Medial is to the left, posterior is down. Scale bar = 2 mm.

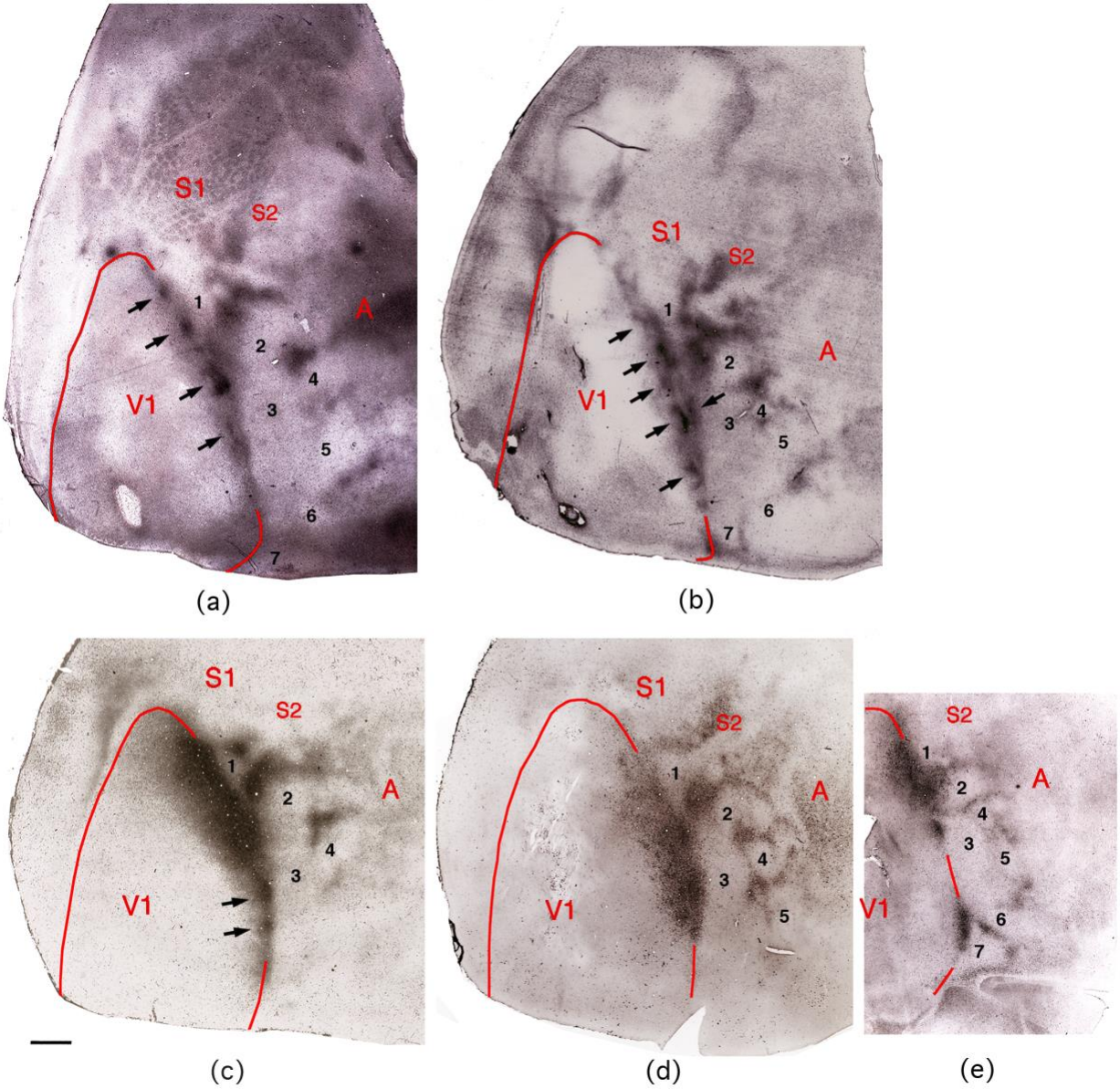
S1
S2
A
V1
1
2
3
4
5
6
7
(a)
(b)
(c)
(d)
(e)

Figure 24: Schematic map of the visual field in right rabbit V1 showing the approximate locations within V1 of 14 tracer injections performed in 5 albino rabbits.

The representation of the horizontal meridian is approximate. All injections in the same animal are represented by the symbol next to the respective case number. The tracers used in each animal are indicated in the text. HM: horizontal meridian, VM: vertical meridian.

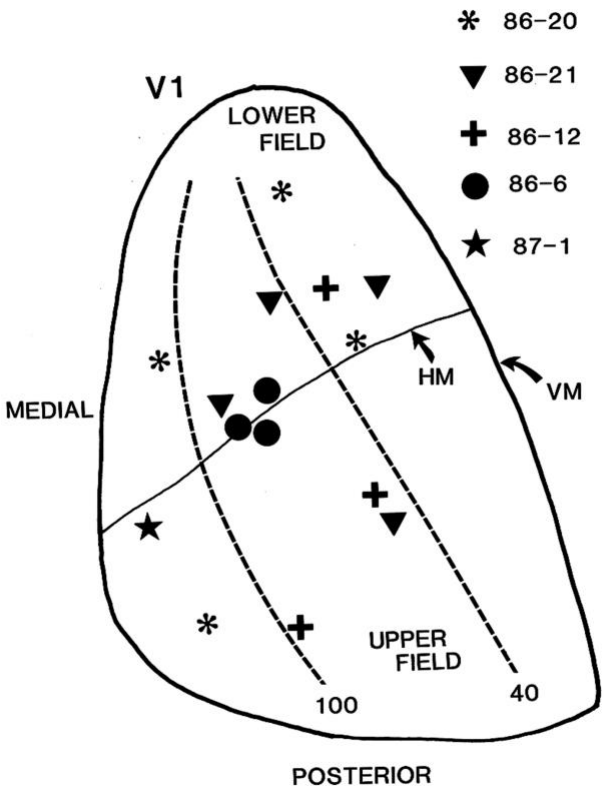
86-20
86-21
86-12
86-6
87-1
V1
LOWER FIELD
HM
VM
MEDIAL
UPPER FIELD
100
40
POSTERIOR

Figure 25: Data from case 86-21.

A. Labeling pattern following a mediolateral sequence of tritiated proline (black outlines), GB (green) and FB (blue) injections across V1. Callosal connections are indicated in grey. **B.** Addition of a posterior injection of RB (red) illustrates the labeling pattern resulting from an anteroposterior sequence of injections. Arrows indicate tentative visual areas. **C.** Summary of tentative visual areas identified from this case. AL: anterolateral, LM: lateromedial, PL: posterolateral, P: posterior, LLa: laterolateral anterior, LI: laterointermediate. Scale bars = 2 mm.

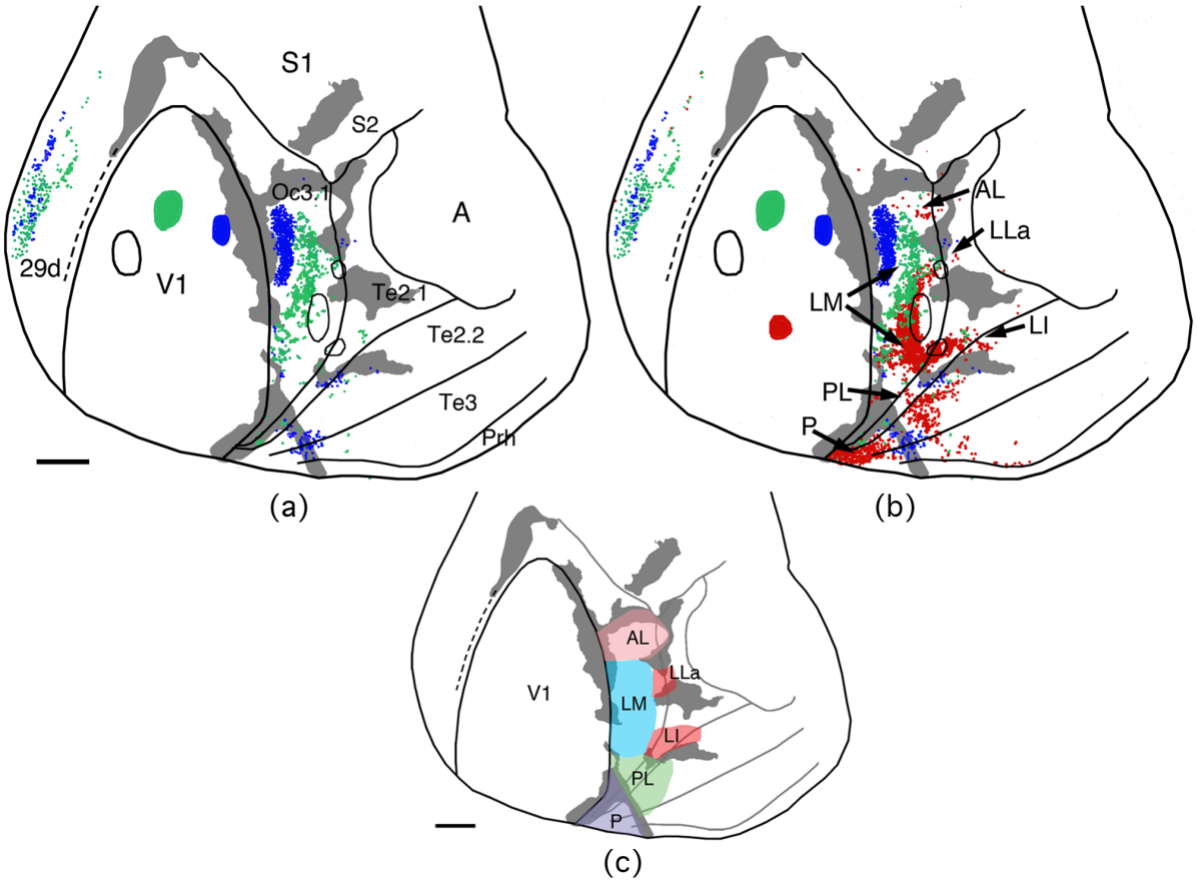
S1
S2
Oc3.1
A
29d
V1
Te2.1
Te2.2
Te3
Prh
(a)
AL
LLa
LM
LI
PL
P
(b)
V1
AL
LLa
LM
LI
PL
P
(c)

Figure 26: Labeling pattern produced by three closely spaced injections of RB, GB and FB (case 86-6).

A mirror-image reversal of the RB-FB-GB labeling sequence (arrow) suggests the location of the LM/LI border. Medial is to the left, posterior is down. TP: temporal posterior area. Scale bar 2 = mm.

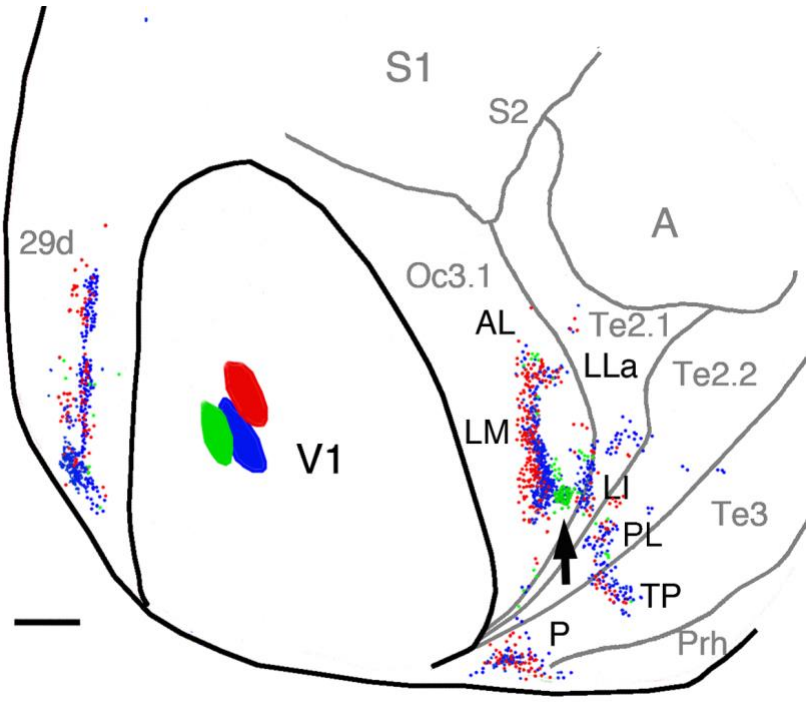
S1
S2
A
29d
Oc3.1
AL
Te2.1
LLa
Te2.2
LM
V1
LI
Te3
PL
TP
P
Prh

Figure 27: Data from case 86-12.

A. and **B.** Labeling pattern resulting from an anteroposterior sequence of FB and RB injections. Callosal pattern (shown in Figure 23A) is indicated in grey. Medial is to the left, posterior is down. Scale bar = 2 mm.

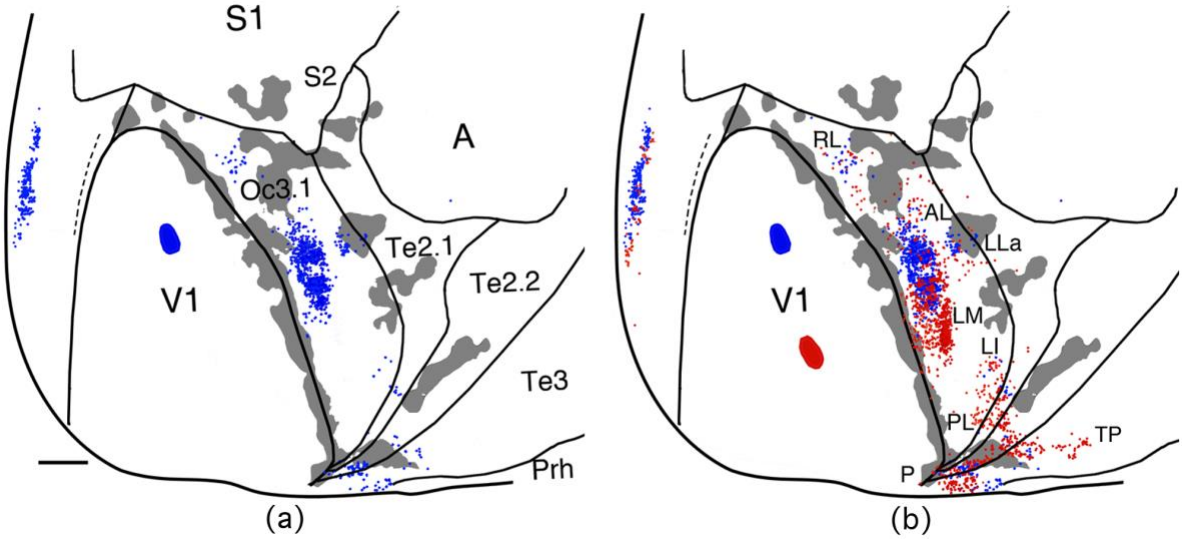
S1
S2
A
Oc3.1
Te2.1
Te2.2
Te3
V1
Prh
(a)
RL
AL
LLa
V1
LM
LI
PL
TP
P
(b)

Figure 28: Data from case 86-20.

A. The myelin pattern (also shown in Figure 2(a)) is related to the callosal pattern (yellow contour) and to labeling resulting from injections of tritiated proline, RB and FB. **B.** The location of putative visual areas is indicated. Callosal pattern represented in grey. Medial is to the left, posterior is down. Scale bar = 2 mm.

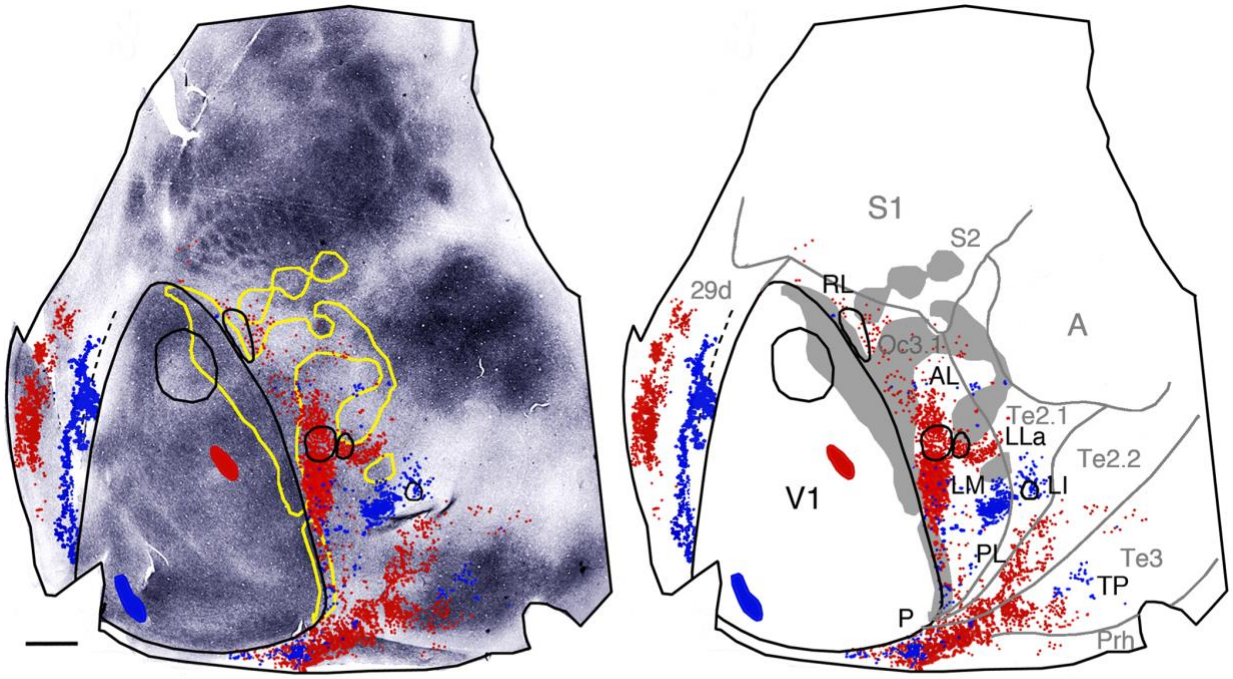

(a) (b)

Figure 29: Tentative diagram of rabbit visual areas and topography derived from present study, and comparison with the rat.

A. and **B.** The callosal pattern (grey) is based on case 86-21 (Figure 25). **A.** Location and name of putative visual areas. M: medial area. **B.** Approximate representations of the mediolateral (red arrows) and anteroposterior (blue arrows) axes in V1. Lack of arrows indicates insufficient data. **C.** Diagram of rat visual areas based on physiological and anatomical studies. Callosal pattern is represented in grey. A: anterior area, AM: anteromedial area, PM: posteromedial area, PR: pararhinal area. Scale bars = 2 mm.

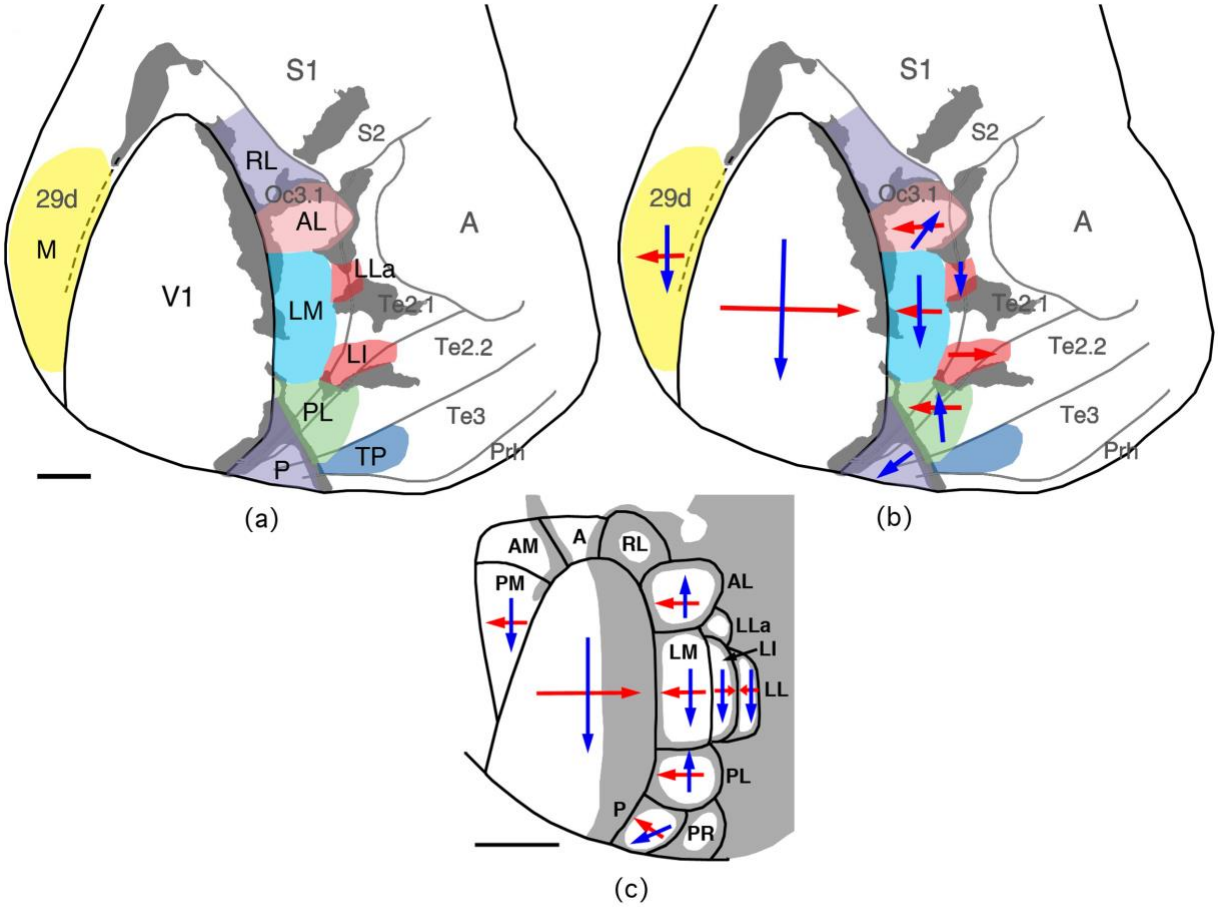
S1
S2
RL
Oc3.1
AL
A
29d
M
V1
LM
LLa
Te2.1
LI
Te2.2
PL
Te3
TP
P
Prh
(a)
S1
S2
29d
Oc3.1
A
Te2.1
Te2.2
Te3
Prh
(b)
AM
A
RL
PM
AL
LLa
LI
LM
LL
PL
P
PR
(c)

SUMMARY AND CONCLUSIONS

Previous studies in albino rats reported that a narrow region in lateral striate cortex (V1) is highly binocular, and that input from the ipsilateral eye to this region comes through the callosum. In contrast, a recent study in pigmented Long Evans rats showed that this region is nearly exclusively dominated by responses from the contralateral eye even though it is richly innervated by the callosum. Here, in experiment 1, we replicated the previous results in albino rats, and tested the hypothesis that the inability of callosal connections to relay input from the ipsilateral eye to lateral striate cortex in Long Evans rats is a consequence of both the existence of ocular dominance columns (ODCs) in V1, and the segregation of callosal connections into patches overlapping ipsilateral ODCs in the binocular region of V1 (Laing et al., 2015). We predicted that in albino rats, input from both eyes intermix in the binocular region, without segregating into ODCs, and that callosal connections are not patchy as in Long Evans rats. Retinal input to V1 was revealed using the transneuronally transported tracer WGA-HRP, and callosal connections were revealed using cortical injections of anatomical tracers. Confirming our predictions, we found that inputs from both eyes are intermixed in the binocular zone, without segregating into ODCs. Similarly, we found that callosal connections in albino rats are not patchy, but instead are distributed throughout the binocular segment and LS. We propose that, as a consequence of these changes, the binocular region in albino rats includes lateral striate cortex, being therefore larger in size than the binocular region in Long Evans rats. Our findings provide insight about the role of callosal connections in generating binocular cells, and suggest that albino rats may be a useful model for studying factors that regulate the segregation of eye specific input in mammalian visual cortex, as well as the spatial correlation between eye specific domains and callosal connections in striate cortex.

Blindness early in life induces permanent alterations in brain anatomy, including dramatic reductions in the surface area of primary visual cortex (V1). Bilateral enucleations early in development caused greater reductions in primary visual cortex surface area than do enucleations at later times. However, the time at which cortical surface area expansion is no longer sensitive to enucleation has not been clearly established in previous studies, despite being an important milestone for visual cortical development. Using histological and MRI techniques, we investigated, in experiment 2, how reductions in the surface area of V1depends on the timing of blindness onset in rats, ferrets and humans. To compare data across species, we translated the post-conception ages of each species to a common neurodevelopmental event-time scale. We found that the relationship between V1 surface area and the age of blindness onset is strikingly similar across species. Blindness starting early during cortical expansion induces large reductions in V1 surface area, as much as 40% in rats and ferrets, while blindness occurring at later event times has progressively smaller effects. Moreover, the period of susceptibility to blindness as a function of age of deprivation onset is remarkably consistent across species. Longitudinal measurements confirmed that enucleation early in development severely disrupted cortical expansion. Our results also show that the critical period for the effect of blindness on V1 surface area ends well before the visual cortex reaches its normal, mature size. By incorporating extant data from other species, we further refined the estimates of the end of the critical period for the effect of visual deprivation on the surface area of V1, and generalized the observation that this critical period closes before expansion of visual cortex is complete. These findings will further our understanding of the mechanisms controlling cortical growth, and guide the interpretation of the effects of blindness onset on human cortical development.

Previous studies in rabbits identified an array of extrastriate cortical areas anatomically connected with V1, but did not describe their internal topography. To address this issue, in experiment 3 we injected multiple anatomical tracers into different regions in V1 of the same animal and analyzed the topography of resulting extrastriate labeled fields with reference to the patterns of callosal connections and myeloarchitecture revealed in tangential sections of the flattened cortex. Our results extend previous studies and provide further evidence that rabbit extrastriate areas resemble the visual areas in rats and mice not only in their general location with respect to V1, but also in their internal topography. Moreover, extrastriate areas in the rabbit maintain a constant relationship with myeloarchitectonic borders and features of the callosal pattern. These findings highlight the rabbit as an alternative model to rats and mice for advancing our understanding of cortical visual processing in mammals, especially for projects benefiting from a larger brain.

BIBLIOGRAPHY FOR CHAPTER 1

Antonini, A., Fagiolini, M., & Stryker, M.P. (1999, June, 1). Anatomical correlates of functional plasticity in mouse visual cortex. *Journal of Neuroscience, 19*(11), 4388-4406. https://doi-org.offcampus.lib.washington.edu/10.1523/JNEUROSCI.19-11-04388.1999.

Bosking, W.H., Kretz, R., Pucak, M.L., & Fitzpatrick, D. (2000, March, 15). Functional specificity of callosal connections in tree shrew striate cortex. *Journal of Neuroscience, 20*(6), 2346-2359. https://doi-org.offcampus.lib.washington.edu/10.1523/JNEUROSCI.20-06-02346.2000.

Casagrande, V.A. & Harting, J.K. (1975, October, 17). Transneuronal transport of tritiated fucose and proline in the visual pathways of tree shrew Tupaia glis. *Brain Research, 96*(2), 367-372. https://doi.org/10.1016/0006-8993(75)90749-0.

Conde-Ocaziones, S., Altavini, T.S., Wunderle, T., & Schmidt, K.E. (2018, February). Motion contrast in primary visual cortex: A direct comparison of single neuron and population encoding. *European Journal of Neuroscience, 47*(4), 358-369. https://doi-org.offcampus.lib.washington.edu/10.1111/ejn.13786.

Cusick, C.B., & Lund, R.D. (1981). The distribution of the callosal projection to the occipital visual cortex in rats and mice. *Brain. Res. 214*:239-259.

Cusick, C.G., MacAvoy, M.G., & Kaas, J.H. (1985, May, 1). Interhemispheric connections of cortical sensory areas in tree shrews. *The Journal of Comparative Neurology, 235*(1), 111-128. https://doi-org.offcampus.lib.washington.edu/10.1002/cne.902350109.

Diao, Y.C., Wang, Y.K., & Pu, M.L. (1983). Binocular responses of cortical cells and the callosal projection in the albino rat. *Experimental Brain Research, 49*(3), 410-418.

Diao Y.C., Xiao Y.M., Bu M.L. (1987) Callosal projections in the visual cortex and the vertical meridian of the visual field in the albino rat. *Scientia Sinica, Series B* 30(2):141-8.

Laing, R.J., Bock, A.S., Lasiene, J., & Olavarria, J.F. (2012, October, 1). Role of retinal input on the development of striate–extrastriate patterns of connections in the rat. *The Journal of Comparative Neurology, 520,* 3256-3276. doi: 10.1002/cne.23096.

Laing, R.J., Turecek, J., Takahata, T., & Olavarria, J.F. (2015, October). Identification of eye-epecific domains and their relation to callosal connections in primary visual cortex of Long Evans rats. *Cerebral Cortex, 25*(10), 3314-3329. DOI: 10.1093/cercor/bhu128.

Lund, R.D. (1965, September, 24). Uncrossed visual pathways of hooded and albino rats. *Science, 149*(3691), 1506-1507. doi: 10.1126/science.149.3691.1506.

Marzi, C.A., Antonini, A., Di Stefano, M., & Legg, C.R. (1980, September, 15). Callosum-dependent binocular interactions in the lateral suprasylvian area of Siamese cats which

lack binocular neurons in areas 17 and 18. *Brain Research, 197(1),* 230-235. https://doi.org/10.1016/0006-8993(80)90450-3.

Mesulam, M.M. (1978, February, 1). Tetramethyl benzidine for horseradish peroxidase neurohistochemistry: a non-carcinogenic blue reaction product with superior sensitivity for visualizing neural afferents and efferents. *Journal of Histochemistry and Cytochemistry, 26(2),* 106-117. DOI: 10.1177/26.2.24068.

Minciacchi, D., & Antonini, A. (1984, August). Binocularity in the visual cortex of the adult cat does not depend on the integrity of the corpus callosum. *Behavioral Brain Research, 13(2),* 183-192. https://doi.org/10.1016/0166-4328(84)90148-7.

Olavarria, J.F., & Van Sluyters, R.C. (1985, September, 1). Organization and postnatal development of callosal connections in the visual cortex of the rat. *The Journal of Comparative Neurology, 239(1),* 1-26. https://doi-org.offcampus.lib.washington.edu/10.1002/cne.902390102.

Olavarria, J.F. (2001, May, 14). Callosal connections correlate preferentially with ipsilateral cortical domains in cat areas 17 and 18, and with contralateral domains in the 17/18 transition zone. *The Journal of Comparative Neurology, 433(4),* 441-457. https://doi-org.offcampus.lib.washington.edu/10.1002/cne.1152.

Olavarria, J.F. (2002). Influence of topography and ocular dominance on the functional organization of callosal connections in cat striate cortex. in *The Cat Primary Visual Cortex*, B. Payne, and A. Peters, eds., Academic Press, New York, USA, 259-294.

Pettigrew, J.D., Ramachandran, V.S., & Bravo, H. (1984). Some neural connections subserving binocular vision in ungulates. *Brain, Behavior and Evolution, 24(2-3),* 65-93. https://doi-org.offcampus.lib.washington.edu/10.1159/000121306.

Richter, C.P., & Warner, C.L. (1974, March). Comparison of Weigert stained sections with unfixed, unstained sections for study of myelin sheaths. *Proceedings of the National Academy of Sciences of the United States of America, 71(3)*, 598-601.

Routtenberg, A. & Glickman, S.E. (1964, August). Visual Behavior in albino and hooded rats. *Journal of Comparative and Phyiological Psychology, 58,* 140-142.

Ruthazer, E.S., Basker, G.E., Stryker, M.P. (1999). Development and organization of ocular dominance bands in primary visual cortex of the sable ferret. *Journal of Comparative Neurology, 407*:151–165.

Thurlow, G.A., & Cooper, R.M. (1988, August, 22). Metabolic activity in striate and extrastriate cortex in the hooded rat: Contralateral and ipsilateral eye input. *The Journal of Comparative Neurology, 274(4),* 595-607. https://doi-org.offcampus.lib.washington.edu/10.1002/cne.902740408.

White, L.E., Bosking, W.H., Williams, S.M., & Fitzpatrick, D. (1999). Maps of central visual space in ferret V1 and V2 lack matching inputs from the two eyes. *Journal of Neuroscience, 19*:7089–7099.

Zeki, S., & Fries, W. (1980, February, 29). A function of the corpus callosum in the Siamese cat. *Proceeding of the Royal Society of London B: Biological Sciences 207(1167),* 249-258.

BIBLIOGRAPHY FOR CHAPTER 2

Andrews, T.J., Halpern, S.D., & Purves, D. (1997). Correlated size variations in human visual cortex, lateral geniculate nucleus, and optic tract. *Journal of Neuroscience, 17:*2859-2868.

Anurova, I., Renier, L.A., DeVolder, A.G., Carlson, S., & Rauschecker, J.P. (2015). Relationship between cortical thickness and functional activation in the early blind. *Cerebral Cortex, 25:*2035-2048.

Bock, A.S. & Olavarria, J.F. (2011). Neonatal enucleation during a critical period reduces the precision of cortico-cortical projections in visual cortex. *Neuroscience Letters 501*:152-156.

Bock, A.S., Kroenke, C.D., Taber, E.N., & Olavarria, J.F. (2012). Retinal input influences the size and corticocortical connectivity of visual cortex during postnatal development in the ferret. *The Journal of Comparative Neurology, 520*:914-932.

Bock, A.S., Olavarria, J.F., Leigland, L.A., Taber, E.N., Jespersen, S.N., & Kroenke, C.D. (2010). Diffusion tensor imaging detects early cerebral cortex abnormalities in neuronal architecture induced by bilateral neonatal enucleation: An experimental model in the ferret. *Frontiers in Systems Neuroscience, 4:*Article 149.

Bock, A.S., Binda, P., Benson, N.C., Bridge, H., Watkins, K.E., & Fine, I. (2015). Resting-State Retinotopic Organization in the Absence of Retinal Input and Visual Experience. *Journal of Neuroscience, 35*(36):12366-82.

Bridge, H., Cowey, A., Ragge, N., & Watkins, K. (2009). Imaging studies in congenital anophthalmia reveal preservation of brain architecture in 'visual' cortex. *Brain, 132*:3467-3480.

Clancy, B., Kersh, B., Hyde, J., Darlington, R.B., Anand, K.F.S., & Finlay, B.L. (2007). Web-based method for translating neurodevelopment from laboratory species to humans. *Neuroinformatics, 5*:79-94.

Dale, A.M., Fischl, B., & Sereno, M.I. (1999). Cortical surface-based analysis. I. Segmentation and surface reconstruction. *NeuroImage, 9*:179-194.

Darlington, R.B., Dunlop, S.A., & Finlay, B.L. (1999). Neural development in metatherian and eutherian mammals: Variation and constraint. *The Journal of Comparative Neurology, 411:*359-368.

Dehay, C. & Kennedy, H. (2007). Cell-cycle control and cortical development. *Nature Reviews Neuroscience, 8:*438-450.

Dehay, C., Savatier, P., Cortay, V., & Kennedy, H. (2001). Cell-cycle kinetics of neocortical precursors are influenced by embryonic thalamic axons. *Journal of Neuroscience, 21*:201-214.

Dehay, C., Horsburgh, G., Berland, M., Killackey, H., & Kennedy, H. (1989). Maturation and connectivity of the visual cortex in monkey is altered by prenatal removal of retinal input. *Nature, 337*:265-267.

Dehay, C., Horsburgh, G., Berland, M., Killackey, H., & Kennedy, H. (1991). The effects of bilateral enucleation in the primate fetus on the parcellation of visual cortex. *Developmental Brain Research, 62:*137-141.

Dehay, C., Giroud, P., Berland, M., Killackey, H., & Kennedy, H. (1996). Contribution of thalamic input to the specification of cytoarchitectonic cortical fields in the primate: effects of bilateral enucleation in the fetal monkey on the boundaries, dimensions, and gyrification of striate and extrastriate cortex. *The Journal of Comparative Neurology, 367:*70-89.

Duffy, K.R., Murphy, K.M., & Jones, D.G. (1998). Analysis of the postnatal growth of visual cortex. *Visual Neuroscience, 15:*831-839.

Duncan, R.O. & Boynton, G.M. (2003). Cortical magnification within human primary visual cortex correlates with acuity thresholds. *Neuron, 38*(4), 659-671.

Finlay, B.L. & Darlington, R.B. (1995). Linked regularities in the development and evolution of mammalian brains. *Science, 268:*1578-1584.

Fischl, B., Rajendran, N., Busa, E., Augustinack, J., Hinds, O., Yeo, B.T.T., Mohlberg, H., Amunts, K., & Zilles, K. (2008). Cortical folding patterns and predicting cytoarchitecture. *Cerebral Cortex, 18:*1973-1980.

Giedd, J.N., Raznahan, A., Alexander-Bloch, A., Schmitt, E., Gogtay, N., & Rapoport, J.L. (2015). Child psychiatry branch of the National Institute of Mental Health longitudinal structural magnetic resonance imaging study of human brain development. *Neuropsychopharmacology, 40*:43-49.

Herrmann, K., Antonini, A., & Shatz, C.J. (1994). Ultrastructural evidence for synaptic interactions between thalamocortical axons and subplate neurons. *European Journal of Neuroscience, 6:*1729-1742.

Huttenlocher, P.R. (1990). Morphometric study of human cerebral cortex development. *Neuropsychology, 28:*517-527.

Jiang, F., Stecker, G.C., Boynton, G.M., & Fine, I. (2016). Early Blindness Results in Developmental Plasticity for Auditory Motion Processing within Auditory and Occipital Cortex. *Frontiers in Human Neuroscience, 10:*324.

Jiang, J., Zhu, W., Shi, F., Liu, Y., Li, J., Qin, W., Li, K., Yu, C., & Jiang, T. (2009). Thick visual cortex in the early blind. *Journal of Neuroscience, 29:*2205 -2211.

Johnson, J.K. & Casagrande, V.A. (1993). Prenatal development of axon outgrowth and connectivity in the ferret visual system. *Visual Neuroscience, 10:*117-130.

Kalia, A., Lesmes, L.A., Dorr, M., Gandhi, T., Chatterjee, G., Ganesh, S., & Sinha, P. (2014). Development of pattern vision following early and extended blindness. *Proceedings of the National Academy of Sciences of the United States of America*, *111*(5), 2035-9.

Karlen, S.J. & Krubitzer, L. (2009). Effects of bilateral enucleation on the sizes of visual and nonvisual areas of the brain. *Cerebral Cortex, 19*:1360-1371.

Knutsen, A.K., Kroenke, C.D., Chang, Y.V., Taber, L.A., & Bayly, P.V. (2013). Spatial and temporal variations of cortical growth during gyrogenesis in the developing ferret brain. *Cerebral Cortex, 23:*488-498.

Laing, R.J., Bock, A.S., Lasiene, J., & Olavarria, J.F. (2012). Role of retinal input on the development of striate-extrastriate patterns of connections in the rat. *Journal of Comparative Neurology, 520:*3256-3276.

Laing, R.J., Turecek, J., Takahata, T., Olavarria, J.F. (2015). Identification of eye-specific domains and their relation to callosal connections in primary visual cortex of Long Evans rats. *Cerebral Cortex 25:*3314-3329.

Lepore, N., Voss, P., Lepore, F., Chou, Y-Y., Fortin, M., Gougoux, F., Lee, A.D., Brun, C., Lassonde, M., Madsen, S.K., Toga, A.W., Thompson, P.M. (2010). Brain structure changes visualized in early-and late-onset blind subjects. *NeuroImage 49:*134-140.

Massé, I.O., Guillemette, S., Laramée, M-E., Bronchti, G., Boire, D. (2014). Strain differences of the effect of enucleation and anophthalmia on the size and growth of sensory cortices in mice. *Brain Research, 1588:*113-126.

Missler, M., Eins, S., Merker, H-J., Rothe, H., Wolff, J.R. (1993). Pre- and postnatal development of the primary visual cortex of the common marmoset. I. A changing space for synaptogenesis. *The Journal of Comparative Neurology, 333:*41-52.

Moreno-Juan, V., Filipchuk, A., Antón-Bolaños, N., Mezzera, C.1., Gezelius, H., Andrés, B., Rodríguez-Malmierca, L., Susín, R., Schaad, O., Iwasato, T., Schüle, R., Rutlin, M., Nelson, S., Ducret, S., Valdeolmillos, M., Rijli, F.M., López-Bendito, G. (2017). Prenatal thalamic waves regulate cortical area size prior to sensory processing. *Nature Communications, 8:*14172.

Munzel, U. & Hothorn, L.A. (2001). A unified approach to simultaneous rank test procedures in the unbalanced one-way layout. *Journal of Biometrics, 43:*553-569.

Olavarria, J.F., Malach, R., VanSluyters, R.C. (1987). Development of visual callosal connections in neonatally enucleated rats. *The Journal of Comparative Neurology, 260:*321-348.

Olavarria, J., Van Sluyters, R.C.. (1985). Organization and post- natal development of callosal connections in the visual cortex of the rat. *The Journal of Comparative Neurology, 239:*1–26.

Olavarria, J., Van Sluyters, R.C. (1995). Overall pattern of callosal connections in visual cortex of normal and enucleated cats. *The Journal of Comparative Neurology, 363:*161-176.

Olavarria, J.F. & Hiroi, R. (2003). Retinal influences specify cortico-cortical maps by postnatal day six in rats and mice. *The Journal of Comparative Neurology, 459:*156-172.

Olavarria, J.F., Bock, A.S., Leigland, L.A., & Kroenke, C.D. (2012). Deafferentation-induced plasticity of visual callosal connections: predicting critical periods and analyzing cortical abnormalities using diffusion tensor imaging. *Neural Plasticity:* Article 250196.

Park, H-J., Lee, J.D., Kim, E.Y., Park, B., Oh, M-K., Lee, S.C., & Kim, J-J. (2009). Morphological alterations in the congenital blind based on the analysis of cortical thickness and surface area. *NeuroImage, 47:*98-106.

Purves, D. & LaMantia, A. (1993). Development of blobs in the visual cortex of macaques. *The Journal of Comparative Neurology, 334:*169-175.

Ptito, M., Schneider, F.C.G., Paulson, O.B., & Kupers, R. (2008) Alterations of the visual pathways in congenital blindness. E*xperimental Brain Research, 187:*41-49.

Rakic, P. (1988). Specification of cerebral cortical areas. *Science, 241:*170-176

Rakic, P., Suner, I., & Williams, R.W. (1991). A novel cytoarchitectonic area induced experimentally within the primate visual cortex. *Proceedings of the National Academy of Science, 88:*2083-2087.

Raznahan, A., Shaw, P., Lalonde, F., Stockman, M., Wallace, G.L., Greenstein, D., Clasen, L., Gogtay. N., & Giedd, J.N. (2011). How does your cortex grow? *Journal of Neuroscience, 31:*7174-7177.

Reillo, I., Romero, C.D.J., Garcia-Cabezas, M.A., & Borrell, V. (2011). A role for intermediate radial glia in the tangential expansion of the mammalian cerebral cortex. *Cerebral Cortex, 21:*1674-1694.

Richter, C.P. & Warner, C.L. (1974) Comparison of Weigert stained sections with unfixed, unstained sections for study of myelin sheaths. *Proceedings of the National Academy of Sciences, 71:*598-601.

Stevens, A.A., Snodgrass, M., Schwartz, D., Weaver, K. (2007). Preparatory activity in occipital cortex in early blind humans predicts auditory perceptual performance. *Journal of Neuroscience, 40:*10734-10741.

Sugita, S., Otani, K. (1984). Quantitative analysis of the striate cortex in the mutant microphthalmic rat. *Experimental Neurology, 85:*584-596.

Verma, A.S., Fitzpatrick, D.R. (2007). Anophthalmia and microphthalmia. *Orphanet Journal of Rare Diseases, 2:*47.

Workman, A.D., Charvet, C.J., Clancy, B., Darlington, R.B., Finlay, B.L. (2013). Modeling transormations of neurodevelopmental sequences across mammalian species. *Journal of Neuroscience, 33:*7368-7383.

Yuodelis, C., & Hendrickson, A. (1986). A qualitative and quantitative analysis of the human fovea during development. *Visual Research, 26*(6), 847-855.

BIBLIOGRAPHY FOR CHAPTER 3

Bousfield, J.D. (1977). Columnar organization and the visual cortex of the rabbit. *Brain Research, (136)*1, 154-158.

Bousfield, J.D. (1978). Some properties of extrastriate visual units in the cortex of the rabbit. *Brain Research, (149)*2, 365-378.

Bravo, H., Olavarria, J., & Martinich, S. (1990). Patterns of interhemispheric and striate-peristriate connections in visual cortex of the Southamerican marsupial *Marmosa elegans* (mouse opossum). *Anatomy and Embryology, (182)*6, 583-589.

Choudhury, B.P., & Gent, J.P. (1973). The corpus callosum and the rabbit's visual cortex. *Brain Research, (52),* 433-436.

Clarke, R.J., Datskovsky, B.W., Grigonis, A.M., & Murphy, E.H. (1992). Transcallosally evoked responses in the visual cortex of normal and monocularly enucleated rabbits. *Experimental Brain Research, (91)*2, 296-302.

Cowan, W.M., Gottlieb, D.I., Hendrickson, J.L., Price, J.L., & Woolsey, T.A. (1972). The autoradiographic demonstration of axonal connections in the central nervous system. *Brain Research, (37)*1, 21-51.

Cowey, A., & Perry, V.H. (1979). The projection of the temporal retina in rats, studied by retrograde transport of horseradish peroxidase. *Experimental Brain Research, (35)*3, 457-464.

Chai, X., Li, L., Wu, K., Zhou, C., Cao, P., & Ren. Q. (2008). C-sight visual prostheses for the blind. *IEEE Engineering in Medicine and Biology Magazine, (27)*5, 20-28.

Coogan, T.A., & Burkhalter, A. (1993). Hierarchical organization of areas in rat visual cortex. *Journal of Neurosci*ence, (13)9, 3749–3772.

Dias, I.A., Bahia, C.P., Franca, J.G., Houzel, J.C., Lent, R., Mayer, A.O., Santiago, L.F., Silveira, C.L., Picanço-Diniz, C.W., & Pereira, A. (2014). Topography and architecture of visual and somatosensory areas of the agouti. *Journal of Comparative Neurology, (522)*11, 2576-2593.

Espinoza, S.G., Thomas, H.C. (1983). Retinotopic organization of striate and extrastriate visual cortex in the hooded rat. *Brain Research*, 272(1), 137–144.

Fleischhauer, K., Zilles, K., & Schleicher, A. (1980). A revised cytoarchitectonic map of the neocortex of the rabbit (*Oryctolagus cuniculus*). *Anatomy and Embryology, (161)* 2, 121-143.

Gallyas, F. (1979). Silver staining of myelin by means of physical development. *Neurological Research, (1)*2, 203–209.

Garrett, M.E., Nauhaus, I., Marshel, J.H. & Callaway, E.M. (2014). Topography and areal organization of mouse visual cortex. *Journal of Neuroscience*, 34(37), 12587–12600.

Glickfeld, L.L., Reid, R.C., & Andermann, M.L. (2014). A mouse model of higher visual cortical function. *Current Opinion in Neurobiology, (24)*1, 28–33.

Gould, H.J. III. (1984). Interhemispheric connections of the visual cortex in the grey squirrel (*Sciurus carolinensis*). *Journal of Comparative Neurology, (223)*2, 259-301.

Holländer, H., & Hälbig, W. (1980). Topography of retinal representation in the rabbit cortex: an experimental study using transneuronal and retrograde tracing techniques. *Journal of Comparative Neurology*, (193)3, 701-710.

Hughes, A., & Wilson, M.E. (1969). Callosal terminations along the boundary between visual areas I and II in the rabbit. *Brain Research, (12)*1, 9-25.

Hughes, A., & Vaney, D.I. (1982). The organization of binocular cortex in the primary visual area of the rabbit. *Journal of Comparative Neurology, (204)*2, 151-164.

Jijiwa, H. (1973). Binocular and callosal areas of the visual system of the rabbit. *The Japanese Journal of Physiology, (23)*5, 465-476.

Kaas, J.H., Krubitzer, L.A., & Johanson. K.L. (1989). Cortical connections of areas 17 (V-I) and 18 (V-II) of squirrels. *Journal of Comparative Neurology, (281)*3, 426-446.

Kaas, J.H. & Balaram, P. (2014). Current research on the organization and function of the visual system in primates. *Eye and Brain*, (6)1, 1-4.

Laing, R.J., Bock, A.S., Lasiene, J., & Olavarria, J.F. (2012). Role of retinal input on the development of striate-extrastriate patterns of connections in the rat. *Journal of Comparative Neurology, (520)*14, 3256-3276.

Laing, R.J., Turecek, J., Takahata, T., & Olavarria, J.F. (2014). Identification of eye-specific domains and their relationship to callosal connections in primary visual cortex of Long Evans rats. *Cerebral Cortex*, Jun 26; pii: bhu128. [Epub ahead of print].

Laramée, M.E. & Boire, D. (2015). Visual cortical areas of the mouse: comparison of parcellation and network structure with primates. *Frontiers in Neural Circuits*, (8), article 149.

Ledoux, M.S., Whitworth R.H. Jr., & Gould, H.J. III (1987). Interhemispheric connections of the somatosensory cortex in the rabbit. *Journal of Comparative Neurology,* (258)1, 145-157.

Marshel, J.H., Garrett, M.E., Nauhaus, I., & Callaway, E.M. (2011). Functional specialization of seven mouse visual cortical areas. *Neuron*, vol. 72, no. 6, pp. 1040–1054, 2011.

Martinich, S., Pontes, M.N., & Rocha-Miranda, C.E. (2000). Patterns of corticocortical, corticotectal, and commissural connections in the opossum visual cortex. *Journal of Comparative Neurology, (416)*2, 224-244.

Mathers, L.H., Douville, A., & Chow, K.L. (1977). Anatomical studies of a temporal visual area in the rabbit. *Journal of Comparative Neurology, (171)*2, 147-156.

Mesulam, M.M. (1978). Tetramethyl benzidine for horseradish peroxidase neurohistochemistry: A non-carcinogenic blue reaction-product with superior sensitivity for visualizing neural afferents and efferents. *Journal of Histochemistry and Cytochemistry, (26)*2, 106-117.

Miller, M.J., Weiss, C. Song, X., Iordanescu, G., Disterhoft, J.F., & Wyrwicz, A.M. (2008). Functional magnetic resonance imaging of delay and trace eyeblink conditioning in the primary visual cortex of the rabbit. *Journal of Neuroscience, (28)*19, 4974-4981.

Montero, V.M., Bravo, H., & Fernandez, V. (1973). Striate-peristriate cortico-cortical connections in the albino and gray rat, *Brain Research*, 53(1), 202–207.

Montero, V.M., Rojas, A., & Torrealba, F. (1973). Retinotopic organization of striate and peristriate visual cortex in the albino rat," *Brain Research,* (53)1, 197–201.

Montero, V.M. (1981). Comparative studies on the visual cortex. in *Cortical Sensory Organization*, C.N. Woolsey, ed., Humana Press, Clifton, New Jersey, USA, vol. 2, 45-81.

Montero, V.M. (1993). Retinotopy of cortical connections between the striate cortex and extrastriate visual areas in the rat. *Experimental Brain Research,* (94)1, 1–15.

Müller-Paschinger, I.B., & Tömböl, T. (1989). Cortico-cortical and subcortico-cortical afferent connection of the rabbit's primary visual cortex. A horseradish peroxidase study. *Anatomy and Embryology, (180)*1, 81-88.

Newton, J.R., Sikes, R.W., & Skavenski, A.A. (2002). Cross-modal plasticity after monocular enucleation of the adult rabbit. *Experimental Brain Research, (144)*4, 423–429.

Olavarria, J., & Torrealba, F. (1978). The effect of acute lesions of the striate cortex on the retinotopic organization of the lateral peristriate cortex in the rat," *Brain Research,* 151(2), 386-391

Olavarria, J. (1979). A horseradish peroxidase study of the projections from the latero-posterior nucleus to three lateral peristriate areas in the rat. *Brain Research,* (173)1, 137–141.

Olavarria, J. & Montero, V.M. (1981). Reciprocal connections between the striate cortex and extrastriate cortical visual areas in the rat. *Brain Research,* 217(2), 358–363.

Olavarria, J., Mignano, L.R., & Van Sluyters, R.C. (1982). Pattern of extrastriate visual areas connecting reciprocally with striate cortex in the mouse. *Experimental Neurology,* 78(3), 775-779.

Olavarria, J. & Montero, V.M. (1984). Relation of callosal and striate-extrastriate cortical connections in the rat: morphological definition of extrastriate visual areas. *Experimental Brain Research,* (54)2, 240–252.

Olavarria, J., & Van Sluyters, R.C. (1985). Organization and postnatal development of visual callosal connections in the rat. *Journal of Comparative Neurology, (239)*1, 1-26.

Olavarria, J. & Montero, V.M. (1989). Organization of visual cortex in the mouse revealed by correlating callosal and striate- extrastriate connections. *Visual Neurosci*ence, (3)1, 59–69.

Olavarria, J., & Montero, V. (1990). Elaborate organization of visual cortex in the hamster. *Neuroscience Research, (8)*1, 40-47.

Olavarria, J.F., & Li, C.P. (1995). Effects of neonatal enucleation on the organization of callosal linkages in striate cortex of the rat. *Journal of Comparative Neurology, (361)*1, 138-151.

Olavarria, J.F. (1996). Non mirror-symmetric patterns of callosal linkages in areas 17 and 18 in cat visual cortex. *Journal of Comparative Neurology, (366)*4, 643-655.

Olavarria, J.F. (2002). Influence of topography and ocular dominance on the functional organization of callosal connections in cat striate cortex. in *The Cat Primary Visual Cortex*, B. Payne, and A. Peters, eds., Academic Press, New York, USA, 259-294.

Paolini, M., & Sereno, M.I. (1998). Direction selectivity in the middle lateral and lateral (ML and L) visual areas in the California ground squirrel. *Cerebral Cortex, (8)*4, 362–371.

Porada, I., Bondar, I., Spatz, W.B. & Krüger, J. (2000). Rabbit and monkey visual cortex: more than a year of recording with up to 64 microelectrodes. *Journal of Neuroscience Methods, (95)*1, 13-28.

Provis, J.M., & Watson, C.R. (1981). The distribution of ipsilaterally and contralaterally projecting ganglion cells in the retina of the pigmented rabbit. *Experimental Brain Research, (44)*1, 82-92.

Rosa, M.G., & Krubitzer, L.A. (1999). The evolution of visual cortex: where is V2? *Trends in Neuroscience, (22)*6, 242-248.

Roth, M.M., Helmchen, F., & Kampa, B.M. (2012). Distinct functional properties of primary and posteromedial visual area of mouse neocortex," *Journal of Neuroscience, (32)*28, 9716–9726.

Sanderson, K.J. Dreher, B., & Gayer, N. (1991). Prosencephalic connections of striate and extrastriate areas of rat visual cortex. *Experimental Brain Research,* vol. 85, no. 2, pp. 324-334, 1991.

Schuett, S., Bonhoeffer, T., & Hübener, M. (2002). Mapping retinotopic structure in mouse visual cortex with optical imaging. *Journal of Neurosci*ence, 22(15), 6549–6559.

Sun, J., Chen, Y., Chai, X., Ren, Q., & Li, L. (2013). Penetrating electrode stimulation of the rabbit optic nerve: parameters and effects on evoked cortical potentials. *Graefe's Archive for Clinical and Experimental Ophthalmology, (251)*11, 2545–2554.

Swadlow, H.A., Weyand, T.G., & Waxman,S.G. (1978). The cells of origin of the corpus callosum in rabbit visual cortex. *Brain Research, (156)*1, 129-134.

Thomas, H.C., & Espinoza, S.G. (1987). Relationships between inter-hemispheric cortical connections and visual areas in hooded rats. *Brain Research, (417)*2, 214–224.

Thompson, J.M., Woolsey, C.N., & Talbot, S.A. (1950). Visual areas I and II of cerebral cortex of rabbit. *Journal of Neurophysiology, (13)*4, 277-288.

Towns, L.C., Giolli, R.A. & Haste, D.A. (1977). Corticocortical fiber connections of the rabbit visual cortex: A fiber degeneration study. *Journal of Comparative Neurology, (173)*3, 537-560.

Vaudano, E., Legg, C.R., & Glickstein, M. (1991). Afferent and efferent connections of temporal association cortex in the rat: a horseradish peroxidase study. *European Journal of Neuroscience, (3)*4, 317–330.

Vermaercke, B., Gerich, F.J., Ytebrouck, E., Arckens, L., Op de Beeck, H.P. & Van den Bergh, G. (2014). Functional specialization in rat occipital and temporal visual cortex. *Journal of Neurophysiol*ogy, 112(8) pp. 1963–1983, 2014.

Vogt, B.A., Sikes, R.W., Swadlow, H.A., & Weyand. T.G. (1986). Rabbit cingulate cortex: cytoarchitecture, physiological border with visual cortex, and afferent cortical connections of visual, motor, postsubicular, and intracingulate origin. *Journal of Comparative Neurology, (248)*1, 74-94.

Wang, Q. & Burkhalter, A. (2007). Area map of mouse visual cortex. *Journal of Comparative Neurology,* (502)3, 339–357.

Wang, Q., Gao, E., & Burkhalter, A. (2011). Gateways of ventral and dorsal streams in mouse visual cortex," *Journal of Neuroscience,* vol. 31, no. 5, pp. 1905–1918, 2011.

Wang, Q., Sporns, O., & Burkhalter, A. (2012). Network analysis of corticocortical connections reveals ventral and dorsal processing streams in mouse visual cortex," *Journal of Neuroscience, (32)*13, 4386–4399.

Weyand, T.G., & Swadlow, H.A. (1986). Thalamic inputs to visual areas 1 and 2 in the rabbit. *Journal of Comparative Neurology, (250)*4, 521-528.

Weber, J.T., Casagrande, V.A., & Harting, J.K. (1977). Transneuronal transport of [^{3}H] proline within the visual system of the grey squirrel. *Brain Research, (129)*2, 346-352.

Wong, P., & Kaas, J.H. (2008). Architectonic subdivisions of neocortex in the gray squirrel (*Sciurus carolinensis*). *Anatomical Record*, (291)10, 1301-1333.

Woolsey, C.N., Sitthi-Amorn, C., Keesey, U.T., & Holub, R.A. (1974). Multiple representations of the visual field in the cerebral cortex. *American Association of Neurological Surgeons*, St. Louis Meeting, vol. 6.